IEEE P1597.2™/D6.4
Draft Recommended Practice for Validation of Computational Electromagnetics Computer Modeling and Simulations

Prepared by the P1597.2 Working Group of the

IEEE Electromagnetic Compatibility Society (EMC-S) Standards Development Committee

IEEE Standards Activities Department
Standards Licensing and Contracts
445 Hoes Lane, P.O. Box 1331
Piscataway, NJ 08855-1331, USA

Abstract: <Select this text and type or paste Abstract—contents of the Scope may be used>
Keywords: <Select this text and type or paste keywords>

Introduction

(This introduction is not part of IEEE P1597.2/D6.4, Draft Recommended Practice for Validation of Computational Electromagnetics Computer Modeling and Simulations .)

The development of standards and recommended practices for computational electromagnetics (CEM) computer modeling and simulation and code validation has been a topic of much interest within the electromagnetics (EM) community primarily since the mid 1980s. This has been due to advancements in computer hardware and software technologies as well as the arrival of new CEM codes and applications as we know them today. The areas of concern include, but are not limited to analyzing printed circuit board radiated and conducted emissions/immunity, system-level EMC, radar cross section (RCS) of complex structures, and the simulation of various electromagnetic environment effects (E^3) problems. In particular, there are concerns regarding the lack of well-defined methodologies to achieve code-to-code or even simulation-to-measurement validations within a consistent level of accuracy.

P1597.2 is a companion document to the P1597.1 Standard. The scope of P1597.1 is to develop a standard for the validation of CEM computer modeling and simulation techniques and codes in differing electromagnetic compatibility (EMC) applications. The standard provides a basis for analytical and empirical validation of CEM codes and configurations focusing on several key areas.

The scope of this P1597.2 project is to develop a recommended practice for use in CEM computer modeling and simulation applications to guide the electromagnetic compatibility (EMC) design of printed circuit boards to large, complex systems. Areas to be addressed include:

— General guidelines for creating CEM models.

— Development of modeling methodologies for small-to-large scale canonical, standard validation, and benchmark problems.

— Reducing uncertainty and errors in modeling applications.

— Developing fundamental modeling techniques that are consistent with collaborative, multi-disciplinary engineering applications.

The recommended practice will aid modelers and analysts in the selection and application of appropriate modeling and simulations methodologies, physics, and solution techniques to achieve accurate results and to complement measurements and EMC design tasks for a range of progressively complex problems.

Patents

Attention is called to the possibility that implementation of this recommended practice may require use of subject matter covered by patent rights. By publication of this recommended practice, no position is taken with respect to the existence or validity of any patent rights in connection therewith. The IEEE shall not be responsible for identifying patents or patent applications for which a license may be required to implement an IEEE standard or for conducting inquiries into the legal validity or scope of those patents that are brought to its attention.

Participants

At the time this draft recommended practice was completed, the P1597.2 Working Group had the following membership:

Andrew L. Drozd, *Chair*

Bruce Archambeault, *Vice-chair*

Charles Bunting, *Secretary*

Vignesh Rajamani, Assistant *Secretary*

Bronwyn Brench, *Technical Editor*

Colin Brench	James Durbano	Antonio Orlandi
Heinz-Dietrich Brüns	Jun Fan	Al Ruehli
Darren Carpenter	Heyno Garbe	Christian Schuster
Samuel Connor	Tim Harrington	Hermann Singer
Alistair Duffy	Doug Howard	

The following members of the balloting committee voted on this recommended practice. Balloters may have voted for approval, disapproval, or abstention.

(to be supplied by IEEE)

CONTENTS

1. Overview 1

1.1 Scope 1
1.2 Purpose 1
1.3 Background 1

2. Normative references 2

3. Acronyms and abbreviations 3

4. CEM modeling and simulation validation process 4

4.1 General 4
4.2 Levels of model validation 5

5. Problem sets 5

5.1 Problem categories and validation problems 5
5.2 Canonical validation problems 6
5.3 Benchmark validation problems 25
5.4 Standard validation problems 35
5.5 Publication of reference problems and results on the WEB 44

6. Self references for model validation 48

6.1 General 48
6.2 Computational based self referenced models 49
6.3 Geometry based self referenced models 50

7. Numerical calculation of the validation rating using the Feature Selective Validation technique 51

7.1 Implementing the Feature Selective Validation (FSV) technique 52
7.2 The procedure 52
7.3 Grade and Spread 67

Annex A (informative) Bibliography 70

Annex B (informative) Basic descriptions of common CEM techniques 78

B.1 Adaptive Integral Method (AIM) 78
B.2 Analytical Closed-Form Techniques 78
B.3 Bi-Conjugate Gradient Method with Fast Fourier Transform (BCG-FFT) 78
B.4 Boundary Element Method (BEM) 78
B.5 Conjugate Gradient Method (CGM) 78
B.6 Fast Multi-Pole Method (FMM) 79
B.7 Finite-Difference Frequency-Domain (FDFD) 79
B.8 Finite-Difference Time-Domain (FDTD) 79
B.9 Finite Element Method (FEM) 79
B.10 Finite Integration Technique (FIT) 80
B.11 Finite-Volume Time-Domain (FVTD) 80

B.12 Generalized Multi-pole Technique (GMT - Moment Method) ... 80
B.13 Geometrical Optics (GO) ... 81
B.14 Geometrical/Uniform Theory of Diffraction (GTD/UTD) ... 81
B.15 Hybrid Lumped Circuit and Quasi-Transmission Line Method ... 81
B.16 Hybrid Techniques ... 81
B.17 Method of Moments (MoM) ... 82
B.18 Multiple Multi-Pole (MMP) ... 82
B.19 Partial Element Equivalent Circuit (PEEC) Model ... 82
B.20 Pseudo-Spectral Time-Domain Method (PSTD) ... 82
B.21 Shooting Bouncing Rays (SBR), Physical Optics (PO), Physical Theory of Diffraction (PTD) ... 82
B.22 Singularity Expansion Method (SEM) ... 83
B.23 Spectral Domain Approach (SDA) ... 83
B.24 Thin-Wire Time Domain Method (TWTD), Time-Domain Moment Method (TDMM) ... 83
B.25 Transmission Line Method (TLM) ... 83
B.26 Vector Parabolic Equation Technique (VPE) ... 84

Annex C (informative) Guidelines on the selection of CEM techniques and codes ... 85

C.1 Background ... 85
C.2 Typical techniques for EMC modeling problems ... 86
C.3 Commonly used CEM techniques ... 88

Annex D (normative) Validation problems: special cases ... 92

D.1 TSAM validation program ... 92
D.2 CEM and human exposure to electromagnetic fields ... 96

Annex E (informative) Identifying sources of error in CEM modeling and simulation ... 100

E.1 Modeling complex large-scale problems ... 100
E.2 Model-limited errors ... 100
E.3 Procedural errors ... 100
E.4 Technique-limited errors ... 101
E.5 Problem-dependent errors ... 101
E.6 Numerical errors ... 101
E.7 Interpretive errors ... 102

Annex F (informative) Guidelines for reporting solver performance ... 103

F.1 General ... 103
F.2 Description ... 103
F.3 Detailed level descriptions ... 104
F.4 Examples ... 105

Annex G (informative) Combinatorial modeling rules ... 107

G.1 General ... 107
G.2 Integrating component contributions to achieve a total budget solution ... 107
G.3 Bounding uncertainty ... 107

Annex H (informative) Data used for FSV comparison ... 108

Annex I (informative) Glossary ... 110

Draft Recommended Practice for Validation of Computational Electromagnetics Computer Modeling and Simulations

1. Overview

1.1 Scope

This recommended practice is a companion document for IEEE P1597.1™/D4.3[1]. It provides examples and problem sets to be used in the validation of computational electromagnetics (CEM) computer modeling and simulation techniques, codes, and models. It is applicable to a wide variety of electromagnetic (EM) applications including but not limited to the fields of antennas, signal integrity (SI), radar cross section (RCS), and electromagnetic compatibility (EMC). This document shows how to validate a particular solution data set by comparing it to the data set obtained by measurements, alternate codes, canonical, or analytic methods.

1.2 Purpose

This recommended practice serves as an aid to CEM modelers and analysts in the selection and application of appropriate computer modeling and simulation methodologies, physics, and solution techniques to achieve accurate results. It also serves to complement measurements and EM design tasks for a range of progressively complex problems through the use of modeling problem examples for small-to-large scale canonical, benchmark, and standard validation problems. Finally, this recommended practice provides a detailed description of a validation process, the FSV method, that compares a particular solution data set to a reference data set.

1.3 Background

In general, CEM techniques and codes, and the manner in which they are used to analyze a given problem, can produce quite different results. These results are affected by the way in which the underlying physic formalisms have been implemented within the codes including the mathematical basis functions, numerical solution methods, numerical precision, and the use of building blocks (primitives) to generate computational models.

[1] For information on normative references, see Clause 2.

Despite all CEM codes having their basis in Maxwell's equations of one form or another, their accuracy and convergence rate depends on how the physics equations are cast (e.g., integral or differential form, frequency or time domain), what numerical solver approach is used (full or partial wave, banded or partitioned matrix, non-matrix), inherent modeling limitations, approximations, and so forth. The physics formalism, available modeling primitives (canonical surface or volumetric objects, wires, patches, facets), analysis frequency, and time or mesh discretization further conspire to affect accuracy, solution convergence, and overall validity of the computer model.

The critical areas that must be addressed include model accuracy, convergence, and techniques or code validity for a given set of canonical, benchmark, and standard validation models. For instance, uncertainties may arise when the predicted results using one type of CEM technique do not agree favorably or consistently with the results of other techniques or codes of comparable type or even against measured data on benchmark models. Furthermore, it can be difficult to compare the results between certain techniques or codes despite their common basis in Maxwell's equations. Exceptions can be cited, in particular, when comparing the results of "similar" codes grouped according to their physics, solution methods, and modeling element domains. Nevertheless, disparities even among codes in a certain "class" have been observed. Many examples can be cited where fairly significant deviations have been observed between analytical or computational techniques and empirical based methods. Differences are not unexpected, but the degree of disparity in certain cases cannot be readily explained nor easily discounted, which has led to the often asked question, "…which result is accurate?"

The annexes at the end of this document supplement the main body by providing more detailed information, data sets, and guidelines. Annex A is the bibliography for the overall document and allows the interested reader to pursue more detailed information on a given topic. Annex B provides a brief summary of over twenty-five CEM techniques, allowing the reader to gain insight into some of the possible methods that can be selected for validation. Annex C describes some of the more common CEM techniques and provides guidelines on how to match the appropriate CEM techniques or codes to the CEM modeling and simulation problems being faced. Annex D gives some special case validation problems involving complex systems. Annex E identifies many common sources of errors that can be introduced into the CEM modeling and simulation process. By understanding how and why these errors may occur, it is sometimes possible to prevent these errors. If the errors cannot be corrected, this knowledge provides valuable insight into why a specific simulation does not match expected validation results. Annex F provides guidelines for reporting solver performance, an aspect of CEM modeling and simulation that is closely related to accuracy validations. Because accuracy and performance are related and are frequently reported together, this annex provides information necessary to uniformly report performance. Annex G outlines several combinatorial modeling rules to follow when performing piecewise simulations in order to ensure the highest level of accuracy in the ultimate result. Annex H provides the data used to perform the FSV validation process in Clause 7. Annex I is the glossary and includes the definitions of many terms that are specific to this document.

2. Normative references

The following referenced documents are indispensable for the application of this document. For dated references, only the edition cited applies. For undated references, the latest edition of the referenced document (including any amendments or corrigenda) applies.

IEEE P1597.1™ (Draft 4.3, 6 June 2008), Draft Standard for Validation of Computational Electromagnetics Computer Modeling and Simulation.

IEEE EMC-S TC-9, *Problem Categories*, Web site <http://www.ewh.ieee.org/cmte/tc9/Problems/index.html>.

IEEE German EMC Chapter, *AG Numerische Modellierung*, Web site, <http://www.ewh.ieee.org/r8/germany/emc/ag_num/index.html>.

Balanis, Constantine A., *Antenna Theory: Analysis and Design, Second Edition*, John Wiley & Sons, Inc., 1996. (See sub-clauses 5.2.1.1, 5.2.1.2, and 5.2.1.4).

Archambeault, B., Pratapneni, S., Zhang, L., Wittwer, D. C., and Chen, J., "A proposed set of specific standard EMC problems to help engineers evaluate EMC modeling tools," *IEEE International Symposium on Electromagnetic Compatibility*, vol. 2, pp. 1335–1340, Aug. 2001. (See sub-clauses 5.4.1.1, 5.4.1.2, and 5.4.2.1).

Rajamani, V., Bunting, C. F., Deshpande, M. D., and Khan, Z. A., "Validation of Modal/MoM in shielding effectiveness studies of rectangular enclosures with apertures," *IEEE Transactions on Electromagnetic Compatibility*, vol. 48, pp. 348-353, May 2006. (See sub-clause 5.4.2.2).

Archambeault, B., Ruehli, A., "Introduction to 2001 special challenging EMC modeling problems," *IEEE International Symposium on Electromagnetic Compatibilit*y, vol. 2, pp. 799–804, Aug. 2001. (See sub-clause 5.4.3).

Woo, A. C., Wang, H. T. G., Schuh, M., and Sanders, M., "Benchmark Plate Radar Targets for the Validation of Computational Electromagnetics Programs," *IEEE Antennas and Propagation Magazine*, vol. 34, no. 6, pp. 52–56, Dec. 1992. (See sub-clause 5.5.4).

Woo, A. C., Wang, H. T. G., Schuh, M., and Sanders, M., "Benchmark Plate Radar Targets for the Validation of Computational Electromagnetics Programs," *IEEE Antennas and Propagation Magazine*, vol. 35, no. 1, pp. 84–89, Feb. 1993. (See sub-clause 5.5.4).

AFRL-DE-TR-2003-1092, "Vlasov Antenna Data for Electromagnetic Code Validation," Air Force Research Laboratory (AFRL) Directed Energy Directorate Final Report, Greenwood, A., and Hendricks, K., June 2003. (See sub-clause 5.5.4).

3. Acronyms and abbreviations

For the purposes of this Recommended Practice, the following terms and definitions apply. Annex B of this document, *The Authoritative Dictionary of IEEE Standards Terms, Seventh Edition*, and ANSI C63.14-1998 should be referenced for terms not defined in this clause.

ABC	Absorbing Boundary Condition
ADM	Amplitude Difference Measure
CEM	computational electromagnetics
E	electric field
EM	electromagnetic
EMC	electromagnetic compatibility
EMCC	Electromagnetic Code Consortium
EMC-S	Electromagnetic Compatibility Society (of the IEEE)
EMI	electromagnetic interference
FDM	Feature Difference Measure
FDTD	Finite-Difference Time-Domain
FSV	Feature Selective Validation
GDM	Global Difference Measure
MoM	Method of Moments
NASA	National Aeronautics and Space Administration
NEC	Numerical Electromagnetics Code
PCB	printed circuit board
PEC	perfectly electrically conducting
PEEC	Partial Element Equivalent Circuit
RCS	radar cross section
SE	shielding effectiveness

TC-9	Technical Committee 9 (on CEM, of the IEEE EMC-S)
TEM	transverse electromagnetic
TLM	Transmission Line Method
TSAM	Transformable Scale Aircraft-like Model

4. CEM modeling and simulation validation process

4.1 General

The validation process for modeling and simulation results is dependent on exactly what is being validated and what data is available to support the validation. The preferred process is to validate the unknown case against a known reference. To this end, standard problems and other means of obtaining a reference are described in IEEE P1597.1™/D4.3[2] together with a procedure to compare the resulting data sets. Where no suitable reference case can be obtained, validation is possible by using self referencing schemes. While less encompassing, these schemes still permit a high level of confidence to be achieved. The flow chart shown in Figure 1 provides the route that is taken.

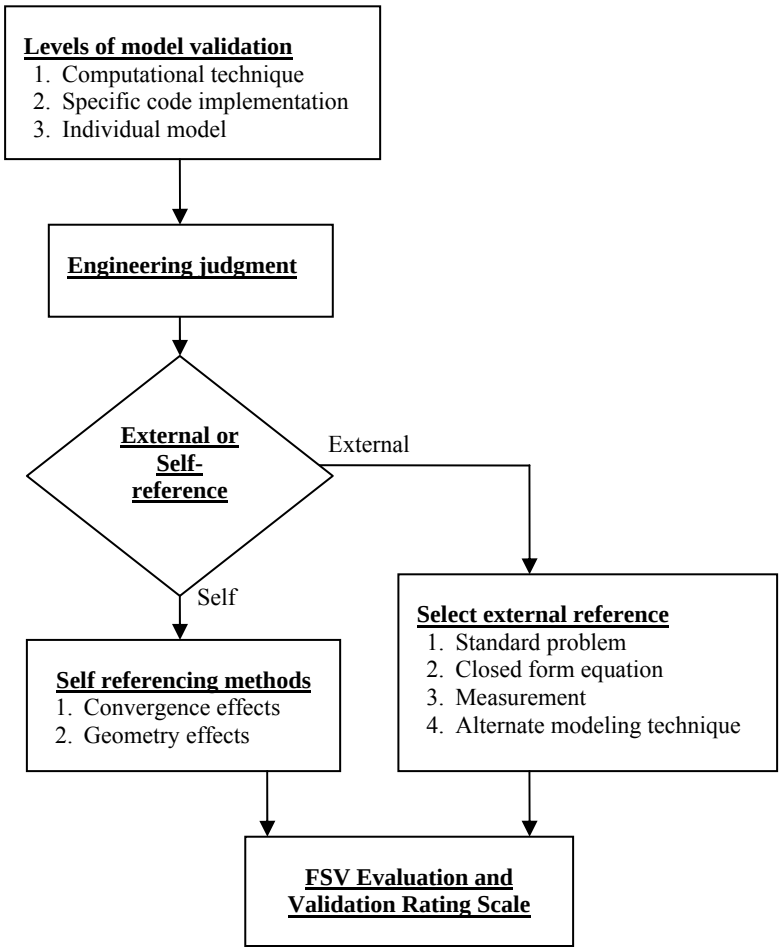

Figure 1—Validation flow chart

[2] See Clause 2 for normative references.

NOTE—The terms "modeling" and "simulation" can, in most places, be used interchangeably.

This recommended practice provides a wide variety of reference problems that are similar to the types of problems encountered at the work place, and the results of these given problems can be used to compare to the user's problem and hence validate a modeling or simulation tool. The Feature Selective Validation (FSV) method is a means to consistently compare the model being validated to the reference data, and Clause 7 contains additional information to support the implementation of the FSV method and to provide assistance in the interpretation of the results produced by the method.

4.2 Levels of model validation

There are three different levels to a complete model validation. When deciding how to validate a model, it is important to consider which levels of validation are needed. The levels are:

a) Mathematical level: Computational technique validation

b) Implementation level: Individual software code implementation validation

c) Model level: Specific model validation

The first level determines if the underlying computational technique is correct. The second expands this to include a particular code implementation, and the third includes the specific details of a model. For a complete model validation, all three of these levels are required to be correct. See IEEE P1597.1™/D4.3[3] for more details on these three levels of validation and how they are analyzed and compared using external and self references, and the Feature Selective Validation (FSV) procedure.

NOTE—The term "numerical" could be used equally in place of "computational" – the authors of this document have chosen to use the term "computational."

5. Problem sets

5.1 Problem categories and validation problems

There are many different types of EM modeling and simulation problems, and the use of well defined cases with known solutions are an excellent means of validating a modeling tool or procedure. However, it is impossible to define every possible case and create a suitable reference problem. Therefore a variety of validation cases were created to span the range of problems that may be encountered. Users are encouraged to select validation cases that most closely match their types of problems, recognizing that more than one validation case may be needed to cover the range of problems they are interested in. It should be noted that the library of standard cases is dynamic and additional materials will be added over time.

This recommended practice defines three types of validation cases: canonical, benchmark, and standard. In the following sub-clauses, multiple problems of each of the three types are provided, along with a final sub-clause, 5.5, that points to an alternate "living" source (continuously updated) of validation problems from which users may choose.

The simplest problems are straightforward canonical problems, which often provide significant challenges for full-wave EM techniques and codes due to the need to "break" the physical geometry into small parts. The input impedances (real and imaginary) and far field radiation patterns are detailed for each problem. These canonical validation problems have a closed form solution that will allow comparison of the user's simulation results to the theoretical results.

[3] See Clause 2 for normative references.

The next level in complexity is "benchmark" validation problems. These problems tend to have a simple geometry with only a few objects, so they represent specific types of problems often encountered in the field of EMC. Although these problems do not have closed form solutions, many of them have been previously solved by a number of different codes and techniques. Thus, the user's simulation results should be compared against these previously obtained results.

The highest level of complexity is "standard" validation problems. These problems have a complex geometry and are intended to represent real-world scenarios. As with the benchmark validation problems, no closed form solution is available but many of these problems have been solved by a number of different codes and techniques. Once again, the user's simulation results should be compared against these previously obtained results.

Unless otherwise specified, all equations in this document are MKS rationalized.

5.2 Canonical validation problems

5.2.1 Antenna canonical validation problems

5.2.1.1 Finite length dipole antenna input impedance

The dipole antenna is one of the simplest structures in EMC problems, as shown in Figure 2. The values of the real and imaginary input impedance are well known for a dipole antenna; the impedance varies versus frequency (wavelength compared to the antenna physical length).

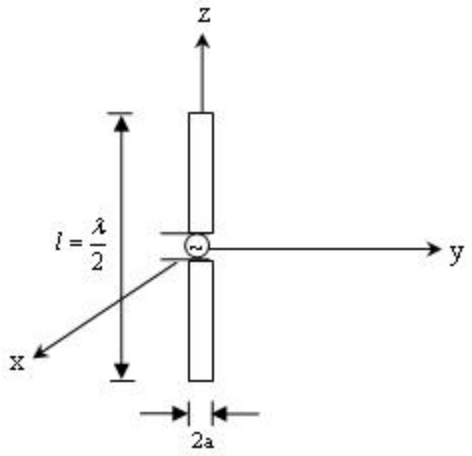

Figure 2—Dipole antenna geometry (where *a* << *l*)

Assuming the antenna is located in free space, the real and imaginary parts of the input impedance at the input terminals are given by Equation (1) from Figure 2.

$$R_{in} = \frac{R_r}{\sin^2(kl/2)}$$
$$X_{in} = \frac{X_m}{\sin^2(kl/2)} \quad (1)$$

where

R_{in} is the input resistance at the input (feed) terminals
X_{in} is the input reactance at the input (feed) terminals
R_r is the radiation resistance at the current maximum
X_m is the radiation reactance at the current maximum
k is the wave number
l is the length of the antenna

NOTE—The radiation resistance and reactance for an assumed current distribution result in sine and cosine integral expressions that are readily available in any graduate level antenna text. The radiation resistance is also the antenna input impedance because the current maximum for a half-wavelength dipole occurs at the input terminals.

The input impedance of a dipole for varying lengths (in wavelengths) has been computed and provided in an Excel® file *5-2-1-1-Dipole_Input_Impedance.xls* (see IEEE EMC-S Web site[4]). The radius of the dipole is assumed to be very small compared to the length.

While many different simulation techniques can be used for this problem, it is likely that a surface based technique, such as the Method of Moments (MoM), is best suited for this problem. This is because only a few unknowns (surface currents) would be needed for this problem, versus a volume based technique where the surrounding air would be required to be part of the model.

Reference:

Balanis, Constantine A., *Antenna Theory: Analysis and Design, Second Edition*, John Wiley & Sons, Inc., 1996. (See normative reference clause 2).

5.2.1.2 Finite length dipole antenna far field radiation pattern

Many software packages have, as an option, the capability to display antenna patterns. In order to explore the capability of a code to predict far field radiation patterns, it is useful to validate against a well known solution. The far field pattern for a dipole in free space, as shown in Figure 3, can be useful to validate the ability of a simulation code to correctly find far fields.

The far field of an antenna is defined as the field for observation points sufficiently distant from an antenna so that the field is considered to be completely transverse electromagnetic (no component of the electric and magnetic field in the direction of propagation). This distance is commonly taken to be

$$R_{\min} = \frac{2D^2}{\lambda}$$

where

$R_{\min}$ is the minimum distance considered to be the far field distance
D is the maximum dimension of the antenna
λ is the wavelength

[4] See Clause 2 for normative references.

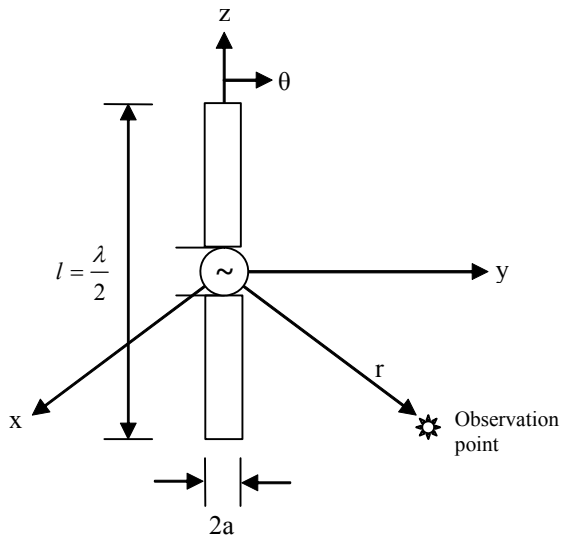

Figure 3—Dipole antenna geometry (where *a* << *l*)

From Balanis, *Antenna Theory*[5], the far fields for a dipole antenna are given in Equation (2) and Equation (3).

$$
\begin{aligned}
&E_r \approx E_\phi = 0 \\
&E_\theta = j\eta \frac{I_0 e^{-jkr}}{2\pi r}\left[\frac{\cos\left(\frac{kl}{2}\right)\cos\theta - \cos\left(\frac{kl}{2}\right)}{\sin\theta}\right] \\
&H_r = H_\theta = 0 \\
&H_\phi \approx j\frac{I_0 e^{-jkr}}{2\pi r}\left[\frac{\cos\left(\frac{kl}{2}\right)\cos\theta - \cos\left(\frac{kl}{2}\right)}{\sin\theta}\right]
\end{aligned}
\tag{2}
$$

So,

$$
\begin{aligned}
&|E| = \frac{I_0\eta}{2\pi r}\left[\frac{\cos\left(\frac{kl}{2}\right)\cos\theta - \cos\left(\frac{kl}{2}\right)}{\sin\theta}\right] \\
&|H| = \frac{I_0}{2\pi r}\left[\frac{\cos\left(\frac{kl}{2}\right)\cos\theta - \cos\left(\frac{kl}{2}\right)}{\sin\theta}\right]
\end{aligned}
\tag{3}
$$

where

[5] See Clause 2 for normative references.

E is the electric field
H is the magnetic field
I_0 is the maximum current through the antenna
η is the intrinsic wave impedance
l is the length of the wire
r is the distance to the observer
k is the wave number
θ is the angle from the z axis

The far field pattern (E and H) for a half wave dipole is calculated and a sample graph is provided in Figure 4. The computed result can be found in the Excel® file *Dipole antenna far field.xls* (see IEEE EMC-S Web site[6]). The field is plotted for θ = 0° to 360°. The field values are in decibels.

While many different simulation techniques can be used for this problem, it is likely that a surface based technique, such as the MoM, is best suited for this problem. This is because only a few unknowns (surface currents) would be needed for this problem vs. a volume based technique where the surrounding air, as well as the air to the distant observation point in the far field would be required to be part of the model.

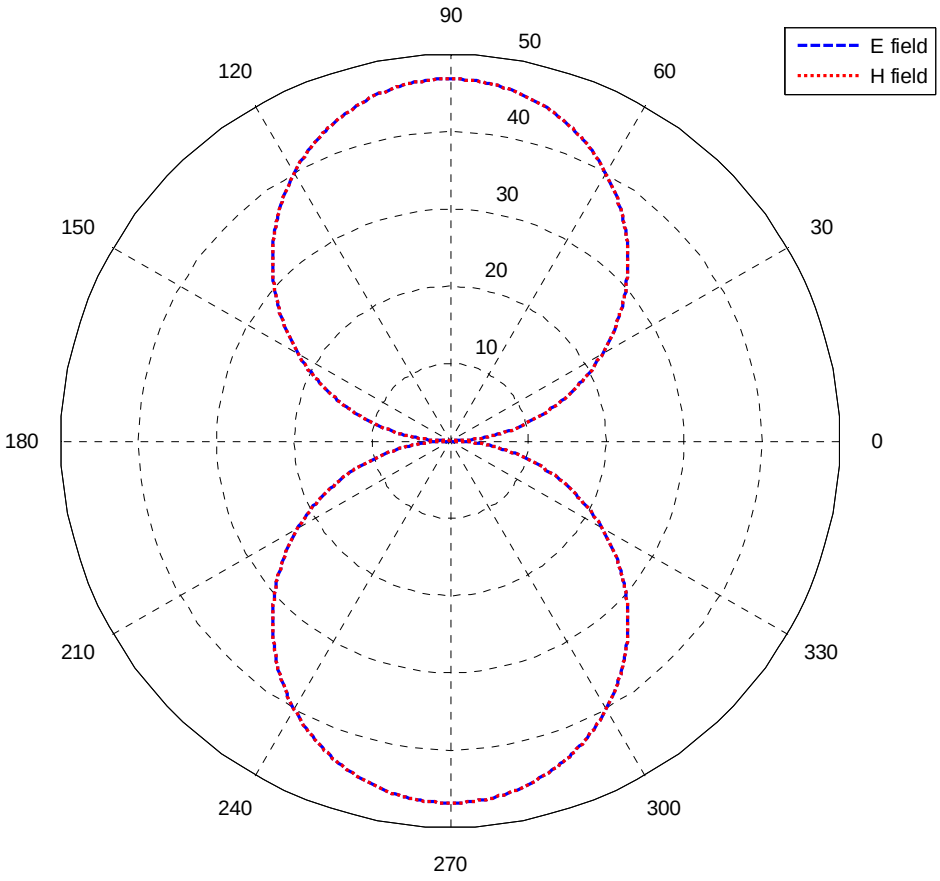

Figure 4—Far field pattern of a half wave dipole

References:

[6] See Clause 2 for normative references.

Balanis, Constantine A., *Antenna Theory: Analysis and Design, Second Edition*, John Wiley & Sons, Inc., 1996. (See normative reference clause 2).

[B76] Kraus, John D., and Marhefka, Ronald J., *Antennas For All Applications*, Third edition

5.2.1.3 Loop antenna radiation resistance

Consider the geometry of Figure 5 for a wire loop antenna in free space.

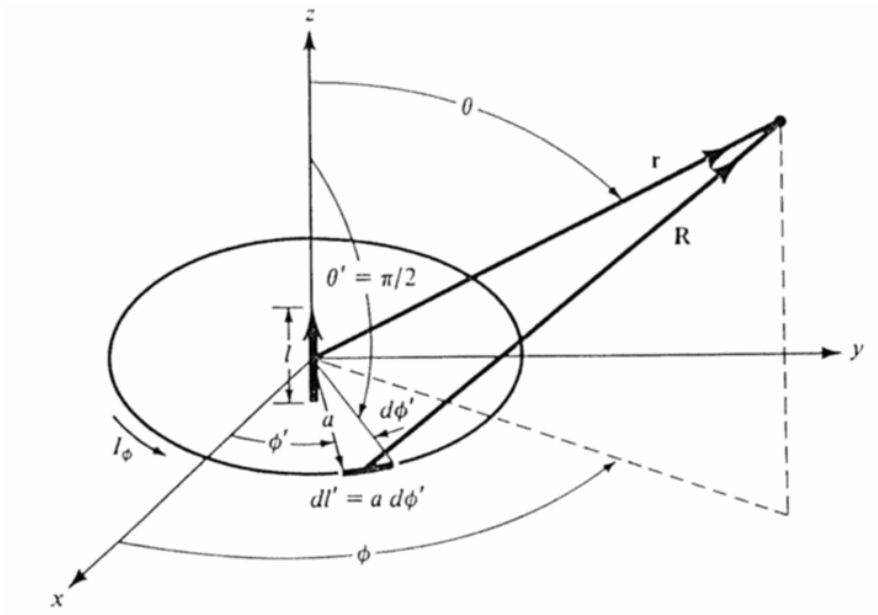

Figure 5—Geometry for circular loop (Balanis 0)

A loop antenna can be considered equivalent to an infinitesimal magnetic dipole where the axis is perpendicular to the plane of the loop. Invoking duality, the fields radiated by a small loop are given by

$$H_r = j\frac{ka^2 I_0 \cos\theta}{2r^2}\left[1+\frac{1}{jkr}\right]e^{-jkr}$$
$$H_\theta = -\frac{(ka)^2 I_0 \cos\theta}{4r}\left[1+\frac{1}{jkr}-\frac{1}{(kr)^2}\right]e^{-jkr} \quad (4)$$
$$E_\phi = \eta\frac{(ka)^2 I_0 \sin\theta}{4r}\left[1+\frac{1}{jkr}\right]e^{-jkr}$$

where

- H is the magnetic field
- E is the electric field
- I_0 is the maximum current through the antenna
- η is the intrinsic wave impedance
- r is the distance to the observer
- k is the wave number
- a is the radius of the loop

θ is the angle from the normal to the loop (from z axis)

These expressions are valid everywhere except the origin.

Loop antennas with electrically small circumferences or perimeters have small radiation resistances that are usually less than their loss resistances. The radiation resistance of the loop can be increased and made comparable to the characteristic impedance of practical transmission lines by increasing (electrically) its perimeter and/or the number of turns.

Please note that the input impedance (of an antenna) is the impedance presented by an antenna at its terminals. The radiation resistance of an antenna is the ratio of the power radiated by an antenna to the square of the RMS antenna current referred to a specified point. The total power radiated is equal to the power accepted by the antenna minus the power dissipated in the antenna.

For the geometry depicted in Figure 5, the radiation resistance depends on the electrical size of the loop. When the internal radius, a, of the loop is large with respect to the wavelength, λ, the radiation resistance will vary considerably from that of, for example, a small loop. Different approximations of radiation resistance for varying loop sizes are compared below.

When the radius of the loop is large ($a \geq \lambda/2$)

$$R_r \approx 60\pi^2\left(\frac{C}{\lambda}\right)$$

When the radius of the loop is intermediate ($\lambda/6\pi \leq a \leq \lambda/2$)

$$R_r \approx \frac{1}{ka}\left[-2J_1(2ka) + \int_0^{2ka} J_0(y)dy\right]$$

When the radius of the loop is small ($a < \lambda/6\pi$)

$$R_r \approx 20\pi^2\left(\frac{C}{\lambda}\right)^4$$

where

R_r is the radiation resistance
C is the circumference of the loop
k is the wave number, $2\pi/\lambda$
a is the radius of the loop
$J_p(y)$ is a Bessel function of the first kind of order p.

Each of the representative plots of the radiation resistance are shown in Figure 6, Figure 7, and Figure 8.

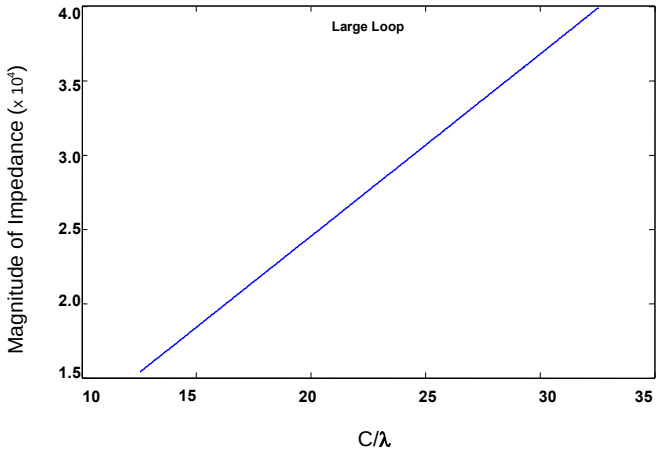

Figure 6—Radiation resistance of a large loop antenna

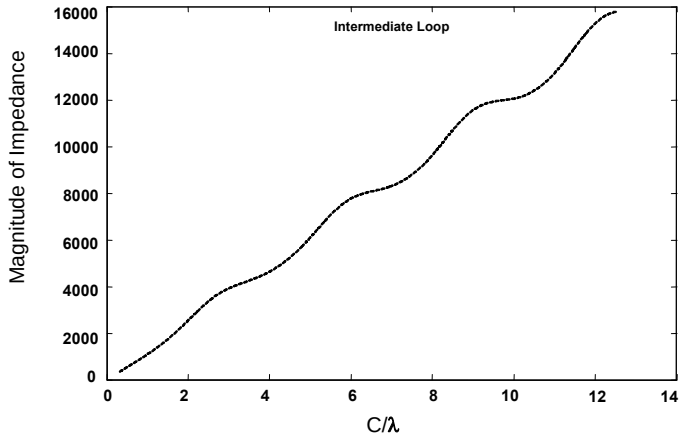

Figure 7—Radiation resistance of a intermediate size loop antenna

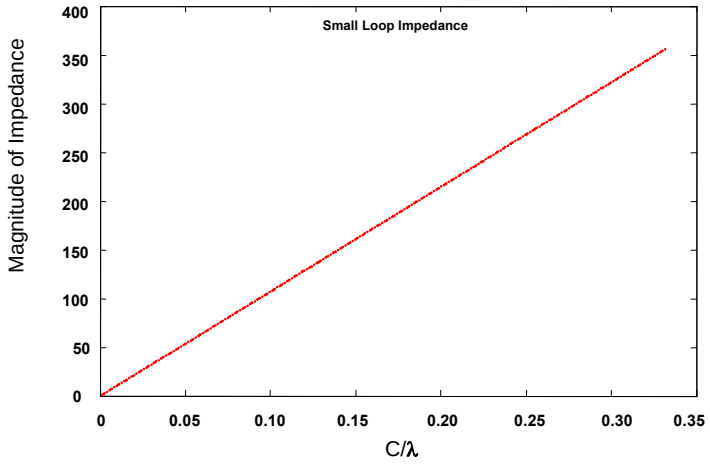

Figure 8—Radiation resistance of a small loop antenna

The magnitude of the radiation resistance of a loop antenna where the radius varies from small to large (compared to wavelength) is computed. The results are presented in an Excel® file, *loop antenna radiation resistance.xls* (see IEEE EMC-S Web site[7]).

While many different simulation techniques can be used for this loop antenna problem, it is likely that a surface based technique, such as the MoM, is best suited for this problem. This is because only a few unknowns (surface currents) would be needed for this problem as opposed to a volume based technique where the surrounding air would be required to be part of the model.

Reference:

Balanis, Constantine A., *Antenna Theory: Analysis and Design, Second Edition*, John Wiley & Sons, Inc., 1996. (For further information only, see normative reference clause 2).

5.2.1.4 Loop antenna far field radiation pattern

The field pattern of electrically small antennas of any shape (circular, elliptical, square, rectangular, etc.) is similar to that of an infinitesimal dipole with a null perpendicular to the plane of the loop and with its maximum along the plane of the loop. The far field pattern for a loop antenna can be useful to validate the ability of a simulation code to correctly find far fields assuming a constant current distribution. The fields for a loop antenna in free space are given in Equation (5).

$$\begin{aligned} E_r &\cong E_\theta = 0 \\ E_\phi &\cong \frac{ak\eta_0 I_0 e^{-jkr}}{2r} J_1(ka\sin\theta) \\ H_r &\cong H_\phi = 0 \\ H_\theta &\cong -\frac{akI_0 e^{-jkr}}{2r} J_1(ka\sin\theta) \end{aligned} \tag{5}$$

where

E is the electric field at the center
H is the magnetic field
a is the internal radius of the loop
k is the wave number
η_0 is the intrinsic impedance of free space
r is the distance between the observer and the center of the loop antenna
J_1 is a Bessel function of the first kind order 1
I_0 is the maximum current through the loop
θ is the angle from the normal to the loop (from z axis)

An example plot is shown in Figure 9.

[7] See Clause 2 for normative references.

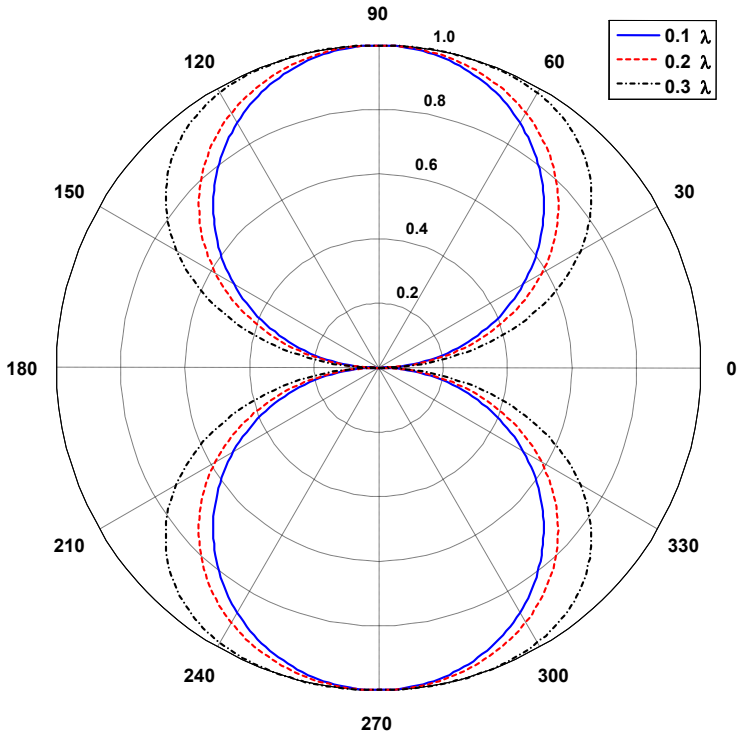

Figure 9—Normalized radiated field pattern

The results are grouped in an Excel® file *Loop Antenna_Farfield.xls*, consisting of five worksheets (see IEEE EMC-S Web site[8]). The first worksheet includes some notes about the problem; for more detail, see Balanis, *Antenna Theory*[9]. The next three worksheets have the calculated data for loop antennas whose radii are 0.1λ, 0.2λ, and 0.3λ respectively. The final worksheet contains the comparison of the three mentioned cases and plots for radiated field pattern and radiated field intensity. All the data presented are normalized to the maximum value.

While many different full wave simulation techniques can be used for this problem, it is likely that a surface based technique, such as the MoM, is best suited for this problem. This is because only a few unknowns (surface currents) would be needed for this problem as opposed to a volume based technique where the surrounding air, as well as the air to the distant observation point in the far field, would be required to be part of the model.

Reference:

Balanis, Constantine A., *Antenna Theory: Analysis and Design, Second Edition*, John Wiley & Sons, Inc., 1996. (See normative reference clause 2).

5.2.2 Signal integrity canonical validation problems

5.2.2.1 Coaxial problem

[8] See Clause 2 for normative references.
[9] See Clause 2 for normative references.

The (centered, round) coaxial line is a very simple structure with well-known closed form expressions for the fundamental transverse electromagnetic (TEM) mode. TEM mode propagation is, strictly speaking, only possible for purely lossless, linear, and isotropic media. Therefore, in this problem, conductors are perfectly electrically conducting (PEC) and the dielectric is free space, as shown in Figure 10.

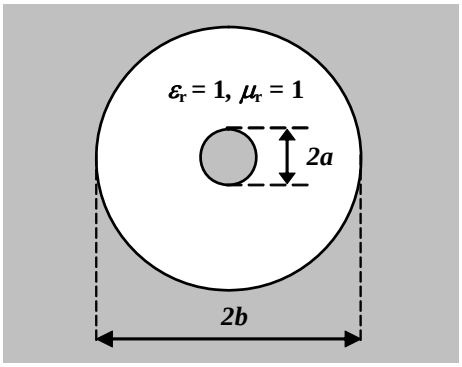

Figure 10—Coaxial problem geometry

Modeling and simulation results can be compared with the following theoretical results:

— Inductance per unit length (in F/m): $L' = \frac{\mu_0}{2\pi} \cdot \ln(b/a)$

— Capacitance per unit length (in H/m): $C' = \frac{2\pi\varepsilon_0}{\ln(b/a)}$

— Characteristic impedance (in Ohm): $Z_0 = \sqrt{\frac{L'}{C'}} = \sqrt{\frac{\mu_0}{\varepsilon_0}} \cdot \frac{\ln(b/a)}{2\pi} = \eta_0 \cdot \frac{\ln(b/a)}{2\pi}$

— Phase velocity (in m/s): $v_{ph} = \frac{1}{\sqrt{L'C'}} = \frac{1}{\sqrt{\mu_0\varepsilon_0}} = c_0$

where

a is the radius of the inner conductor
b is the radius of the outer conductor
μ_0 is the permeability of free space
ε_0 is the permittivity of free space
η_0 is the wave impedance of free space
c_0 is the speed of light in free space

Reference:

[B94] David M. Pozar, *Microwave Engineering*, 2nd edition, Wiley, New York, 1998

5.2.2.2 Parallel Wire Problem

The arrangement of two, parallel, round wires of equal diameter, in a homogeneous dielectric medium, is another simple structure with well-known closed form expressions for the fundamental TEM mode. TEM mode propagation is, again, only possible for purely lossless, linear, and isotropic media and, for this problem, conductors are PEC and the dielectric is free space, as shown in Figure 11.

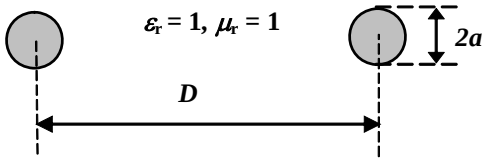

Figure 11—Parallel wire problem geometry

Modeling and simulation results can be compared with the following theoretical results:

— Inductance per unit length (in F/m): $L' = \frac{\mu_0}{\pi} \cdot \cosh^{-1}(D/2a)$

— Capacitance per unit length (in H/m): $C' = \frac{\pi\varepsilon_0}{\cosh^{-1}(D/2a)}$

— Characteristic impedance (in Ω): $Z_0 = \sqrt{\frac{L'}{C'}} = \sqrt{\frac{\mu_0}{\varepsilon_0}} \cdot \frac{\cosh^{-1}(D/2a)}{\pi} = \eta_0 \cdot \frac{\cosh^{-1}(D/2a)}{\pi}$

— Phase velocity (in m/s): $v_{ph} = \frac{1}{\sqrt{L'C'}} = \frac{1}{\sqrt{\mu_0\varepsilon_0}} = c_0$

where

a is the radius of each wire
D is the separation between the centers of the two wires
μ_0 is the permeability of free space
ε_0 is the permittivity of free space
η_0 is the wave impedance of free space
c_0 is the speed of light in free space

Reference:

[B94] David M. Pozar, *Microwave Engineering*, 2nd edition, Wiley, New York, 1998.

5.2.2.3 Strip line impedance problem

The symmetrical strip line trace on a printed circuit board (PCB) is a simple structure and very common in high-speed circuit designs. Its geometry is shown in Figure 12. The strip line characteristic impedance, which is a critical design aspect for signal integrity, is a closed-form formula and is given in Equation (6). However, it should be noted that this is not a pure canonical problem, and that this equation is approximate and no exact solution is available.

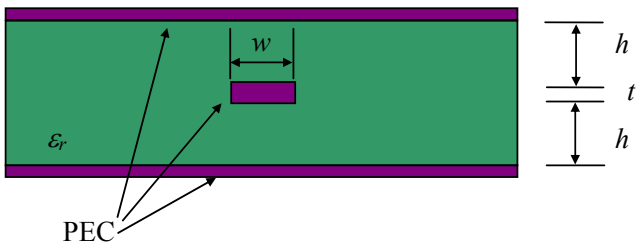

Figure 12—Strip line problem geometry

$$Z_0 = \frac{60}{\sqrt{\varepsilon_r}} \ln\left[\frac{4(2h+t)}{0.67\pi(0.8w+t)}\right] \tag{6}$$

where

Z_0 is the characteristic impedance of the strip line trace
w is the width of the strip line trace
t is the thickness of the strip line trace
h is the distance between the trace and the planes
ε_r is the relative permittivity of the dielectric material

Reference:

[B68] IPC-2251; "Design Guide for the Packaging of High Speed Electronic Circuits," Association Connecting Electronics Industries, Nov. 2003.

5.2.2.4 Microstrip impedance and attenuation validation problem

The microstrip trace on a PCB is a simple structure and very common in high-speed circuit designs. Its characteristic impedance and attenuation, which are critical design aspects for signal integrity, are known as closed-form formulas. This problem is not a pure canonical problem with an exact solution; however, it can be a meaningful validation tool, especially for PCBs.

For the microstrip geometry shown in Figure 13, the characteristic impedance, Z_0, is given in Equation (7) (from Wadell, *Transmission Line Design Handbook* [B123]). It must be noted that this equation will not give an exact solution, but it will give a useful, "good" approximation.

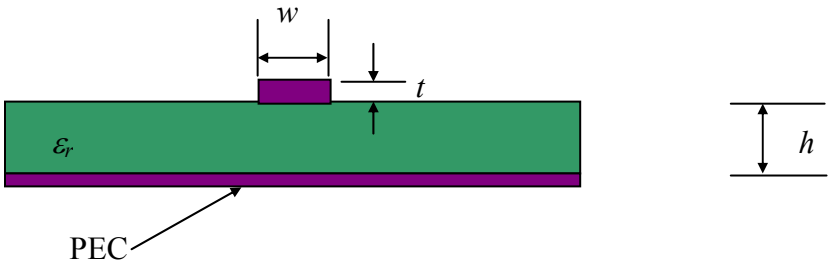

Figure 13—Microstrip problem geometry

$$Z_0 = \frac{60}{\sqrt{2}\sqrt{\varepsilon_{eff}+1}} \ln\left\{1+\frac{4h}{w'}\left[\frac{14+\frac{8}{\varepsilon_{eff}}}{11}\frac{4h}{w'} + \sqrt{\left(\frac{14+\frac{8}{\varepsilon_{eff}}}{11}\right)^2\left(\frac{4h}{w'}\right)^2 + \frac{1+\frac{1}{\varepsilon_{eff}}}{2}\pi^2}\right]\right\} \tag{7}$$

where

Z_0 is the characteristic impedance of the microstrip trace

H is the dielectric layer thickness
ε_{eff} is the effective permittivity of the microstrip trace
w is an intermediate term

The w' term is a function of the microstrip geometry and the relative permittivity as

$$w' = w + \left(\frac{1 + \frac{1}{\varepsilon_r}}{2} \right) \frac{t}{\pi} \ln \left[\frac{4e}{\sqrt{\left(\frac{t}{h}\right)^2 + \left(\frac{\frac{1}{\pi}}{\frac{w}{t} + 1.1} \right)^2}} \right]$$

where

w is the width of the microstrip trace
t is the thickness of the microstrip trace
ε_r is the relative permittivity of the dielectric material
e is the natural logarithm base

The effective permittivity (ε_{eff}) can be obtained from one of the two equations listed below, depending on the value of w / h. When $w / h \leq 1$

$$\varepsilon_{eff} = \frac{\varepsilon_r + 1}{2} + \frac{\varepsilon_r - 1}{2} \left[\left(1 + \frac{12h}{w} \right)^{-0.5} + 0.04 \left(1 - \frac{w}{h} \right)^2 \right]$$

When $w / h \geq 1$

$$\varepsilon_{eff} = \frac{\varepsilon_r + 1}{2} + \frac{\varepsilon_r - 1}{2} \left(1 + \frac{12h}{w} \right)^{-0.5}$$

The attenuation factors of the microstrip trace are also given as closed-form expressions as the characteristic impedance. Again it shall be noted that these expressions are not exact solutions but are good approximations. The overall attenuation is caused by both conductor and dielectric losses (from Wadell, *Transmission Line Design Handbook* [B123]). In other words,

$$\alpha = \alpha_c + \alpha_d$$

where

α is the overall attenuation factor of the microstrip trace
α_c is the attenuation factor of the microstrip trace due to conductor losses
α_d is the attenuation factor of the microstrip trace due to dielectric losses

The attenuation factor due to dielectric losses (α_d) is expressed as

$$\alpha_d = \frac{20\pi}{\ln 10}\frac{\varepsilon_r}{\varepsilon_{eff}}\frac{\varepsilon_{eff}-1}{\varepsilon_r-1}\frac{\tan\delta}{c}\sqrt{\varepsilon_{eff}}\,f \tag{8}$$

where

$\tan\delta$ is the loss tangent of the dielectric material

f is the frequency

c is the velocity in free space

The attenuation factor due to conductor losses (α_c) can be obtained from one of the two equations listed below, depending on the value of w / h. When $w / h \leq 1$

$$\alpha_c = \frac{10R_s}{\pi \ln 10}\frac{\left(\frac{8h}{w}-\frac{w}{4h}\right)\left(1+\frac{h}{w}+\frac{h}{w}\frac{\partial w}{\partial t}\right)}{hZ_0\exp(Z_0/60)} \tag{9}$$

When $w / h \geq 1$

$$\alpha_c = \frac{Z_0 R_s}{720\pi^2 h \ln 10}\left[1+\left(\frac{0.44h^2}{w^2}\right)+\frac{6h^2}{w^2}\left(1-\frac{h}{w}\right)^5\right]\left(1+\frac{w}{h}+\frac{\partial w}{\partial t}\right) \tag{10}$$

where

R_s is the surface resistance of the conductor

$\frac{\partial w}{\partial t}$ is an intermediate term

The $\frac{\partial w}{\partial t}$ term is determined from one of the two expressions listed below, depending on the value of w / h.

When $\frac{w}{h} \leq \frac{1}{2\pi}$ then $\frac{\partial w}{\partial t} = \left(\frac{1}{\pi}\right)\ln\frac{4\pi w}{t}$

When $\frac{w}{h} \geq \frac{1}{2\pi}$ then $\frac{\partial w}{\partial t} = \left(\frac{1}{\pi}\right)\ln\frac{2h}{t}$

The surface resistance of the conductor (R_s) is given as

$$R_s = \sqrt{\frac{\omega\mu}{2\sigma}}$$

where

μ is the permeability of the dielectric material

σ is the conductivity of the conductor

While many different full wave simulation techniques can be used for this problem, it is likely that a volume based technique, such as the Finite-Difference Time-Domain (FDTD) technique, is best suited for this problem. This is because the volume of the dielectric is important to the solution. Surface based techniques may be able to solve this problem using equivalent surface currents at the air-dielectric interface, or by other methods.

References:

[B123] Wadell, Brian C., *Transmission Line Design Handbook*, Artech House, 1991, Chapter 3.

[B44] Edwards, T.C., *Foundations for Microstrip engineering*, John Wiley, New York, 1981

[B91] Paul, C.R., *Introduction to EMC*, John Wiley, New York, 1992

5.2.3 Scattering canonical validation problems

5.2.3.1 Reflection/scattering from a PEC sphere

The scattering of a plane wave by a sphere is a classic problem and is often used as the reference because of its symmetry. This is used to measure the scattering properties like the RCS of other targets. As the problem has been extensively studied by many authors, only an outline of the problem is sketched and references will be provided for the interested reader. The RCS, or scattering cross section, σ_s, (in square meters) can be defined as:

$$\sigma_s = \lim_{r\to\infty}\left[4\pi r^2 \frac{\left|\vec{E}^s\right|^2}{\left|\vec{E}^i\right|^2}\right]$$

where

r is the distance from the target to the observation point
$\vec{E}^s$ is the scattered electric field
$\vec{E}^i$ is the incident electric field

For a sphere of radius a, it can be shown that, assuming geometrical optics ($a >> \lambda$) and a perfectly reflecting sphere, the incident plane-wave radiation is uniformly scattered in all directions (isotropic scattering) and the RCS is given as $\sigma_s = \pi a^2$.

When the wavelength is not small compared with the sphere radius, the calculation is much more complicated. This region where the wavelength is not small compared to the radius is called the Mie region or resonance region. After several developments from different authors Mie, G., *A Contribution to the Optics of Turbid Media* [B83], Stratton, J. A., *Electromagnetic Theory* [B110], Kerr, D. E., et al., *Propagation of Short Radio Waves* [B72], Blake, L. V., *Radar Range-Performance Analysis* [B16], the solution is given in Equation (11)

$$\frac{\sigma_s}{\pi a^2} = \frac{1}{k^2}\left|\sum_{n=1}^{\infty}(-1)^n(2n+1)(a_n + b_n)\right|^2 \qquad (11)$$

where

σ_s is the RCS
a is the radius of the sphere
k is the wave number
n is an index referring to the order of the spherical Bessel function used to express the solution behavior

a_n and b_n (for a perfectly conducting sphere) are given by

$$a_n = \frac{j_n(\alpha)}{h_n^{(2)}(\alpha)}$$

$$b_n = \frac{-\left[\alpha j_n(\alpha)\right]'}{\left[\alpha h_n^{(2)}(\alpha)\right]'}$$

where

j_n is the spherical Bessel function of the first kind

$h_n^{(2)}$ is the spherical Hankel function of the second kind, respectively.

α is ka, the argument of the Bessel and Hankel functions

The primes denote the differentiation with respect to the argument of the Bessel and Hankel functions, α. The plot of the RCS is given in Figure 14 (Barton, *Modern Radar System Analysis* [B11]).

The RCS for a sphere of radius a is calculated and the results are reported in the Excel® file *rcs_sphere.xls* (see IEEE EMC-S Web site[10]). The behavior is indeed oscillatory with a peak of approximately 5.4 dB at $a = \lambda / 2\pi$.

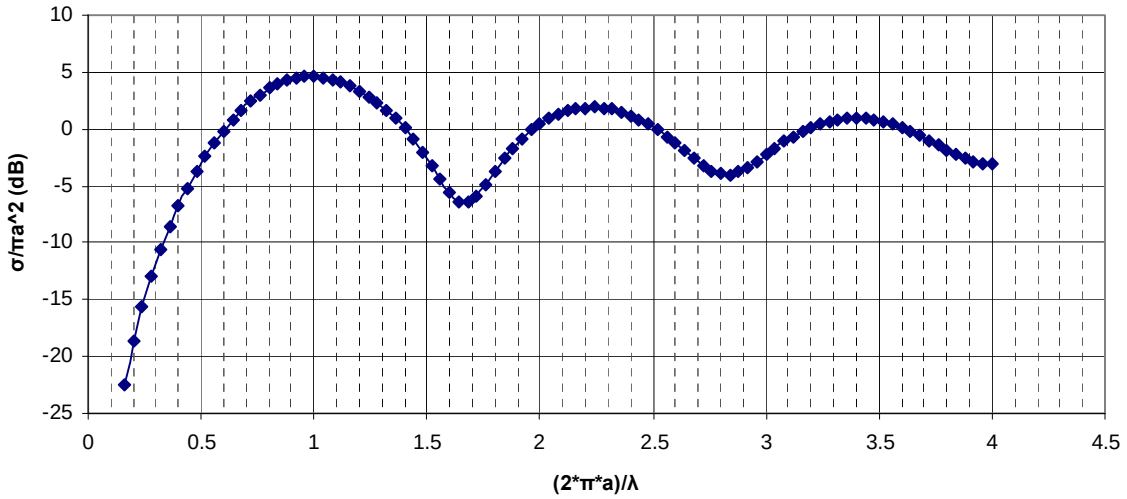

Figure 14—RCS of a perfectly conducting sphere

While many different full wave simulation techniques can be used for this problem, it is likely that a surface based technique, such as the MoM, is best suited for this problem. This is because only a few unknowns (surface currents) would be needed for this problem versus a volume based technique where the surrounding air, as well as the air to the distant observation point in the far field would be required to be part of the model. Another useful technique could be the Geometrical Theory of Diffraction (GTD).

References:

[B113] Sullivan, Roger J., *Microwave Radar: imaging and advanced concepts*, Norwood, MA: Artech House, 2000.

[10] See Clause 2 for normative references.

[B11] Barton, D. K., *Modern Radar System Analysis*, Norwood, MA: Artech House, 1988. (Updated version: *Radar System Analysis and Modeling*, Artech House, 2005.)

[B74] Knott, E. F., Shaffer, J. F., and Tuley, M. T., *Radar Cross Section*, *2nd Edition*, Norwood, MA: Artech House, 1993. (Corrected reprint: SciTech Publishing, 2004.)

[B96] Ruck, G. T., et al., *Radar Cross Section Handbook*, (2 Volumes), New York: Plenum Press, 1970. (Reprinted by Peninsula Publishing.)

[B35] Crispin, J. W. and Siegel, K. M., *Methods of Radar Cross Section Analysis*, New York: Academic Press, 1968.

[B83] Mie, G., *A Contribution to the Optics of Turbid Media, Especially Colloidal Metallic Suspensions*, Annals of Physics, Vol. 25, 1908, pp. 377-445

[B110] Stratton, J. A., *Electromagnetic Theory*, New York: McGraw-Hill, 1941. (Re-issued by Wiley-IEEE, Jan. 2007.)

[B72] Kerr, D. E., et al., *Propagation of Short Radio Waves,* New York: Dover Publications, 1965. (Rev Sub edition by P. Peregrinus, 1987. also by IEE, 1987.)

[B16] Blake, L. V., *Radar Range-Performance Analysis*, Norwood, MA: Artech House, 1986. (Reprinted by Munro Publishing, 1991.)

5.2.3.2 Transverse electric (TE) reflection/scattering from an infinitely long conducting cylinder

The TE (magnetic field parallel to the axis of the cylinder, permitting the electric field to be considered transverse) scattering of a plane wave by an infinitely long conducting cylinder is a classic problem and is often used as the reference because of its symmetry. As the problem has been extensively studied by many authors, only an outline of the problem is sketched and references will be provided for the interested reader. The scattering cross section, σ_s, or RCS, for two dimensional problems is considered a scattering width (in meters).

$$\sigma_s = \lim_{\rho \to \infty} \left[2\pi\rho \frac{\left|\vec{E}^s\right|^2}{\left|\vec{E}^i\right|^2} \right]$$

where,

ρ is the distance from the target to the observation point
$\vec{E}^s$ is the scattered electric field
$\vec{E}^i$ is the incident electric field

Cylindrical coordinates will be used in the problem description to follow.

Since the cylinder is infinitely long, the problem is two dimensional as shown in Figure 15. We can express the time factor $e^{j\omega t}$ throughout the analysis. For the sake of convenience, we need to express the plane wave in terms of cylindrical waves.

The incident wave may be written as

$$E_z^{\,i} = E_0 e^{-jkx} = E_0 \sum_{n=-\infty}^{\infty} (-j)^n J_n(k\rho) e^{jn\varphi} \tag{12}$$

where

$E_z^{\,i}$ is the incident wave on the cylinder
E_0 is the electric field, treated as a constant amplitude
k is the wave number
J_n is the cylindrical Bessel function of n^{th} order
ρ is the separation between the observer and the centre of the cylinder
ϕ is the angle measured from the x-axis

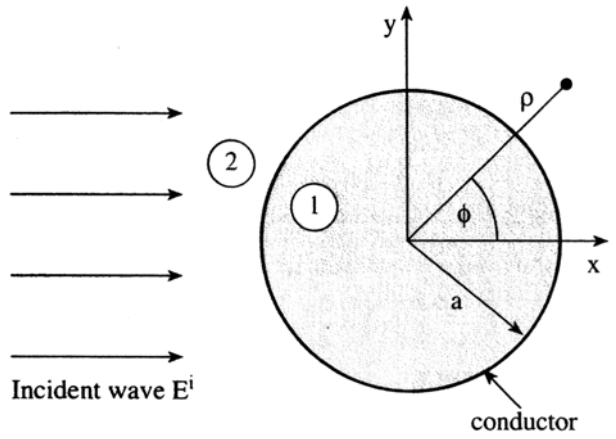

Figure 15—Conducting cylinder scattering canonical problem geometry (Sadiku [B97])

The total field in medium 2 is

$$E_2 = E_z^{\,i} + E_z^{\,s}$$

While the total field in medium 1 is $E_1 = 0$ since medium 1 is conducting. At $\rho = a$, the boundary condition requires that the tangential components of E_1 and E_2 be equal. Hence

$$E_z^{\,i}(\rho = a) + E_z^{\,s}(\rho = a) = 0$$

Substituting the values for the incident and scattered fields, where A_n is a constant,

$$\sum_{n=-\infty}^{\infty} \left[E_0 (-j)^n J_n(ka) + A_n H_n^{(2)}(ka) \right] e^{jn\varphi} = 0$$

From this we obtain

$$A_n = -\frac{E_0 (-j)^n J_n(ka)}{H_n^{(2)}(ka)}$$

Finally substituting A_n and introducing the time factor leads to the scattered wave as

$$E_z^{\ s} = -E_0 e^{j\omega t} a_z \sum_{n=-\infty}^{\infty} (-j)^n \frac{J_n(ka) H_n^{(2)}(k\rho) e^{jn\varphi}}{H_n^{(2)}(ka)} \tag{13}$$

where

E_z^s is the scattered wave on the cylinder
a is the radius of the cylinder
ρ is the separation between the observer and the center of the cylinder
k is the wave number
J_n is the cylindrical Bessel function of n^{th} order
H_n is the cylindrical Hankel function of n^{th} order

The excitation is chosen to be an incoming plane wave of unit amplitude incident normally from the left and the monostatic backscattering angle is phi equal to 180 degrees. Figure 16 shows the bistatic RCS of an infinite conducting cylinder with electric radius equal to one wavelength. The results are provided in an Excel® file, *rcs_cylinder.xls* (see IEEE EMC-S Web site[11]).

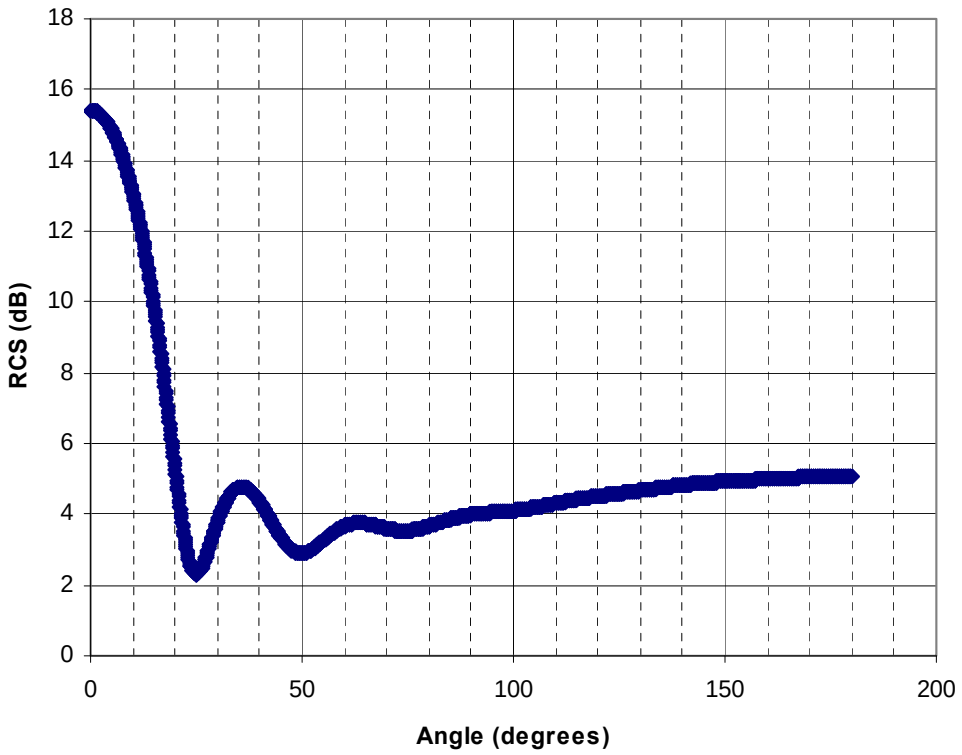

Figure 16—RCS of an infinitely long PEC cylinder

While many different full wave simulation techniques can be used for this problem, it is likely that a surface based technique, such as the MoM, is best suited for this problem. This is because only a few unknowns (surface currents) would be needed for this problem versus a volume based technique where the

[11] See Clause 2 for normative references.

surrounding air, as well as the air to the distant observation point in the far field would be required to be part of the model. Another useful technique could be the Geometrical Theory of Diffraction (GTD).

Reference:

[B97] Sadiku, Matthew N. O., *Numerical Techniques in Electromagnetics*, Boca Raton, FL: CRC Press, 2001.

5.3 Benchmark validation problems

5.3.1 Antenna benchmark validation problems

5.3.1.1 Antenna calibration

In this benchmark validation problem, the effects of imperfect ground planes on the measurement in a typical open area test site (OATS) (as per ANSI C63.5-2006 [B1]) are found for a frequency of 600 MHz as the receive antenna height is varied from 1 m to 4 m above the ground reference. The results of the electric field over height are compared to the theoretical value for a perfect ground (image) plane.

The problem geometry is shown in Figure 17. The dipole antennas are aligned parallel to the *y*-axis and have a length of one-half the wavelength at 600 MHz. The wire radius for the dipole is set to $\lambda/1000$. The distance, *R*, from the coordinate system origin to the antennas is 3 m. The transmit antenna is at a height of 1 m, and the receive antenna height is varied from 1 m to 4 m.

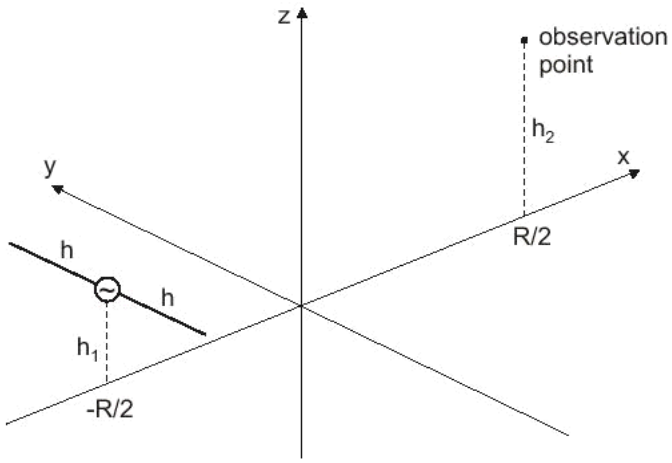

Figure 17—Antenna calibration benchmark problem geometry

The ground (image) plane conditions are varied as follows:

— Ground 1: Perfectly conducting infinite ground plane at $z = 0$

— Ground 2: Perfectly conducting ground plane at $z = 0$ with finite dimensions of 2 m × 4 m. The ground plane is located from $x = \pm 2$ m and $y = \pm 1$ m.

— Ground 3: Wet soil modeled by a homogeneous dielectric media for $z < 0$ with a relative permittivity of 12 and conductivity of 0.04 S/m. The relative permeability is 1.

— Ground 4: Dry soil modeled by a homogeneous dielectric media for $z < 0$ with a relative permittivity of 8 and conductivity of 0.04 S/m. The relative permeability is 1.

The excitation is applied to the transmitting dipole antenna at a frequency of 600 MHz so that a total power of 1 pW is radiated.

The task requires the electric field (in dBμv/m) for each type of ground be plotted for the receive antenna heights of 1.0 m, 1.5 m, 2.0 m, 2.5 m, 3.0 m, 3.5 m, and 4.0 m.

While many different full wave simulation techniques can be used for this problem, it is likely that a surface based technique, such as the MoM, is best suited for this problem. This is because only a few unknowns (surface currents) would be needed for this problem as opposed to a volume based technique where the surrounding air, as well as the air between the source and observation point in the far field, would be required to be part of the model.

References:

IEEE German EMC Chapter, *Numerical Benchmark Problem #11*, Web site <http://www.ewh.ieee.org/r8/germany/emc/ag_num/benchmark.html>. (See normative reference clause 2).

[B1] ANSI C63.5-2006, American National Standard for Electromagnetic Compatibility – Radiated Emission Measurements in Electromagnetic Interference (EMI) Control – Calibration of Antennas (9 kHz to 40 GHz).

5.3.1.2 Coupling from transmitting antenna into transmission line

In this benchmark validation problem, the effect of a nearby monopole antenna on a transmission line is found. Figure 18 shows the physical geometry and dimensions. The entire configuration is placed above an infinite, perfectly conducting, ground (image) plane. The transmission line represents a cable close to the antenna and the antenna dimensions are for a typical high frequency (HF) antenna. The conductors are considered to be perfect conductors. The transmission line is terminated to the ground plane through a 1 kΩ resistor at the right hand end of the transmission line, and is shorted at the left-hand end.

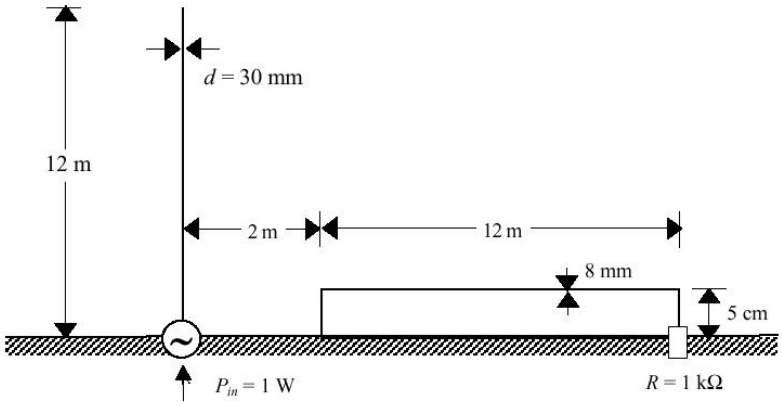

Figure 18—Coupling benchmark problem geometry

The antenna is fed with a 1 W sine wave that varies over the frequency range of 1 MHz to 30 MHz. The internal impedance of the antenna is assumed to be zero.

The results should include the real and imaginary part of the current at the right-hand end of the transmission line (load end), and the real and imaginary part of the monopole antenna's impedance.

While many different full wave simulation techniques can be used for this problem, it is likely that a surface based technique, such as the MoM, is best suited for this problem. This is because only a few unknowns (surface currents) would be needed for this problem as opposed to a volume based technique where the surrounding air, as well as the air to the distant observation point in the far field would be required to be part of the model.

Reference:

IEEE German EMC Chapter, *Numerical Benchmark Problem #3*, Web site <http://www.ewh.ieee.org/r8/germany/emc/ag_num/benchmark.html>. (See normative reference clause 2).

5.3.2 General benchmark validation problems – Thin panel with wire connections above a ground-reference plane

In this benchmark validation problem, an L-shaped antenna is mounted on a finite, thin, rectangular metal plate. The feed point of the antenna is at the base of the vertical conductor, as shown in Figure 19. The open end of the outer shield of the coax cable connects the central point of the rectangular plate with the infinite, perfectly conducting ground plane. All conductors are assumed to be perfectly conducting.

A 1 V source is placed at the top opening of the coax cable, between the center conductor and the cable shield. The frequency range of the source is varied from 1 MHz to 1000 MHz.

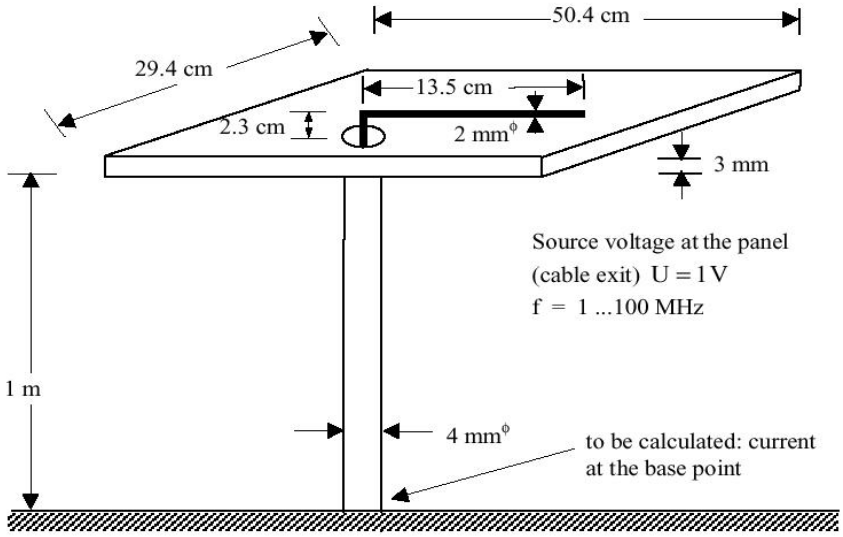

Figure 19—Thin panel benchmark problem geometry

The results should include the induced current (magnitude and phase) at the bottom of the cable on the outer shield of the coax cable. Also, the input impedance (magnitude and phase) of the source should be included.

While many different full wave simulation techniques can be used for this problem, it is likely that a volume based technique, such as the FDTD technique, is best suited for this problem. This is because the volume based technique allows different amplitudes of currents on the top and bottom surface of the plate without additional overhead or unknowns. Surface based techniques could be applied to this problem if a special type of coupling is used between the top and bottom of the plate. Traditional surface based techniques simply replace the different top and bottom currents with an equivalent current. This equivalent current is very sensitive to grid size. If traditional surface based techniques are used, the user is cautioned to create a completely enclosed metal box (no openings) with a source inside, and to observe the amplitude external to the box while adjusting the grid size for a sufficiently accurate result.

Reference:

IEEE German EMC Chapter, *Numerical Benchmark Problem #4*, Web site <http://www.ewh.ieee.org/r8/germany/emc/ag_num/benchmark.html>. (See normative reference clause 2).

5.3.3 Shielding benchmark validation problems

5.3.3.1 Conducting sphere with rectangular loop conductor

In this benchmark validation problem, a perfectly conducting sphere with a radius equal to the wavelength, is connected to a rectangular wire loop at opposite points of the sphere as shown in Figure 20. The wire diameter is specified at 0.00333333λ. The center of the sphere is at $y = 0$.

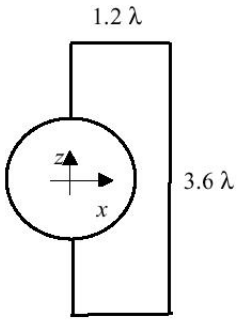

Figure 20—Conducting sphere with rectangular loop benchmark problem geometry

The configuration is fed by a voltage generator with a power of 1 W at the point between the upper vertical wire and the sphere. The frequency is set according to the dimensions of the object.

The results should include the radiation pattern for E_θ in the *x*-*z* plane at $y = 0$, and E_ϕ in the *x*-*y* plane at $z = 0$.

While many different full wave simulation techniques can be used for this problem, it is likely that a surface based technique, such as the MoM, is best suited for this problem. This is because only a few unknowns (surface currents) would be needed for this problem as opposed to a volume based technique where the surrounding air, as well as the air to the distant observation point in the far field (for the radiation pattern) would be required to be part of the model.

Reference:

IEEE German EMC Chapter, *Numerical Benchmark Problem #10*, Web site <http://www.ewh.ieee.org/r8/germany/emc/ag_num/benchmark.html>. (See normative reference clause 2).

5.3.3.2 Resonant frequencies of a metal enclosure

In this benchmark validation problem, the resonant frequencies and "Q" (quality factor) are found for a rectangular enclosure with apertures. The rectangular enclosure is 20 cm x 25 cm x 10 cm high and is constructed of perfectly conducting metal walls. An aperture of 10 cm x 1 cm is centered in each of the walls so that each orthogonal direction includes an aperture. The geometry for this structure is shown in Figure 21.

The source is located inside the rectangular enclosure at x = 8 cm, y = 10 cm, and z = 4 cm. The source amplitude is not specified since the results will be normalized. The results should include a list of all resonant frequencies below 5 GHz and the Q-factor for each frequency.

While many different full wave simulation techniques can be used for this problem, it is likely that a volume based technique, such as the FDTD technique, is best suited for this problem. This is because FDTD uses a time domain approach where all frequencies are excited simultaneously. Frequency domain techniques can also solve this problem, but much care is needed to insure a small enough frequency increment is used (which slows solution time).

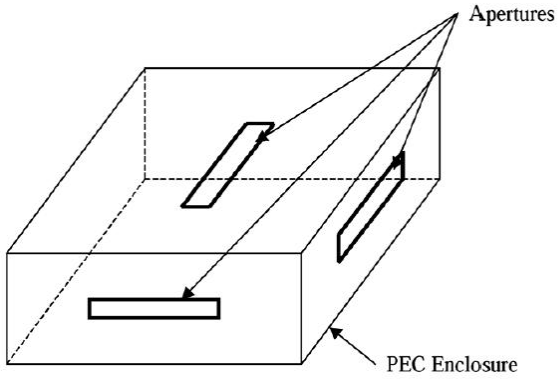

Figure 21—Resonant frequencies benchmark problem geometry

Reference:

IEEE German EMC Chapter, *Numerical Benchmark Problem #17*, Web site <http://www.ewh.ieee.org/r8/germany/emc/ag_num/benchmark.html>. (See normative reference clause 2).

5.3.3.3 Aperture leakage

In this benchmark validation problem, the shielding effectiveness's (SE) of various aperture sizes in an infinite conducting plate are found. Figure 22 shows the configuration. The infinite plate is 5 mm thick.

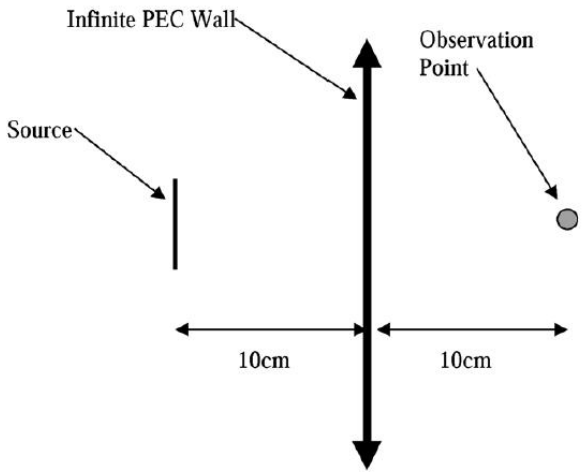

Figure 22—Aperture leakage benchmark problem geometry

The source is a current filament of 1 cm in length and is orientated so its length is perpendicular to the aperture's long dimension. The observation point is 10 cm on the opposite side of the conducting plate and centered on the aperture.

The results should include a plot from 100 MHz to 10 GHz of the differences in the electric field between the case with no metal wall and a metal wall with 2 cm, 3 cm, and 4 cm apertures. The apertures are 5 mm in the short dimension. A plot of the electric field strength (normalized to the source amplitude) for the three aperture sizes and the case with the metal plate and no aperture should also be included.

While many different full wave simulation techniques can be used for this problem, it is likely that a volume based technique, such as the FDTD technique, is best suited for this problem. This is because, depending on the vendor implementation, FDTD allows infinite metal plates by extending them into the absorbing boundary condition (ABC), or mesh truncation technique. Other techniques would be required to create an enclosure where resonances would likely dominate the solution.

Reference:

IEEE German EMC Chapter, *Numerical Benchmark Problem #16*, Web site <http://www.ewh.ieee.org/r8/germany/emc/ag_num/benchmark.html>. (See normative reference clause 2).

5.3.4 Signal integrity benchmark validation problems

5.3.4.1 Multi-conductor configuration above ideal ground-reference

In this benchmark validation problem, the structure consists of two short-circuited conductor loops above an ideally conducting ground as shown in Figure 23. One conductor loop (parts 1 to 3) exhibits a straight line with a 5 m length, whereas the second loop (parts 4 to 7) with a total length of 5 m has a 90 degree kink at the center. Both conductor loops run parallel (length 2.5 m) with a center distance of 10 cm. The height of all horizontal conductors is 10 cm. The radius of all conductors totals 1.75 mm. All conductors are loaded with a distributed resistance $R' = 2\ \Omega/\text{m}$, in order to facilitate the numerical analysis.

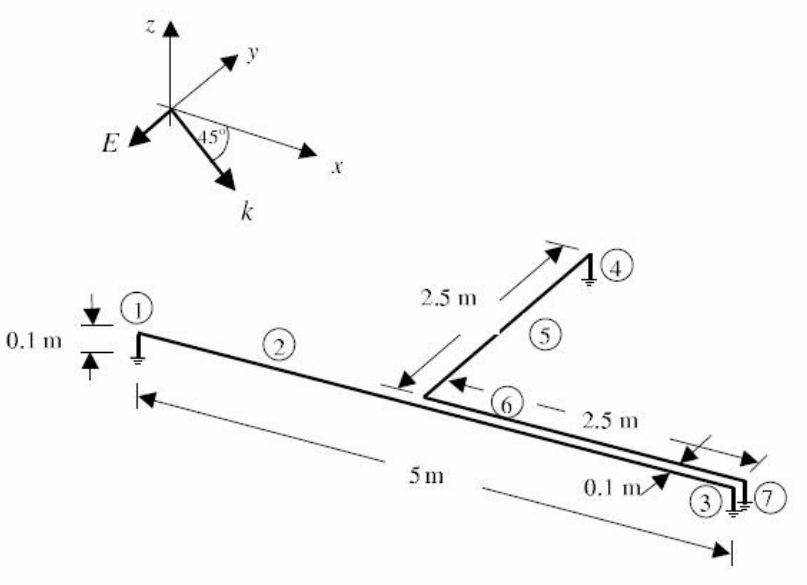

Figure 23—Multi-conductor configuration – geometry

This multi-conductor configuration is excited by a plane wave that is defined according to the following time function: linear rise from zero in 3 ns to a constant value of 1 V/m. The wave vector is the *x*-*z* plane (see Figure 23) and has an angle of -45 degrees against the positive *x*-axis. The E-field vector is horizontally polarized and shows in the -*y* direction.

The following quantities should be found:

a) The time domain current just above the GND connection at locations 3 and 4. These time domain currents should be found for 0 ns to 100 ns.

b) The frequency domain current just above the GND connection at locations 3 and 4. These frequency domain currents should be found for 0 GHz to 1 GHz and displayed using a logarithmic scale (dBμA) for the magnitude.

While many different full wave simulation techniques can be used for this problem, it is likely that a surface based technique or wire based technique, such as the MoM, is best suited for this problem. This is because the surface based technique will only require currents on the wires and, since this problem is wire based, this is the most efficient method. However, other techniques such as volume based techniques (like FDTD) could be used, but will pay a high cost in memory requirements.

Reference:

IEEE German EMC Chapter, *Numerical Benchmark Problem #14*, Web site <http://www.ewh.ieee.org/r8/germany/emc/ag_num/benchmark.html>. (See normative reference clause 2).

5.3.4.2 Propagation delay through dielectric slab

In this benchmark validation problem, the propagation delay through a 5 cm thick dielectric slab is found. The dielectric slab is large enough to be considered infinite in height and width, that is, any end effects will not be part of the final results.

The source is a plane wave approaching from the $x = -\infty$ direction.

The result should include the propagation delay (normalized to free space) for a relative dielectric constant of 2.5, 5.0, and 10.0.

While many different full wave simulation techniques can be used for this problem, it is likely that a volume based technique, such as the FDTD technique, is best suited for this problem. This is because the volume of the dielectric is important to the solution. Surface based techniques may be able to solve this problem using equivalent surface currents at the air-dielectric interface, or by other methods.

Reference:

IEEE German EMC Chapter, *Numerical Benchmark Problem #18*, Web site <http://www.ewh.ieee.org/r8/germany/emc/ag_num/benchmark.html>. (See normative reference clause 2).

5.3.4.3 Microstrip interconnect on PCB with finite ground-reference plane

In this benchmark validation problem, the effect of a microstrip trace over a finite ground-reference plane and near an edge of the finite plane is found. Figure 24 illustrates the configuration. A rectangular ground reference plane of 30 cm by 50 cm and centered at $x = y = 0$ is placed at $z = 0$. A 30 cm long trace is placed as shown near the edge of the reference plane. Figure 25 shows the trapezoidal cross section of the traces, the dielectric slab with a relative dielectric constant of 4.7, and the reference plane. The source and load configurations are shown in Figure 26.

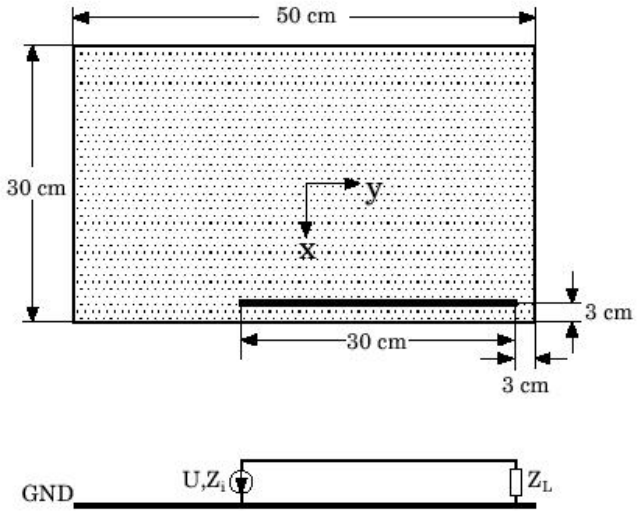

Figure 24—Microstrip interconnect on PCB problem geometry

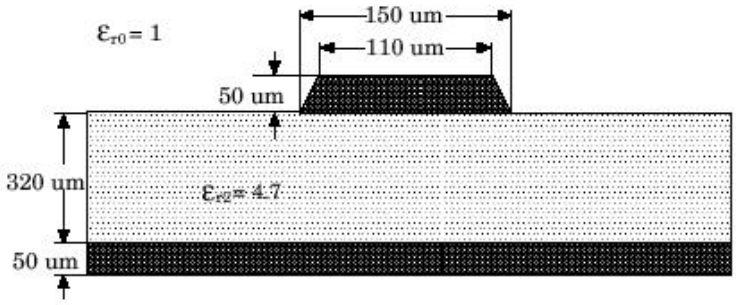

Figure 25—Geometry cross section view

Figure 26—Source and load schematic

The results should include the following values for the frequencies of 96.6666 MHz, 100 MHz, and 233.3333 MHz:

a) A plot of the real and imaginary parts of the current along the length of the trace.

b) A plot of the real and imaginary parts of the current in the reference plane, displayed as an arrow plot to include direction of current flow.

c) A plot of the magnitude of the electric field at a height of 2 cm above the reference plane.

In addition to the above results, the maximum electric field for E_x, E_y, and E_z should be displayed for frequencies from 100 MHz to 1 GHz over a surface 3 m from the center of the reference plane.

The source is a periodic trapezoidal voltage waveform with a rise and fall time of 1.4 ns (based on a 10 % to 90 % amplitude definition), a duty cycle of 50 %, and the total period of 30 ns. The pulse amplitude will vary from 0 V to 5 V.
While many different full wave simulation techniques can be used for this problem, it is noted that this problem combines two difficult items: a dielectric, and far field results at 3 m. A volume based technique such as FDTD could be used to include the dielectric, and then a field extension algorithm applied to get the far field result. Surface based techniques could use an equivalent surface current for the air-dielectric interface, and the 3 m distance is not an issue.

Reference:

IEEE German EMC Chapter, *Numerical Benchmark Problem #12*, Web site <http://www.ewh.ieee.org/r8/germany/emc/ag_num/benchmark.html>. (See normative reference clause 2).

5.3.4.4 Coupled transmission lines

In this benchmark validation problem, a pair of microstrip traces are positioned over an infinite ground-reference plane for a distance of 200 mm. Figure 27 shows the configuration and Figure 28 shows a schematic representation of the configuration.

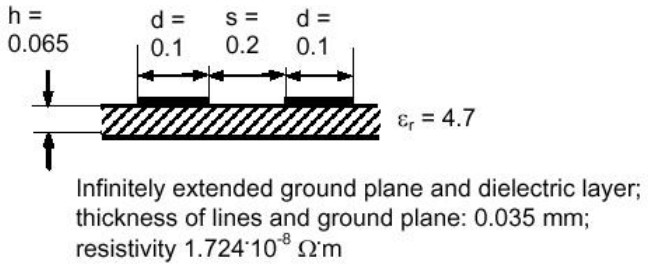

Figure 27—Coupled transmission line problem geometry

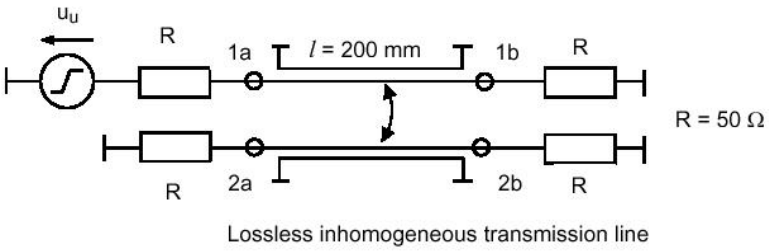

Figure 28—Coupled transmission line problem schematic

The source is a trapezoidal pulse with a rise and fall time of 0.25 ns (based on a 10 % to 90 % amplitude definition) and an amplitude of 2 V. The source impedance is set to 50 ohms, and all lines are terminated with 50 ohms.

The results should include a number of parameters:

a) Characteristic impedance and propagation velocity for the physical geometry for both common mode and differential mode signals.

b) The magnitude of the electric field (E_x, E_y, E_z) 2 cm above the reference plane and centered over the two traces.

c) Time domain plots of the voltage waveform at points 1a, 1b, 2a, and 2b.

d) The frequency domain spectrum of the voltages at 1a, 1b, 2a, and 2b for the case of the trapezoidal pulse being periodically repeated with a rate of 200 MHz.

e) The magnitude of the electric field maximum over a surface of a sphere at 3 m (centered on the center of the two traces) for the same spectrum as (d) above.

While many different full wave simulation techniques can be used for this problem, it is noted that this problem combines two difficult items: a dielectric, and far field results at 3 m. A volume based technique such as FDTD could be used to include the dielectric, and then a field extension algorithm applied to get the far field result. Surface based techniques could use an equivalent surface current for the air-dielectric interface, and the 3 m distance is not an issue.

Reference:

IEEE German EMC Chapter, *Numerical Benchmark Problem #13*, Web site <http://www.ewh.ieee.org/r8/germany/emc/ag_num/benchmark.html>. (See normative reference clause 2).

5.4 Standard validation problems

5.4.1 Printed circuit board standard validation problems

5.4.1.1 Decoupling power/ground-reference planes in PCB standard validation problem

The proper decoupling of power/ground planes is important to both EMC and signal integrity applications. This problem defines a realistic-sized PCB, with capacitors distributed across the entire board. The specifications are given below and a diagram is provided in Figure 29. This problem includes a wide range of frequencies, resonance effects, and the effects of lumped circuit elements.

General Board Description: 4-layer board with 2 solid planes in inner layers; solid planes are separated by 40 mils dielectric FR4 (relative dielectric constant is 4.5).

PCB size: 10 in. x 12 in.

Capacitors: 95 capacitors evenly spaced 1 in. apart, including a 30 mΩ series resistance and 2 nH series inductance.

Source: Located in center of board, with a 1 V sine wave and the frequency scanned from 10 MHz to 1000 MHz.

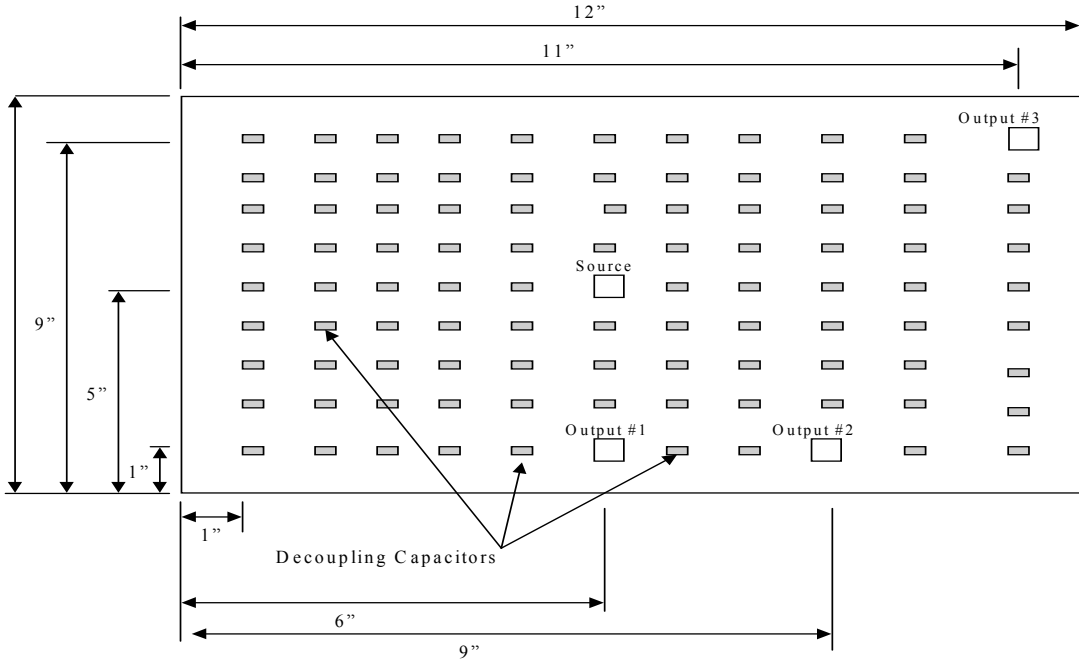

Figure 29—Decoupling capacitor standard validation problem geometry

Figure-of-merit: Voltage at output #1, #2, and #3, relative to input voltage.

Compare the results for the following cases:

a) Board with no capacitors.

b) Board with four capacitors only around source.

c) Board with fully loaded 95 capacitors.

d) Use capacitor values of 0.01 μF, 0.1 μF, and 100 pF.

While many different full wave simulation techniques can be used for this problem, it is likely that a technique that easily allows lumped circuit elements, such as the Partial Element Equivalent Circuit (PEEC) technique, would be best suited. Both volume based techniques and surface based techniques could be used, but the large number of lumped elements may be burdensome.

Reference:

Archambeault, B., Pratapneni, S., Zhang, L., Wittwer, D.C., Chen, J., "A proposed set of specific standard EMC problems to help engineers evaluate EMC modeling tools," *IEEE International Symposium on Electromagnetic Compatibility*, vol. 2, pp. 1335-1340, Aug. 2001. (See normative reference clause 2).

5.4.1.2 Effects of trace crossing split in ground-reference plane

The emissions from a PCB, where a trace is run over a split in the ground-reference plane, is due to a complex interaction of the return current "loop" in the ground-reference plane, and the extra "bunching" of return current near the edge of the ground-reference plane. These effects result in an increase of radiated emissions and electromagnetic interference (EMI) impact. This problem is illustrated in Figure 30, and compares the radiation levels with and without plane splits, as well as the effect of (realistic) stitching capacitors.

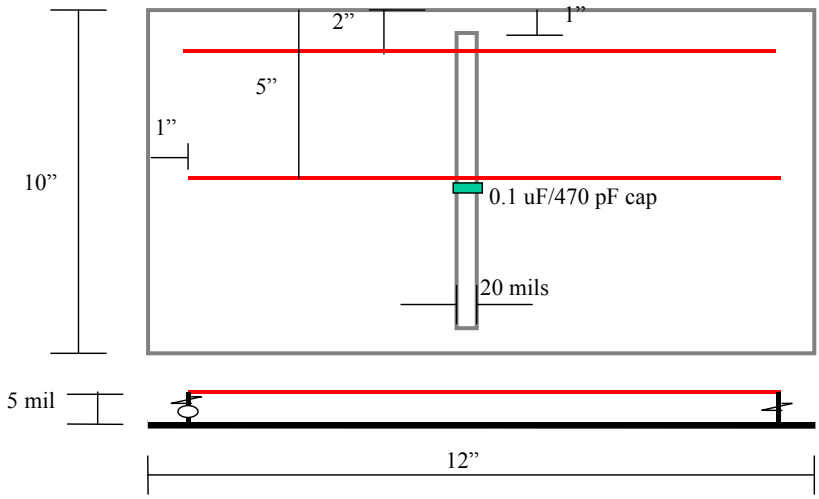

Figure 30—Trace over split plane standard validation problem geometry

Plane size: 10 in. x 12 in.

Trace: 5 mil wide, 10 in. long, 5 mils above the plane, center or close upper edge; dielectric material is FR4.

Slot: 8 in. long, 20 mil wide, center.

Stitching cap: 0.1 μF, consider 2 nH connection inductance and 0.5 Ω parasitic resistance in series, placed right next to the trace.

Source: 3.3 V spread spectrum source from 100 MHz to 2 GHz, 50 Ω source/load termination.

Figure-of-merit: percentage of power radiated into free space, or maximum E-field over a spherical surface 3 m away from the center of the PCB at 100 MHz to 2 GHz range.

Compare the results for the following cases:

a) Board without slot, trace in the middle.

b) Add slot to plane.

c) Move trace to board edge.

d) Add 0.1 μF cap close to trace.

e) Replace 0.1 μF cap with 470 pF cap.

While many different full wave simulation techniques can be used for this problem, it is noted that this problem combines two difficult items: a dielectric, and far field results at 3 m. A volume based technique such as FDTD could be used to include the dielectric, and then a field extension algorithm could be applied to get the far field result. Surface based techniques could use an equivalent surface current for the air-dielectric interface and the 3 m distance would not be an issue.

Reference:

Archambeault, B., Pratapneni, S., Zhang, L., Wittwer, D.C., and Chen, J., "A proposed set of specific standard EMC problems to help engineers evaluate EMC modeling tools," *IEEE International Symposium on Electromagnetic Compatibility*, vol. 2, pp. 1335-1340, Aug. 2001. (See normative reference clause 2).

5.4.2 Shielding standard validation problems

5.4.2.1 Shielding standard validation problem with multiple apertures

The shielding effectiveness (SE) of an enclosure is a complex matter, in which a lot of different phenomena are involved; for example, electrical and geometrical parameters of the material of the walls, apertures and grids, joints and contacts (connections; including the use of gaskets, springs, overlaps, and the like), internal and external cabling and cable feed-through or connectors, and internal boards and back panels. In most cases, the total SE is determined by the combination of all these effects, some with greater impact than others. As a consequence, determining the SE of a real enclosure is not a simple matter. For this problem, a complex metal enclosure has been defined and is shown in Figure 31. This enclosure includes an internal source and apertures with different hole sizes.

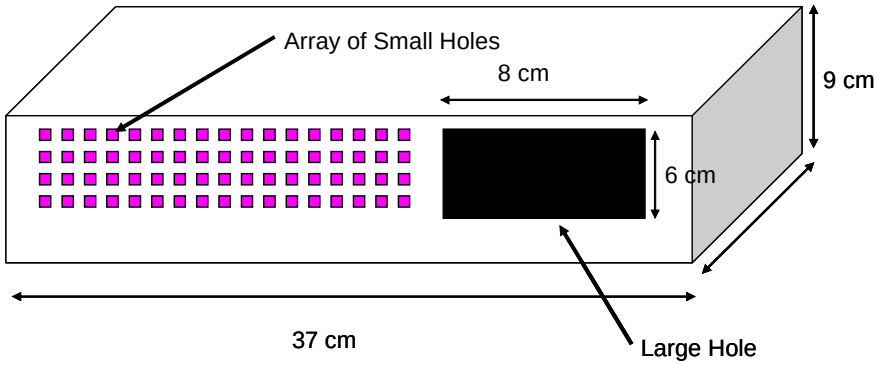

Figure 31—Shielding standard validation problem geometry

Enclosure Dimension: 37 cm × 30 cm × 9 cm; all enclosure walls are made up of perfect electric conductors.

Aperture Dimension: One large hole of 8 cm x 6 cm, plus 68 small holes of 0.2 cm x 0.2 cm, and the spacing between each small hole is 0.2 cm. There are 4 rows and 17 columns of these small holes.

Source Location: A metal plane (26 cm x 28 cm) representing the PCB reference plane and the trace over a dielectric (FR4) bed (thickness: 0.0127 cm) driven by constant amplitude harmonic excitations. The plane is placed horizontally in the enclosure and is 1 cm away from the front panel and 1 cm above the bottom enclosure wall. The trace is centered in the plane perpendicular to the slotted panel. A heat sink (solid metal rectangular object) of 16 cm x 10 cm x 2 cm high and is centered 0.5 cm above the reference plane covering the trace.

Source Definition: A 1 V source with frequency ranging from 100 MHz to 2 GHz, and a 50 Ω source/load termination.

Compare the results for the following cases:

a) With no shield.

b) With small holes and large hole.

c) With small holes only.

d) With large hole only.

While many different full wave simulation techniques can be used for this problem, it is likely that a volume based technique, such as the FDTD technique, is best suited for this problem. This is because the volume based technique allows different amplitudes of currents on the inside and outside surface of the enclosure without additional overhead or unknowns. Surface based techniques could be applied to this problem if a special type of coupling is used between the inside and outside of the plate. Traditional surface based techniques simply replace the different inside and outside currents with an equivalent current. This equivalent current is very sensitive to grid size. If traditional surface based techniques are used, the user is cautioned to create a completely enclosed metal box (no openings) with a source inside, and to observe the amplitude external to the box while adjusting the grid size for a sufficiently accurate result.

Reference:

Archambeault, B., Pratapneni, S., Zhang, L., Wittwer, D.C., and Chen, J., "A proposed set of specific standard EMC problems to help engineers evaluate EMC modeling tools," IEEE International Symposium on EMC, vol. 2, pp. 1335–1340, Aug. 2001. (See normative reference clause 2).

5.4.2.2 Shielding effectiveness of a rectangular enclosure with single and double rectangular apertures

In this benchmark validation problem, the SE of a rectangular enclosure with rectangular apertures in the front wall is calculated for a plane wave at normal angle of incidence. The geometry of the enclosure with one aperture is provided in Figure 32, and the geometry with two apertures is provided in Figure 33.

The SE can be defined as the relative capability of a shield to eliminate undesirable electric and magnetic fields and plane waves. It is given by the formula,

$$E - Shielding\left(dB\right) = -20.0\log\left(\frac{\left|\vec{E}_{int}\right|}{\left|\vec{E}_{ext}\right|}\right)$$

where $\vec{E}_{int}$ is the electric field at a given point inside the enclosure and $\vec{E}_{ext}$ is the field at the same point in absence of the enclosure.

A lossless rectangular cavity with rectangular apertures on its front wall is illuminated by a "*y*" polarized plane wave from outside, as shown in Figure 32 and Figure 33, and the SE of the box is investigated by calculating the field that is developed at the center of the cavity due to the source outside (at normal angle of incidence to the front face) for varying size and number of apertures.

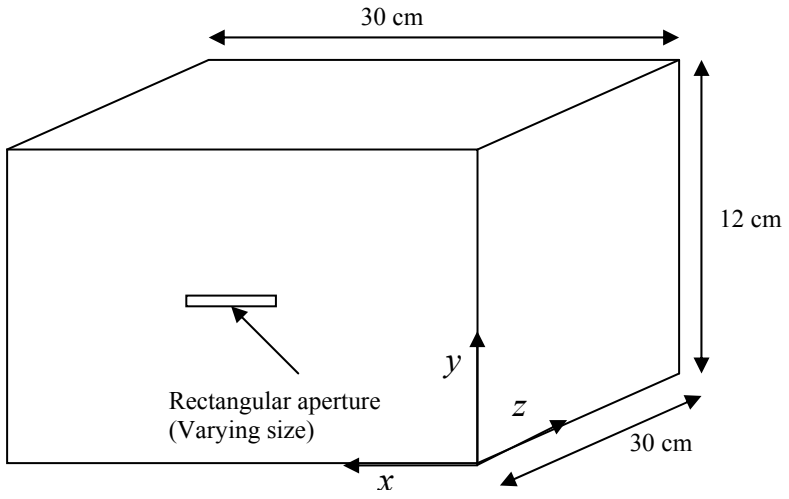

Figure 32—Geometry of the cavity with one aperture at the front wall

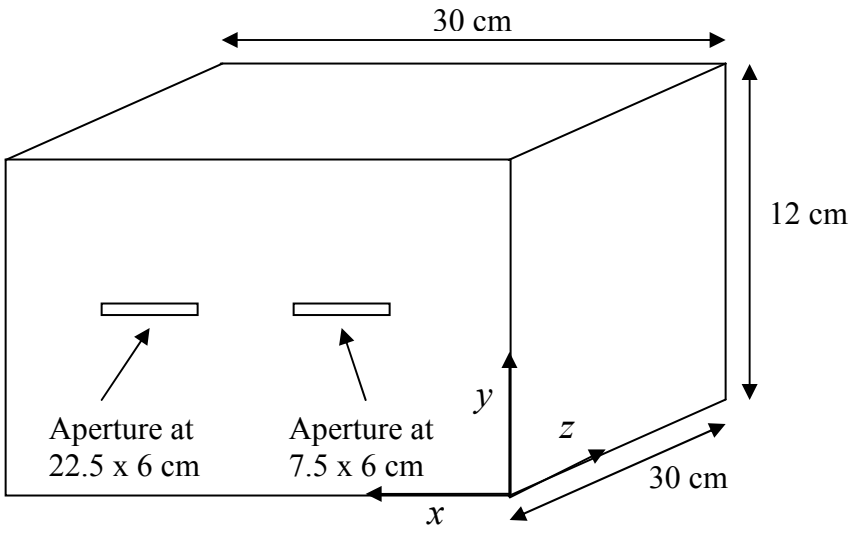

Figure 33—Geometry of the cavity with two apertures at the front wall

Plots of the SE for the frequency range of interest (100 MHz to 1 GHz), computed using two different computational methods, are provided for the one- and two-aperture cases shown in Figure 34 and Figure 35. Two computational methods are used to solve this problem to provide a better understanding and to compare the accuracy of the results.

Problem dimensions:
Cavity size: 30 cm x 12 cm x 30 cm
Single aperture dimensions: 10 cm x 0.5 cm, 10 cm x 10 cm, 15 cm x 6 cm, 20 cm x 8 cm, and 30 cm x 12 cm
Double aperture dimensions: 6 cm x 0.5 cm, 10 cm x 2 cm, and 14 cm x 10 cm

Frequency range of interest: 100 MHz to 1 GHz

Model details: The cavity is a lossless cavity and is PEC. The source is a "*y*" polarized plane wave at normal angle of incidence to the front face of the cavity.

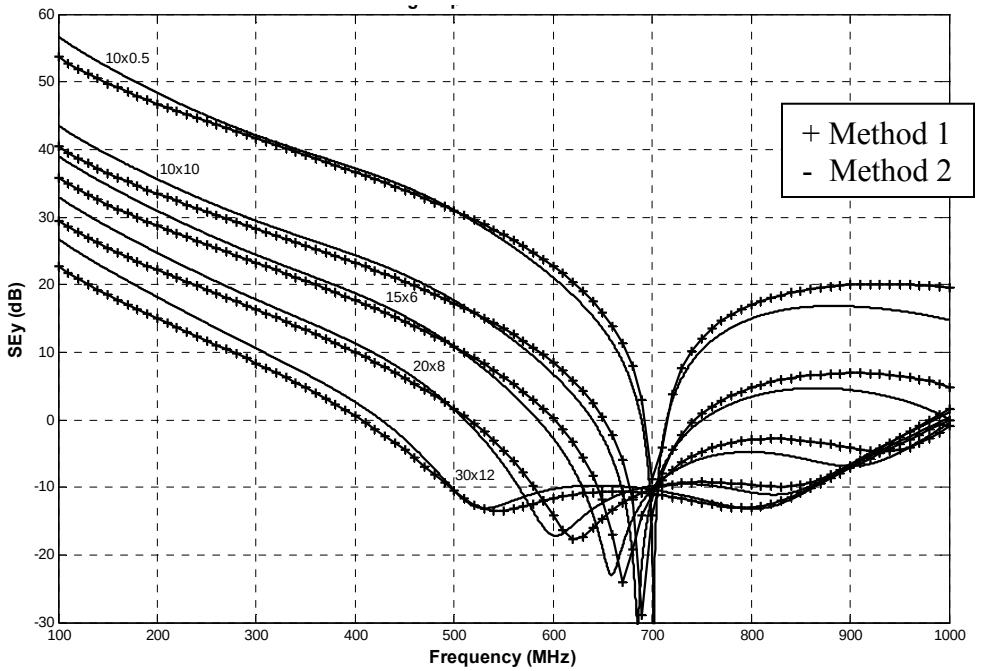

Figure 34—Comparison of SEy results for varying aperture sizes (single aperture)

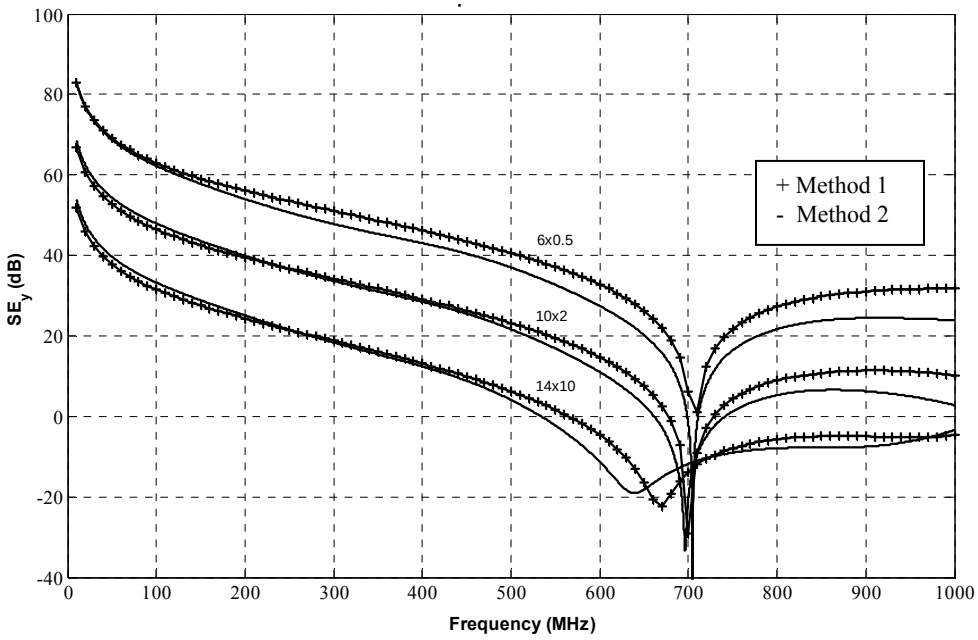

Figure 35—Compared SEy results for varying aperture sizes (two apertures)

In the first computational method, the aperture is represented as a very thin waveguide structure located on an infinite ground plane and hence the aperture fields can be represented using modal expansions. The equivalence principle is used to replace the apertures with equivalent magnetic currents. The internal fields

can be found using cavity Green's functions, and external fields can be found using free space Green's functions with the magnetic currents as the radiating source. The external and internal fields are then matched at the aperture to obtain an integro-differential equation to be solved for unknown magnetic currents using MoM. The excitation source is external and far away from the cavity so that the cavity is illuminated by a plane wave.

In the second computational method, the walls are not assumed to be infinite ground planes, rather they are assumed to be infinitely thin walls with specified dimensions, and the Rao, Wilton, Glisson (RWG) basis functions are used for gridding. This process eliminates the error that can be introduced due to the infinite ground plane assumption. The field at the same point inside the rectangular cavity for the varying size of the apertures (single and double), located on the front wall of the enclosure and illuminated by a plane wave, is computed and compared.

From the results it can be seen that as the aperture size increases, the SE decreases indicating higher field penetration. The self resonance of the cavity can be seen at around 700 MHz and this seems to decrease with an increase in the aperture size. As the frequency increases, the SE decreases for both cases, indicating an increase in field penetration with frequency. The difference between the two methods used in this comparison varies from 2 dB at the low frequency side to about 5 dB at the high frequency side, which points out some limitations of the computational methods in accordance to their assumptions.

Reference:

Rajamani, V., Bunting, C. F., Deshpande, M. D., and Khan, Z. A., "Validation of Modal/MoM in shielding effectiveness studies of rectangular enclosures with apertures," *IEEE Transactions on Electromagnetic Compatibility*, vol. 48, pp. 348-353, May 2006. (See normative reference clause 2).

5.4.3 Signal integrity standard validation problems – Delay line performance standard validation problem

This standard validation problem concerns the performance of a delay line on a PCB. Signal traces are often created in various serpentine shapes to lengthen the trace length and achieve a desired delay. The coupling between the legs of the serpentine delay line can create significant distortion in the pulse, which is not simulated in typical transmission line based simulation tools. The distortion can easily cause timing problems as well as create common mode currents, which can cause EMC problems.

Figure 36 and Figure 37 show the geometry for this challenge problem. The serpentine delay line has a number of closely coupled legs. Results should include the distortion of the delay line and the maximum electric field (100 MHz to 10 GHz) two inches above the board, compared to the same length straight trace case.

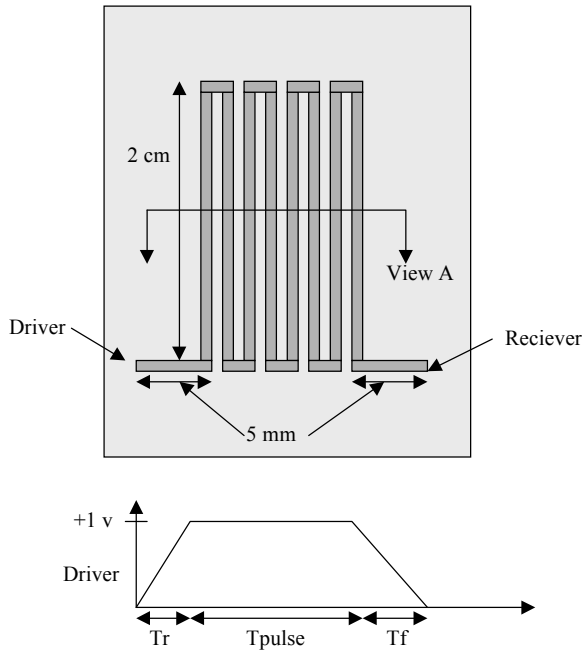

Figure 36—Delay line standard validation problem geometry (top view) (Archambeault & Ruehli 0)

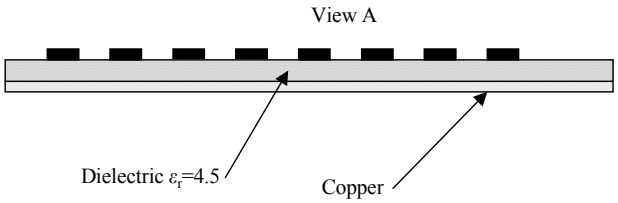

Notes:

1. Traces -- 1 mm wide and 0.2 mm thick
2. Traces 1 mm separation
3. Dielectric Thickness 1 mm
4. Tr = Tf = 200 psec
5. Tpulse = 1 nsec
6. Receiver impedance = line characteristic Z
7. Source Z = 0

Figure 37—Delay line standard validation problem geometry (side view) (Archambeault & Ruehli 0)

While many different full wave simulation techniques can be used for this problem, it is likely that either a surface based technique or a volume based technique would be the best suited. Since the problem source is a time domain pulse, a time domain technique (such as FDTD, finite integration technique (FIT), or PEEC) could be the preferred technique.

Reference:

Archambeault, B., Ruehli, A., "Introduction to 2001 special challenging EMC modeling problems," *IEEE International Symposium on Electromagnetic Compatibility*, vol. 2, pp. 799–804, Aug. 2001. (See normative reference clause 2).

5.5 Publication of reference problems and results on the WEB

5.5.1 IEEE EMC-S web site

The authors of this Recommended Practice, in cooperation with the IEEE EMC-S Technical Committee on CEM (TC-9) and the Applied Computational Electromagnetics Society (ACES), have created a central depository of EMI Modeling Problems, located at the IEEE Entity Web Hosting (EWH) Web site <http://www.ewh.ieee.org/cmte/tc9/> for contributors to provide model and measurement data to share and compare with others. In addition to the data repository, a set of standard challenge problems have been proposed over the past few years, and they are included in this web site.

A committee has been established to review all submittals to this storage location. The submittal must include sufficient detail about how the modeling was accomplished (if any), and how the measurements were conducted (if any) so that the modeling and/or experiments can be easily repeated. The results from these models and/or measurements must be clearly presented, and a simple ASCII text file with the data must be available for downloading. The submittal will be posted on the web once accepted by the review committee and will be available for downloading by interested engineers.

All submittals are expected to contain sufficient information that the user can reproduce the reported results. Model and measurement data or multiple modeling techniques (showing the same results) are preferred so that there is validation within the submittal. Engineers using this data are encouraged to provide their results as further validation of the specific model and results.

The second major purpose of this web location is to provide a central location where interested researchers and engineers can download the details of the various P1597 benchmarks including the IEEE EMC-S TC-9 Challenge and Specific Standard Modeling Problems. These problems have been designed to allow users to highlight strengths and weaknesses of various modeling techniques and tools.

Additional reference validation problems are available at the IEEE German EMC Chapter Web site: <http://www.ewh.ieee.org/r8/germany/emc/ag_num/index.html>[22].

Other problems may also exist. The user is cautioned to carefully consider if the proposed problem is reasonably close to problems of interest to themselves.

5.5.2 Standardized format for validation results on the IEEE EMC-S web site

Typical results that are reported should be in an ASCII file containing tab delimited floating point or fixed-point numbers with the variables defined in an accompanying paragraph that describes the results. An example of floating point numbers is shown in Table 1.

Additionally, the variable definitions may be described in the ASCII file as depicted in Table 2, with fixed point numbers. This table shows how a file might appear when opened using Notepad.

[22] See Clause 2 for normative references.

Table 1—Example ASCII file

3.00000000E+4	-1.02093700E+2
3.01950000E+4	-9.81796800E+1
3.03930000E+4	-1.00031200E+2
3.05910000E+4	-9.28593600E+1
3.07910000E+4	-9.79648400E+1

Table 2—Example 2 ASCII file

S21 port 3-to-14 edge term/decoupling			
Frequency	470pF Cap Only	470 pF & 220 ohm	470 pF & 2.2 ohm
1000000	-7.256636149	-7.370994738	-7.232016122
3248750	-16.60424905	-16.61567806	-16.62946108
5497500	-21.1613668	-20.9192679	-21.16261093
7746250	-24.0761064	-23.4504834	-24.06939862
9995000	-26.23606156	-25.26384536	-26.19843986

5.5.3 Web page documentation

The IEEE EMC-S TC-9 will maintain the process for updating relevant problems to the web page. An email address will reside at the TC-9 web page <http://www.ewh.ieee.org/soc/emcs/tc9/tc9comms.htm>.

Emailing a problem of interest to (P1597.2@ieee.org) alias will forward to the chair of the TC-9 who will direct the submission review process (detailed on the TC-9 web page).

5.5.4 U.S. Department of Defense (DoD) benchmark problems

5.5.4.1 Electromagnetic Code Consortium (EMCC)

The problems described in this section comprise a more extensive set of models that were developed to validate the EM scattering predictions of general purpose CEM codes. These problems cover the cases of relatively simple geometrical objects that are PEC and those that contain other materials including dielectric layers. These codes were developed under funding by the U.S. Department of Defense (DoD) High Performance Computing Modernization Program (HPCMPO) and the Common High Performance Computing Software Support Initiative (CHSSI). The selected problems include those associated with RCS, antenna radiation, and component/system EMC applications. These problems were originally defined and evaluated under a Code Assessment and Benchmark Validation Workshop conducted by the HPCMPO-sponsored Electromagnetic Code Consortium (EMCC). Code assessments and validations were done using both a series of CEM codes (some developed under HPCMPO/CHSSI and EMCC funding) and measurements performed by participating US Government laboratories (Naval Weapons Center, NASA, etc.).

The EMCC is chartered with the development of new CEM algorithms and codes that exploit high performance computing, code parallelization and other solution approaches to reduce computation time and to balance computer load resources for the analysis of complex geometries. The EMCC has catalogued important findings and lessons learned from participating joint government, commercial, and multi-university research initiative (MURI) research and development. This work was done on behalf of advancing the state-of-the-art in CEM modeling and simulation that leverages high performance computing technologies.

The references listed below focus on a subset of the canonical EMCC benchmarks that has been published in the open literature on flat plates and other geometries such as an ogive, almond, cone-sphere, and other cases (each of which are described in 5.5.4.2, 5.5.4.3, and 5.5.4.4). The detailed validation data are contained in these references, and are included herein by reference. In later code validation studies, simulation benchmarks were treated as "code agnostic" i.e., results were plotted and presented without mentioning specific codes, to preclude subjectivism regarding relative accuracy and conclusions on which code/technique outperformed another.

The EMCC has other benchmarks in addition to those highlighted below. An account is required to access the EMCC problem sets. It is the responsibility of the user of this document or the requestor to determine whether access to the EMCC data can be granted.

Some of these problems have distribution restrictions under the International Traffic and Arms Regulations (ITAR) or other DoD security classification restrictions on the compiled data. To obtain an account and to get the data associated with any of the published or unpublished benchmarks, go to their Web site <https://www.vdl.afrl.af.mil/emcc>.

References:

Woo, A. C., Wang, H. T. G., Schuh, M., and Sanders, M., "Benchmark Plate Radar Targets for the Validation of Computational Electromagnetics Programs," *IEEE Antennas and Propagation Magazine*, vol. 34, no. 6, pp. 52-56, December 1992. (See normative reference clause 2).

Woo, A. C., Wang, H. T. G., Schuh, M., and Sanders, M., "Benchmark Plate Radar Targets for the Validation of Computational Electromagnetics Programs," *IEEE Antennas and Propagation Magazine*, vol. 35, no. 1, pp. 84-89, February 1993. (See normative reference clause 2).

AFRL-DE-TR-2003-1092, "Vlasov Antenna Data for Electromagnetic Code Validation," Air Force Research Laboratory (AFRL) Directed Energy Directorate Final Report, Greenwood, A., and Hendricks, K., June 2003. (See normative reference clause 2).

5.5.4.2 Scattering from a plate

The EM scattering results of five plate targets are included by reference here for the following cases, and are illustrated in Figure 38:

— Plate 1: Wedge cylinder

— Plate 2: Wedge-plate cylinder

— Plate 3: Plate cylinder

— Plate 4: Business card

— Plate 5: Wedge cylinder gap

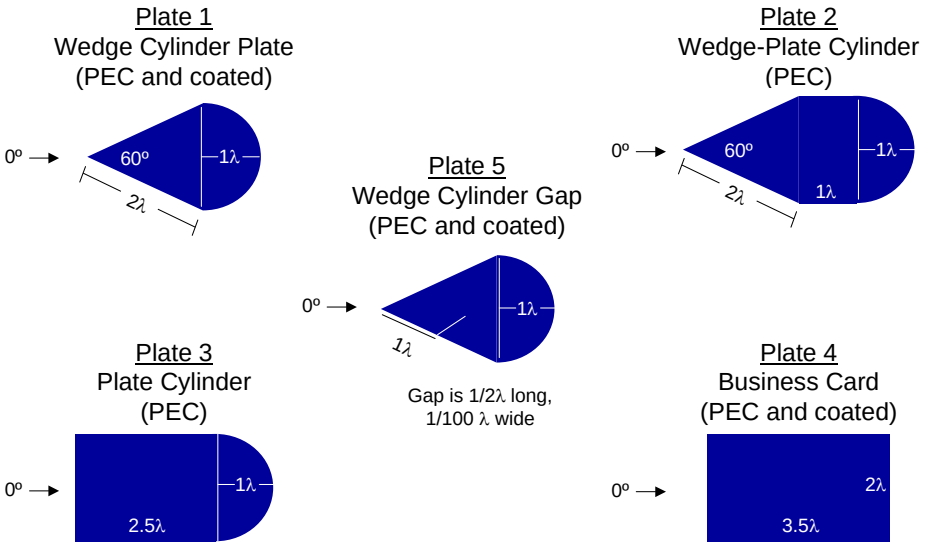

Figure 38—EMCC benchmarks for selected plate geometries

5.5.4.3 Scattering from an ogive and other complex objects

Measured and simulated data on five low cross-section targets are also available for the following:

— Almond

— Ogive

— Double Ogive

— Cone-sphere

— Cone-sphere gap.

These are illustrated in Figure 39.

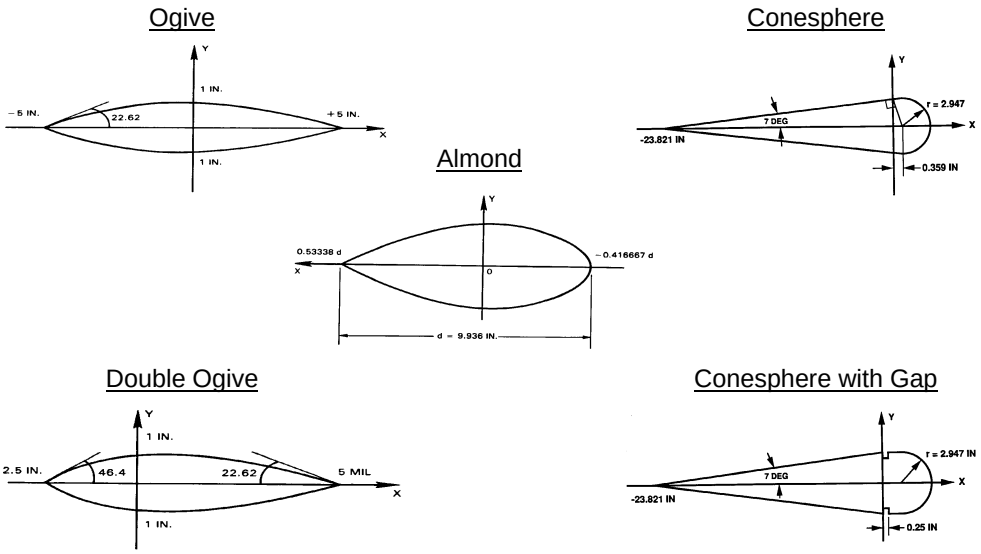

Drawings extracted from NWC TM 7002, Part 2

Figure 39—EMCC scattering benchmarks for an ogive and other complex objects.

5.5.4.4 Other scattering examples

Scattering results are available for the following other geometrical objects:

Dart

Four cavities:

— McDonnell Douglas square aperture
— NASA Ames square aperture
— NAWC square aperture
— NASA Ames cylindrical cavity.

Ice cream sandwich:

— Dielectric slab only
— Dielectric slab with one PEC side
— Dielectric slab with two PEC sides.

6. Self references for model validation

6.1 General

In IEEE P1597.1™/D4.3[23], it is stated that when a model cannot be compared to an external or independent reference, a self referenced model validation shall be performed. This method is less reliable than using an external reference, and requires a higher level of knowledge by the user.

A self referenced model is a secondary model created by changing small details of the primary model. Model validation is performed by running that secondary model and comparing the results to those of the primary. As the self referenced model is created using the same approach as the primary model, it is very easy to carry over errors, e.g. sharing false assumptions. Before validating a particular model it is strongly recommended that the user become familiar with the code or codes being used.

There are two kinds of changes that can be made to the primary model that can create valid secondary models: changes that should not substantially affect the solution, and changes that are expected to have a known effect. These are termed computational effects and geometry effects, respectively.

a) Computational effects can include:
    1) problem grid, segment, or cell size
    2) computational white space domain
    3) absorbing boundary conditions
    4) number of time steps or iterations employed
b) Geometry effects can include:
    1) size of apertures and wires
    2) number of apertures
    3) component placement on PCBs
    4) cavity dimensions

It must be recognized that changing specific details within a complex model is really only validating that particular aspect of the model and is not an all encompassing validation. The goal is to produce results for both the primary and secondary models that can be compared using the FSV procedures, if necessary, as detailed in Clause 7 of IEEE P1597.1™/D4.3. When self referencing is being considered, the best approach is to develop two additional series of models; one that varies computational parameters and a second set that varies the geometric parameters of the model.

6.2 Computational based self referenced models

The goal behind this computational based approach is to create self referenced models by making changes to the primary model's computational set up that should be transparent to the user and provide the same exact answer as the primary model. As the results should be identical, FSV will not be needed to verify the proper performance. It should be noted that each of these changes to the primary model only validates a specific portion of that model and so it is appropriate to use as many changes as possible. The more experienced user should be able to combine multiple changes into one or a few secondary validation models.

The following list describes possible computational parameters that can be varied to create a self referenced model. This list cannot be complete as there are many tools available, each with its own requirements and assumptions. In many cases, self checks are performed within the modeling tool itself and so it may not be necessary to duplicate these checks. For any given model, it is essential that the user determine which aspects of the computational set up need to be more carefully investigated in order to fully validate the primary model.

[23] See Clause 2 on normative references.

a) To validate how the model was digitized, it is necessary to create a model with finer or slightly coarser details. This may take longer to run, but would not be expected to change the results of the simulation to any significant degree.

b) To validate the white space required in a volumetric method, the computational volume can be adjusted. This may be done in one region or around the entire problem geometry, depending upon the nature of the model.

c) To validate the selected boundary conditions, and where the user has a choice, it is prudent to try more than one set of boundary conditions to ensure that the results remain the same. In this case it is essential to verify that there are not different white space requirements for the chosen boundary to function properly.

d) To validate the position of the monitor or solution points, it is recommended that a number of points be located around the intended region. If the points are sufficiently close it is expected that the results would be similar in value. This can help highlight an error where, for example, a field monitor point is placed in a PEC. For some codes these can be included in the primary model with little or no overhead and, when this is the case, it is considered good engineering practice to do so.

e) Validation of the source or sources used to energize a model can be achieved by placing suitable monitor points in the immediate vicinity of the source and using them to ensure that the behavior is as expected. It is often essential to include the source impedance in a model. To verify this has been done correctly, monitoring the current and voltage or the equivalent fields is recommended.

f) Animations may be used to monitor regions of a model for correct operation. Fundamental problems, such as building a model with plates made of dielectric or free space rather than a conductor, will be immediately apparent.

g) Connection checks are important with wire frame models. If the wires that comprise the geometry are not correctly connected, the current distributions will be incorrect. Observing that adjacent segments have very similar currents is one way to detect this error.

h) When looking at simulation results over a given frequency range, perform sanity checks by examining maxima or minima. Do they appear to be in the regions expected or are there gross errors? For example, are there resonances well below the frequency expected given the physical size of the model?

i) To validate whether a time domain code has been run for a sufficient duration, the number of time steps from which the solution is derived can be increased. If the solution has reached steady state, it will not be significantly changed by running for further time steps. For an iterative code, a larger number of iterations can be employed for the same purpose.

The basic goal is to make changes to the model, perhaps a number of them at once, that would not be expected to change the solution. If there is a change, then further work is indicated to find out which variable is the source of error.

6.3 Geometry based self referenced models

In the geometry based self reference approach, the goal is to create self referenced models by modifying the primary model geometry in such a way that the changes in the result can be simply predicted. This approach to validation is limited to the user's understanding of the problem and its expected behavior. Further, it must be noted that for complex models, such predictions may be difficult, and so it is strongly recommended that the user gains experience with less complex portions of the model to be validated, at least as a starting point.

When the dimensions of the primary model are changed, it would be expected that the solution obtained would vary in a predictable manner. For example, increasing the dimensions of a wire or slot will modify

the antenna characteristics accordingly. Similarly, a change in the size of a cavity will shift its resonant points. The following list describes possible model features that can be varied; it should not be considered to be complete. For any given model it is left to the user to determine which features should be examined in detail.

a) It is important to select key or dominant features such as wire or slot length, a cavity, or another major physical attribute that can be varied to perform the geometry validation. Ideally, the data from the primary model will show results that can be clearly identified, such as a fundamental resonance, as being caused by this dominant feature. By changing the geometry of the selected feature by a given amount in a secondary model, it should be expected that the results would reflect this change. Note—there may not be direct correlation due to loading and other effects within the model.

b) Imperfections are an important practical consideration in many computational EM models. Computers are excellent at perfection, and so orthogonal conductors do not interact. In reality there will be cross polarized source components and enclosure walls that are not at 90.00 degrees to one another. Slightly changing the angle of model components should not greatly affect the solution. Other perfect assumptions that must be tested to ensure they have no unintended effects include the symmetry of a model, which can hide certain modes, and the use of perfect material (loss free), which may result in excessively long simulation times and very high Q values.

c) Material variation is another parameter that can be changed in order to produce a known effect. Modifying the permittivity of a dielectric element should change propagation velocity in that region and change the frequencies of any associated resonances.

d) Putting additional output ports or monitor points into a model is a good means to determine proper behavior. For example if there is an intermediate point where a simple voltage or current can be measured it is prudent to do so, and the loading effect of the measurement equipment (50 ohm) should also be included to aid the measurement to model correlation.

e) Ideal sources are often available in CEM tools. It is important to realize that an ideal current source has infinite impedance. If a model exhibits a full-wave resonance and hence very high input impedance, an ideal current source will maintain the source current, which means there will be more energy injected into the model at that resonant frequency. To determine if the source used was appropriate, the source impedance should be changed. This can be most easily done by modifying the resistive component between low and high values. A possible alternative, if care is taken, is to add reactive components; however, in this case the expected results may not be as easy to predict in advance.

f) To determine the importance of coupling between different portions of a model, the spacing between elements may be changed. In this way it is possible to determine if the models are highly dependent upon the geometry; if so it is essential to ensure that the model accurately reflects the real problem spacing.

g) Sub-models are an important step in validating a complex problem. This is simply the process of building a number of small models that can be combined into the final model. A less complex model is more easily validated than a complex one, and if it is known that the parts are valid there can be greater confidence that the combined model is producing the results desired.

For complex models, making changes such as those listed above may well only impact portions of model behavior. Changing a slot length will change the resonances or behavior associated with those slots, but there may be different dominant effects from other parts of the model such as wire lengths or cavity dimensions. For this reason it may be appropriate to use the FSV technique for a comparison of the results.

7. Numerical calculation of the validation rating using the Feature Selective Validation technique

7.1 Implementing the Feature Selective Validation (FSV) technique

Whether the problems to be validated are generated from the previous sets or from data generated by the modeler for a specific problem, the level of agreement needs to be determined between those results and reference results (such as from measurements or other models). The Feature Selective Validation (FSV) method is the accepted technique for doing this. This section contains additional information to support the implementation of the FSV method and to provide assistance in the interpretation of the results produced by the method. No "standard code" is provided, users are free to generate their own using their preferred symbolic solver, high or low level language or to embed within a spreadsheet package as suits their purposes and requirements.

This clause should be read in conjunction with sub-clause 7.4 of IEEE P1597.1™/D4.3[24], from which this section quotes freely and annotates with examples and notes.

At the time of writing, a self contained package is available from the EMC-S TC-9 web site, <http://www.ewh.ieee.org/cmte/tc9/Problems/index.html>[25].

As the main purpose of the FSV will be to quantify changes and variations, small variations caused by differences in implementation should not prove problematic and users are encouraged to look at relative differences and the detailed information to provide intelligence about the comparisons that can then be used to provide a measure of acceptability or to answer whether any changes have been improved sufficiently

7.2 The procedure

7.2.1 Step 1 – Generation of the working data sets

This step sees the input data sets manipulated to create the working data sets. The working data sets contain the same number of data points and have coincident values of the common independent variable.

a) Compare the input data sets to establish the region of overlap within the common independent variable;

b) Identify those data points within each data set that exist within the region of overlap;

c) Identify the number of data points within each data set that exist within the region of overlap;

d) For the input data set with the smallest number of data points within the region of overlap, extract the data points within the region of overlap to form the first working data set;

e) Copy the values of the independent variable from the first working data set to the second working data set;

f) Use the remaining input data set (that with the highest number of data points within the region of overlap), apply linear interpolation within the region of overlap to generate the value of the independent variable at each coincident value of the second working data set;

   When both input data sets have the same number of data points within the region of overlap, either data set may be used in step d, above.

NOTE 1—Obviously, only the portions of the two graphs that overlap can be compared. When visually appraising results where one or other sets extends above or below the other, the temptation may be to extrapolate. This can lead to false comparisons if the system being assessed does not, itself, extrapolate. Hence, FSV is only concerned with the portions of the two graphs that do overlap.

[24] See Clause 2 for normative references.
[25] See Clause 2 for normative references.

NOTE 2—To allow the FSV method to work adequately, all the points in this overlap region need to be coincident. This means that resampling / interpolation may be required. The preferred method of doing this is to resample to the lowest data density of the two data sets being compared. This, effectively, allows down-sampling and reduces the potential to introduce errors. FSV is based on trying to mimic visual comparisons and it is worth asking the question here "has the resampling made the data look different to the original data". If it has, proceed with some caution but practice has shown that this manipulation produces no untoward effects with reasonable data point densities and data which is not excessively noisy (all of these are subjective terms but which are easily recognized with a little experience).

NOTE 3—The expectation is that the data points will be separated by an equal amount (Δx). If the intention is to compare data with logarithmic *x*-axes then the resultant x-axis data should be logarithmically spaced.

NOTE 4—The original data may be in a two column format (such as frequency and data). The x-axis data, such as frequency, can be retained at this stage but does not form part of the current FSV routine.

NOTE 5—The amplitude "*y*-axis" data can be in linear or logarithmic (e.g. dB) units. FSV compares the data without converting between these, i.e., it compares the data as it would appear on the printed page. The user should ensure that the data format is that required to be compared.

NOTE 6—The output from this step of the procedure is two files. Each file contains the data from the respective original data which covers the overlap region and which have the data points co-located.

NOTE 7—Thus, given the data of Figure 40, which has 201 points, a fast Fourier transform (FFT) approach is used requiring zero padding to 256 points. The data was coincident so no resampling or truncation of either data set was required.

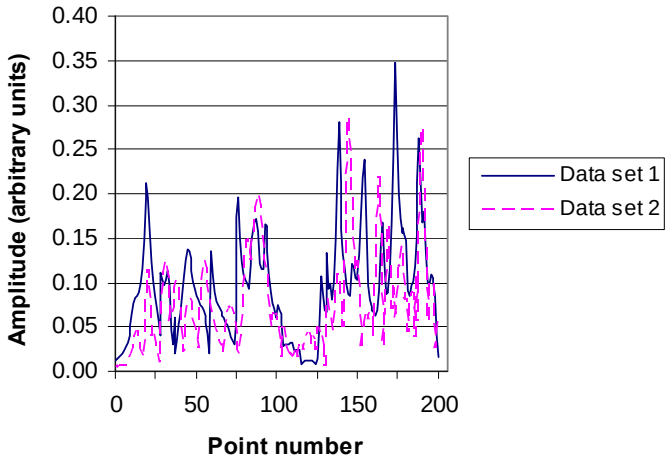

Figure 40—Original data for comparison (refer to Annex F)

7.2.2 Step 2 – Fourier transform both working data sets

Step 2 creates the transformed working data sets.

NOTE 1—Small but noticeable differences may result from using fast or discrete Fourier approaches. For ease of implementation, FFT approaches have been used in the majority of the published work to date.

NOTE 2—The output from this step of the procedure is two files, each containing the transformed data of the files output from stage 1. The transformed data is given in Figure 41.

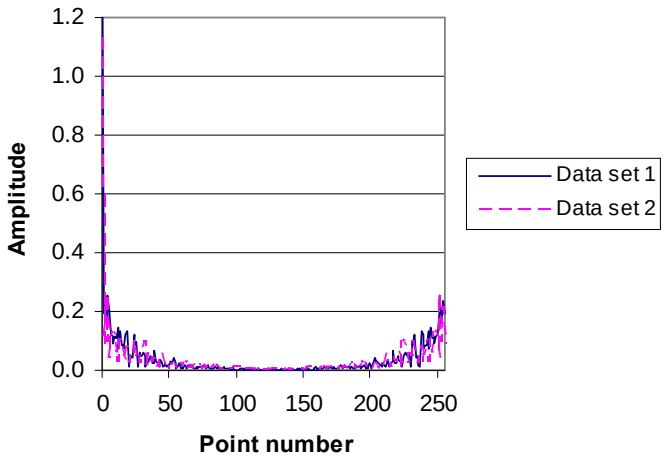

Figure 41 —Fourier transformed data

7.2.3 Step 3 – Apply a low pass filter

The following procedure is to be performed for both transformed working data sets:

a) Perform an inverse Fourier transform on the content of the first four data points within the transformed data set. The vectors returned shall be labeled as $DC_s(n)$, where the subscript, s, is either 1 or 2 and denotes the transformed working data set number.

b) Calculate the sum of the values, S, of the independent variable, starting at the fifth data point and continuing to the end of the data set. Thus:

$$S = \sum_{i=5}^{N} TWDS(i)$$

where

S is the sum of the values of the independent variable;

i is the data set element;

N is the total number of elements within the data set;

$TWDS(i)$ is the ith independent variable within the transformed data set.

c) Determine the "40 %" location. This is the ith data point, at which the sum of the values of the independent variable, starting at the fifth data point and continuing to the ith data point, is greater than or equal to 40 % of the value calculated during step (b). The value of i is systematically increased from the fifth data point until this condition is reached. Thus:

$$\sum_{i=5}^{i_{40\%}} TWDS(i) \geq 0.4S$$

where

S is the sum of the values of the independent variable;

i is the data set element;

$TWDS(i)$ is the ith independent variable within the transformed data set;

$i_{40\,\%}$ is the element containing the "40 %" location.

d) Determine the "break-point" location. This is five data points higher than the "40 %" location determined in step (c). Thus:

$$i_{40\%} = i_{40\%} + 5$$

where

$i_{40\,\%}$ is the element containing the 40 % location;
i_{bp} is the element number of the "break point."

e) Apply the filter displayed as Table 3 to the independent variable values contained within the indicated elements of the transformed working data set to generate the filtered transformed working data set.

Table 3—Filter definition – a

Element Number	Filter Value
I_{bp}-3	1.000
I_{bp}-2	0.834
I_{bp}-1	0.667
I_{bp}	0.500
I_{bp}+1	0.334
I_{bp}+2	0.167
I_{bp}+3	0.000

f) Perform an inverse Fourier transform on the filtered transformed working data set. The vectors returned shall be labeled as $\mathrm{Lo}_s(n)$, where s is either 1 or 2 and denotes the data set number.

NOTE 1—For the purpose of comparison, the data is considered in three regions:

– Region 1. "Low pass" or "DC" which includes the DC level/ offset data.

– Region 2. "Band pass" or "Lo" which includes the bulk of the data concerning the overall shape / envelope of the data set.

– Region 3. "High pass" or "Hi" which includes the bulk of the data concerning the individual (high Q / rapidly changing) features.

NOTE 2—It is important for the analysis that follows that as these "filter" regions are separated out and subsequently inverse transformed to get back to the domain of the data being compared, that they all contain the same number of data points (so if the data coming out of step 1 was two files, each of 250 points, then the DC, Lo, and Hi data that is used in the FSV mathematics each contains 250 points). The data can be reordered, or left in its current state; the following diagrams manipulate the transformed data without reordering. In all cases, references to points and percentages operate at both sides of the DC term.

NOTE 3—To separate these regions, the DC component is considered as that contained in the DC term and the first four data points either side of the DC term, irrespective of the total number of data points in the set. The "Lo" data is that region containing approximately 40 % of the area under the resulting curve.

NOTE 4—Step 3(a) returns two files that are the inverse transform of the first four points with the remaining data being set to zero (to ensure that the inverse transform has the same number of data points as the data being compared).

NOTE 5—To obtain this approximately 40 % knee point (called break point in the method), the total area under the curve is calculated for each data set, minus the first four points, and then the point where 40 % of the total is achieved is recorded for each data set. A small offset of five points is added to each "break point." The same "break point" is applied to both data sets. The "break point" chosen is the lowest of the two individual ones that have been calculated. So, for the example data of Figure 40, the 40 % point for data set 1 was at point 18, and for data set 2 was at point 24. Break point 1 would be 23 (18+5) and Breakpoint 2 would be 29 (24+5). The knee point of the filter for both data sets would thus be point 2.

NOTE 6—The high and low pass (transformed) data is obtained by applying a filter with a linear transition to the transformed data minus the first four points. This transition extends two points above and below the common break point.

NOTE 7—The output from this step is the inverse transformed DC data and the inverse transformed low data.

NOTE 8—The resulting DC data for comparison is given in Figure 42.

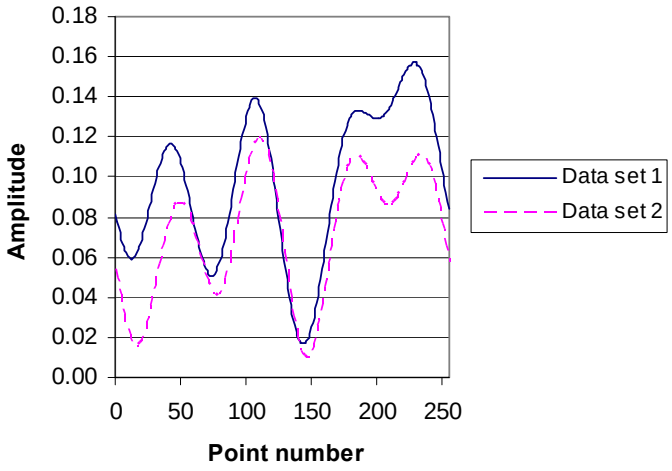

Figure 42—DC data for comparison

NOTE 9—The transformed Lo data is given in Figure 43

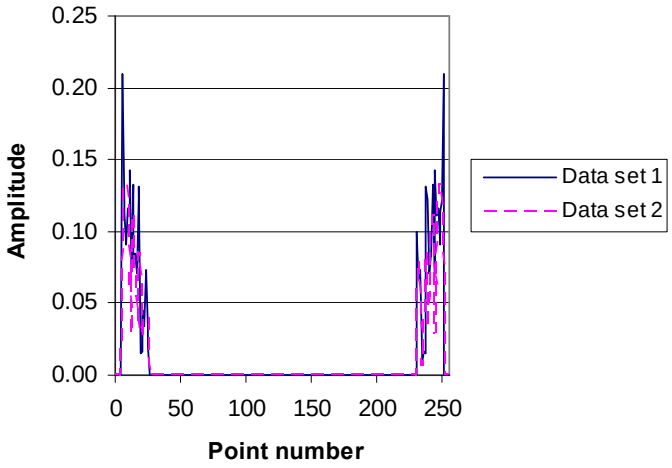

Figure 43—Transformed Lo data

NOTE 10— The Lo data inverse transformed into the original (data) domain is given in Figure 44.

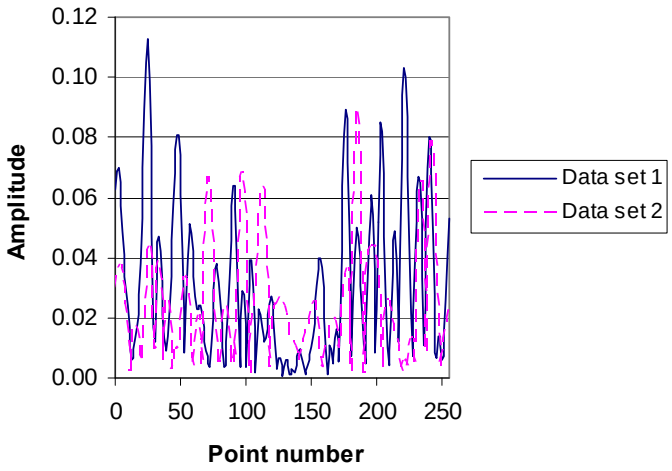

Figure 44—The Lo data to be used for comparison

7.2.4 Step 4 – Apply a high pass filter

The following procedure is to be performed for both transformed working data sets:

a) Apply the filter displayed as Table 4 to the independent variable values contained within the indicated elements of the transformed working data set to generate the filtered transformed working data set.

b) Perform an inverse Fourier transform on the filtered transformed working data set. The vectors returned shall be labeled as $Hi_s(n)$, where s is either 1 or 2 and denotes the data set number.

Table 4—Filter definition – b

Element Number	Filter Value
I_{bp}-3	0.000
I_{bp}-2	0.167
I_{bp}-1	0.334
I_{bp}	0.500
I_{bp}+1	0.667
I_{bp}+2	0.834
I_{bp}+3	1.000

NOTE 1—This continues the process of obtaining the data to be used for the comparison and applies a high pass filter, which overlaps with the low pass filter previously used.

NOTE 2—The output of this step is the Hi data to be used in the comparison.

NOTE 3—The transformed Hi data is given in Figure 45 and the Hi data for comparison is given in Figure 46.

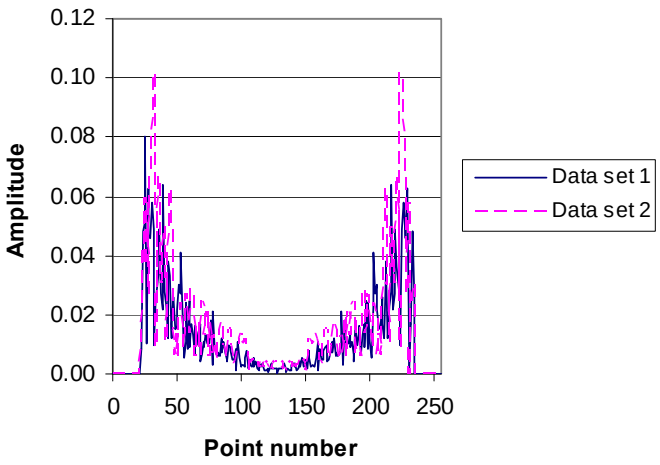

Figure 45—Transformed Hi data

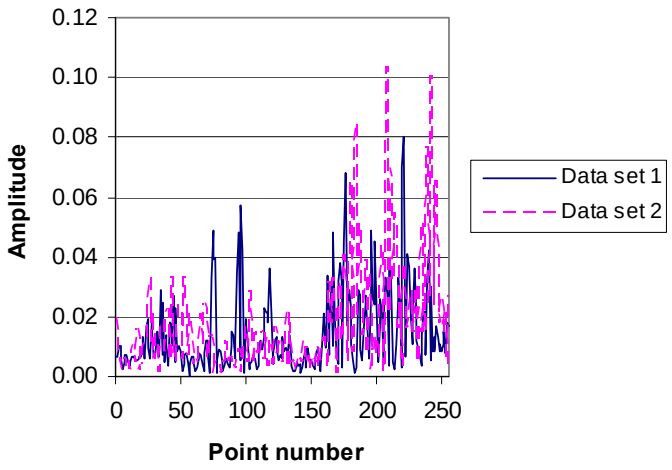

Figure 46—Hi data to be used for comparison

7.2.5 Step 5 – Calculate ADM

For each set of data points within the Working Data Sets, the Amplitude Difference Measure (ADM) is to be calculated using Equation (14).

$$ADM(n) = \left|\frac{\alpha}{\beta}\right| + \left|\frac{\chi}{\delta}\right| \exp\left\{\left|\frac{\chi}{\delta}\right|\right\} \tag{14}$$

where

$$\alpha = \left(\left|\mathrm{Lo}_1(n)\right| - \left|\mathrm{Lo}_2(n)\right|\right)$$

$$\beta = \frac{1}{N}\sum_{i=1}^{N}\left[\left(\left|\mathrm{Lo}_1(i)\right| + \left|\mathrm{Lo}_2(i)\right|\right)\right]$$

$$\chi = \left(\left|\mathrm{DC}_1(n)\right| - \left|\mathrm{DC}_2(n)\right|\right)$$

$$\delta = \frac{1}{N}\sum_{i=1}^{N}\left[\left(\left|\mathrm{DC}_1(i)\right| + \left|\mathrm{DC}_2(i)\right|\right)\right]$$

n is the nth data point

NOTE 1—Here, we are concerned with obtaining the ADM on a point-by-point basis so that it can be compared directly to the data coming from step 1.

NOTE 2—There are two parts to the ADM, one based on the trend and one based on the offset. The offset information has been included in this way so that small differences in the overall levels have little effect but large differences, even if the shape of the data being compared is the same, have a large effect on the ADM value.

NOTE 3—In Equation (14), the terms β and δ need only to be calculated once. They provide a normalizing function and help to ensure that the order of comparison does not influence the final results.

NOTE 4—The terms α and χ need to be calculated on a point-by-point basis.

NOTE 5—The output from this step is a data file / graph which can be compared with the original data to identify the locations of poor comparison: which can then be used to identify any remedial action or changes required to the model or to help identify underlying causes of poor comparison that can be used as part of a report on the validation.

NOTE 6—The point-by-point ADM is given in Figure 47. It clearly shows that there are substantial contributions to poor performance in the bottom third, but particularly in the top third of the data. This corresponds to differences in the lower–Q type structures in the original data.

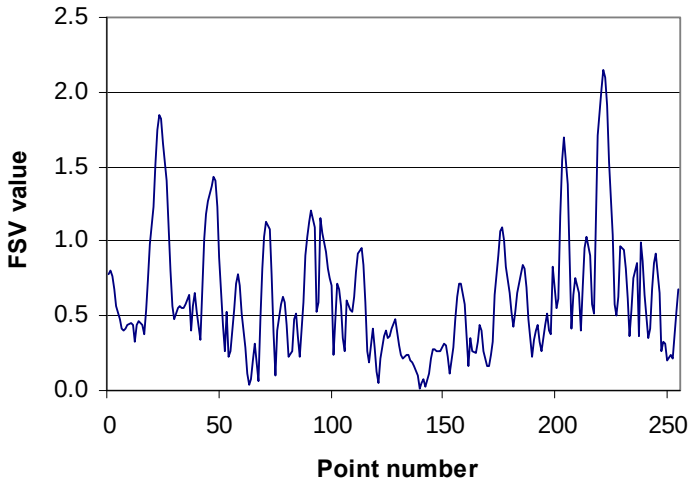

Figure 47—ADM shown on a point-by-point basis

7.2.6 Step 6 – Calculate the mean value of ADM

Calculate the mean value of ADM from Equation (15),

$$ADM = \frac{\sum_{n=1}^{N} ADM(n)}{N} \tag{15}$$

where the mean value of the ADM(n) gives a single-figure measure of "goodness-of-fit".

NOTE 1—The output from this stage is a single number. This can be used to compute the overall difference measure, to compare with other ADMs or to compare to the resulting Feature Difference Measure (FDM) to help in identifying causes of error and any required action.

NOTE 2—N is the number of points used in the analysis and ADM is simply a numerical mean value. For the above data, $N = 0.62$.

7.2.7 Step 7 – Calculate the ADM confidence histogram

Calculate the ADM confidence histogram. The range of values for the ADM and, in fact, the FDM and Global Difference Measure (GDM) can be divided into six categories, each with a natural language descriptor: Excellent, Very Good, Good, Fair, Poor, and Very Poor. These are the terms that are most often used in descriptions of the quality of comparisons. The confidence histogram, like a probability density function, provides some intelligence as to how much emphasis can be placed on the single figure of merit. There is some evidence to show that this mirrors the overall group assessment of any data pair by a number of engineers. The determination of the histogram is simply a case of counting the proportion of points that fall into one of the categories, according to the rule base in Table 5.

Table 5—FSV interpretation scale

FSV value (quantitative)	FSV interpretation (qualitative)
Less than 0.1	Excellent
Between 0.1 and 0.2	Very good
Between 0.2 and 0.4	Good
Between 0.4 and 0.8	Fair
Between 0.8 and 1.6	Poor
Greater than 1.6	Very poor

NOTE 1—The histogram is, effectively, a probability density function using binned data. It is most effectively obtained by taking each point in the ADM(n) individually and adding them to a "tally sheet" for each of the six categories in Table 5, and then divide by the total number of points used.

NOTE 2—It is common, where a data point lies at 0.1, 0.2 etc. to tally the point to the lower category (e.g., "Good" = $0.4 < \text{ADM} \leq 0.8$).

NOTE 3—The confidence histogram is given in Figure 48. It suggests that a large group of people assessing this data for overall trend agreement would broadly agree on the quality of comparison, with the majority agreeing that the comparison is fair, but with a notable proportion assessing the comparison as Good or Poor. Very few people would regard it as Excellent, Very Good, or Very Poor.

NOTE 4—The confidence histogram is used to calculate the Grade and Spread, discussed later.

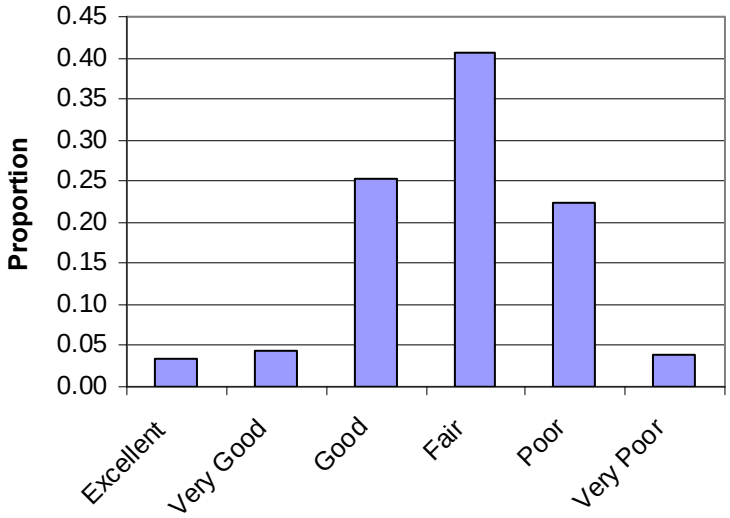

Figure 48—Confidence histogram for ADM

7.2.8 Step 8 – Calculate derivatives in preparation for the FDM calculation

Calculate derivatives in preparation for the FDM calculation. The following components need to be calculated:

a) The first derivatives of the Lo(*f*) and Hi(*f*) data sets

b) The second derivatives of the Hi(*f*) data sets.

The derivatives accentuate the high rate-of-change features in the original data, and differences based on the derivatives are combined in the determination of the FDM. The first derivatives are obtained using a central difference scheme as in Equation (16).

$$\mathrm{Lo}' = \mathrm{Lo}\left(f + N_d\right) - \mathrm{Lo}\left(f - N_d\right) \tag{16}$$

where $N_d = 2$ for the first derivative.

The second derivatives of the Hi data sets are obtained from the first derivatives using a similar approach again, found in Equation (17)

$$\mathrm{Hi}'' = \mathrm{Hi}'\left(f + N_d\right) - \mathrm{Hi}'\left(f - N_d\right) \tag{17}$$

where $N_d = 3$.

c) Equation (18) shows the derivative operators [from Equation (16) and Equation (17)] in terms of templates that "slide across" the original data to generate the first and second derivatives.

$$\begin{aligned} \mathrm{Hi}' &= \begin{bmatrix} 1 & 0 & 0 & 0 & -1 \end{bmatrix}^T \\ \mathrm{Hi}'' &= \begin{bmatrix} 1 & 0 & 0 & 0 & -1 & 0 & -1 & 0 & 0 & 0 & 1 \end{bmatrix}^T \end{aligned} \tag{18}$$

where superscript *T* stands for transpose.

NOTE 1—This straightforward approach using differences above and below the data point ignores any x-axis data because this data cancels in the calculations.

NOTE 2—To illustrate this, the Hi'' data is compared in Figure 49.

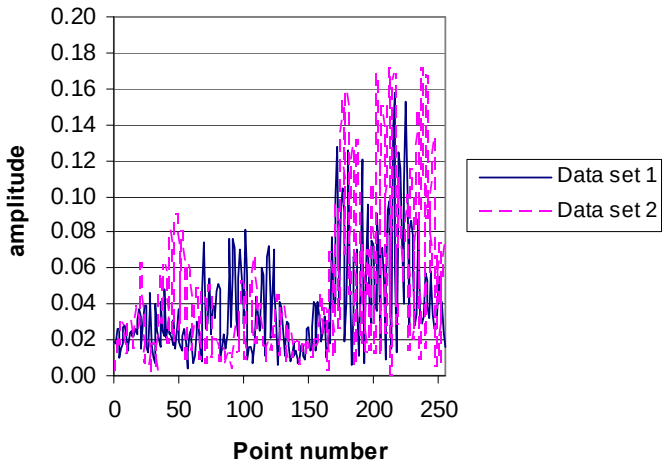

Figure 49—Second derivative of the Hi data

7.2.9 Step 9 – Calculate the point-by-point FDM

Calculate the point-by-point FDM. The FDM is formed from three parts based on the derivatives calculated in step 8. The numerical values in the equations are part of the heuristic and have been determined empirically. Note that because the following equations describe point-by-point values in the numerator, the denominator is based on a mean-value approach, similar to the determination of the ADM. It should be noted that the combination of Equation (19), Equation (20), and Equation (21) results in Equation (22) resolving to the difference between a function of Dataset 1 and a function of Dataset 2.

$$FDM_1(f) = \frac{\left|\mathrm{Lo}_1{}'(f)\right| - \left|\mathrm{Lo}_2{}'(f)\right|}{\frac{2}{N}\sum_{i=1}^{N}\left[\left(\left|\mathrm{Lo}_1{}'(i)\right| + \left|\mathrm{Lo}_2{}'(i)\right|\right)\right]} \tag{19}$$

$$FDM_2(f) = \frac{\left|\mathrm{Hi}_1{}'(f)\right| - \left|\mathrm{Hi}_2{}'(f)\right|}{\frac{6}{N}\sum_{i=1}^{N}\left[\left(\left|\mathrm{Hi}_1{}'(i)\right| + \left|\mathrm{Hi}_2{}'(i)\right|\right)\right]} \tag{20}$$

$$FDM_3(f) = \frac{\left|\mathrm{Hi}_1{}''(f)\right| - \left|\mathrm{Hi}_2{}''(f)\right|}{\frac{7.2}{N}\sum_{i=1}^{N}\left[\left(\left|\mathrm{Hi}_1{}''(i)\right| + \left|\mathrm{Hi}_2{}''(i)\right|\right)\right]} \tag{21}$$

$$FDM(f) = 2\left(\left|FDM_1(f) + FDM_2(f) + FDM_3(f)\right|\right) \quad (22)$$

NOTE 1—These components help to emphasize the feature differences.

NOTE 2—The weighting factors (2, 6, and 7.2) were chosen to balance the FDM against visual assessment.

NOTE 3—The FDM is shown in Figure 50. This reiterates that the main issue to be investigated with this data is in the upper third of the original data.

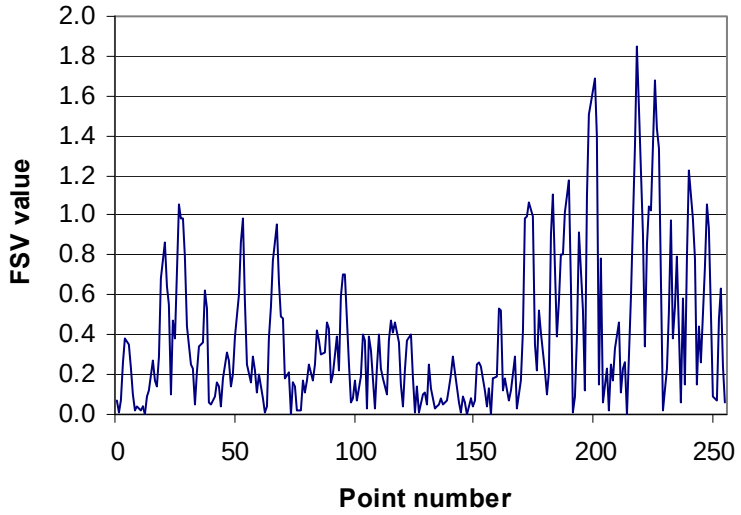

Figure 50—FDM shown on a point-by-point basis

7.2.10 Step 10 – Calculate the single value of FDM

Calculate the single value of FDM. This is done in exactly the same way as for the ADM.

NOTE—The FDM value is 0.39. The implication is that the Features (FDM) make a more substantial contribution to a poor comparison than the Amplitude / Trend information (ADM). As a result, the ADM and FDM would initially point a user to the differences in the upper third of the trace and improvement in the comparison would probably concentrate on the reasons for differences here.

7.2.11 Step 11 – Calculate the FDM confidence histogram

Calculate the FDM confidence histogram. This is done in exactly the same way as was done for the ADM.

NOTE—The histogram is given in Figure 51. Comparing it with the ADM confidence histogram, it suggests that if a group of professionals were looking at the "feature" information in the original data, they would be very split as to the overall conclusion.

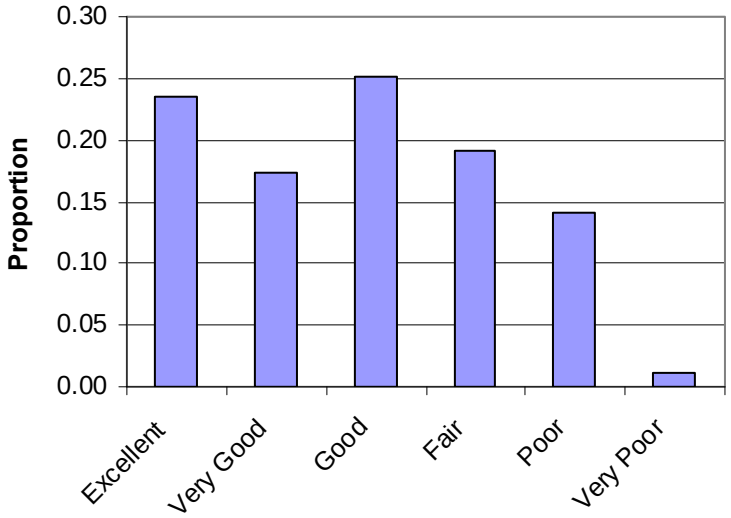

Figure 51—Confidence histogram for the FDM data

7.2.12 Step 12 – Obtain the point-by-point GDM value

Obtain the point-by-point GDM value. The GDM is premised on the ADM and FDM being largely independent, which means that:

$$GDM(f) = \sqrt{ADM(f)^2 + FDM(f)^2} \tag{23}$$

NOTE—The GDM is illustrated in Figure 52. The way the regions that were in poor comparison in both the ADM and FDM have combined can be clearly seen.

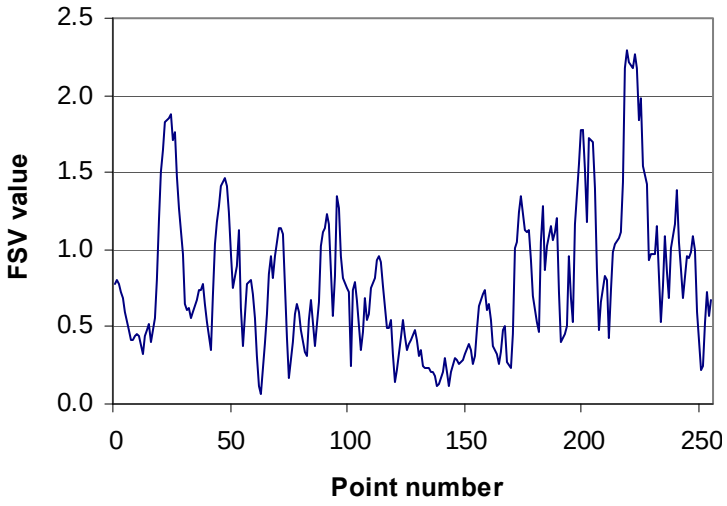

Figure 52—GDM represented on a point-by-point basis

7.2.13 Step 13 – Calculate the overall GDM value and the GDM confidence histogram

Calculate the overall GDM value and the GDM confidence histogram. This follows the same procedure as the ADM and FDM.

NOTE 1—The GDM confidence provides a simple way to assess how the overall comparison would be perceived.

NOTE 2—The overall GDM is 0.80.

NOTE 3—The GDM confidence histogram is shown in Figure 53 and suggests that the overall assessment, taking into account the amplitude and feature information would be more generally accepted as being "Fair."

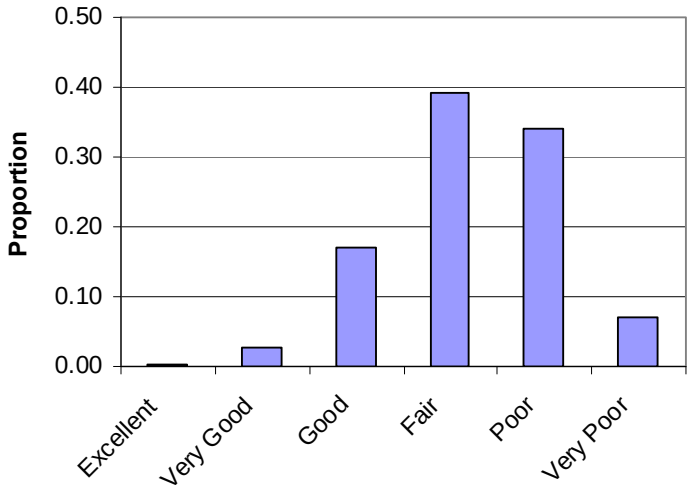

Figure 53—Confidence histogram for the GDM data

7.2.14 Step 14 – Determine the equivalent visual scale values for ADM, FDM, and GDM

Determine the equivalent visual scale values for ADM, FDM, and GDM. As discussed previously, the FSV values can be categorized into a six point, natural language scale. The FSV natural language scale is presented in Table 5. The conversion between the numerical value and natural language descriptor is done using a piecewise conversion. The piecewise approach for this is given in Table 6, where X is the ADM, FDM, or GDM (total or point-by-point), and V is the transformed (visual) scale equivalent.

Table 6—Piecewise visual conversion

If $X \leq 0.1$, then $V = 1 + 10X$
If $X > 0.1$ and $X \leq 0.2$, then $V = 2 + 10\ (X - 0.099)$
If $X > 0.2$ and $X \leq 0.4$, then $V = 3 + 5\ (X - 0.199)$
If $X > 0.4$ and $X \leq 0.8$, then $V = 4 + 2.5\ (X - 0.399)$
If $X > 0.8$ and $X \leq 1.6$, then $V = 5 + 1.25\ (X - 0.799)$
If $X > 1.6$, then $V = 6$

NOTE 1—The purpose of doing this is to allow a direct comparison with visual assessment, if this is done. Thus, if a number of individuals rate a comparison, a mean value can be obtained form this group and compared to a mean value from the analysis.

NOTE 2—A piecewise approach has been used to ensure continuity at the category boundaries and allow a finer level of granularity than is available only with the category descriptors.

NOTE 3—The visual equivalent for this data is 5.0. This is on the boundary of the "Fair" and "Poor" categories.

7.3 Grade and Spread

Another technique that has proved useful in presenting and interpreting FSV data, particularly the confidence histograms, is a "Grade and Spread" diagram. The Spread serves a similar purpose to variance or standard deviation in statistical methods and is a measure of the spread of a distribution. It is measured as the number of categories above and/or below the highest value category that contains a given percentage of the spread – the default value is 85 % but this can be reduced or increased to suit a particular application. The Grade is a measure of quality of the results and serves a similar purpose to skew measurements in statistics. It is found by counting the number of categories, starting with "Excellent" and working towards "Very Poor," required to contain a given percentage of the results – again, the default value is 85 % but this can be reduced or increased depending on the application. Hence, although not mathematically related, the single values of the ADM, FDM or GDM, the Grade and Spread, can be thought of as analogues of the first, second, and third moments of statistics.

To help in the visual presentation of the data, color coding has been used. The categories for the Grade and Spread are as indicated in Table 7. The Grade and Spread chart is particularly useful if a weighting of one of the components (ADM or FDM) is required. An automated weighting approach is shown below based on the Spread. It is based on the concept that a narrower Spread implies a higher confidence in the results and a wider Spread a lower confidence.

Table 7—Grade and Spread classifications

Classification	Grade	Spread
Blue	1 – 2	1 – 2
White	3 – 4	3
Yellow	5	4
Red	6	5 – 6

Typically, results may appear as in Figure 54. Here the ADM and FDM are identical (yellow) which suggests that they should both be given equal weighting. Subsequently, if this was part of a validation process, movement from Yellow to White or Blue would suggest that there has been an overall improvement in the performance.

An alternative Grade and Spread chart is given in Figure 55. This figure suggests that more emphasis could be given to the ADM. In a practical sense, this may mean that the FDM could be overtly de-rated when calculating the overall comparison or when considering actions to be taken to improve the model.

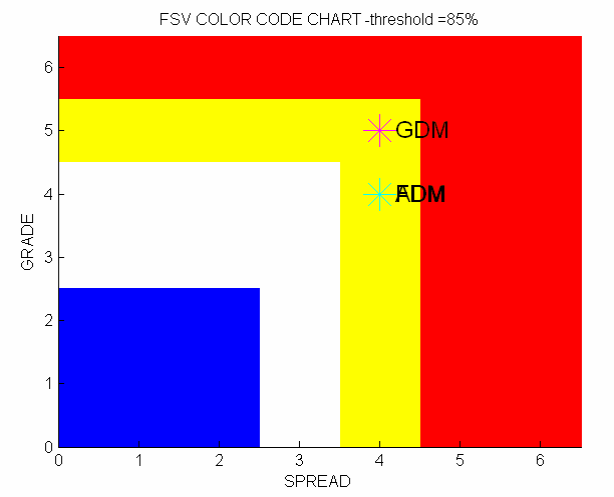

Figure 54—A possible Grade and Spread diagram

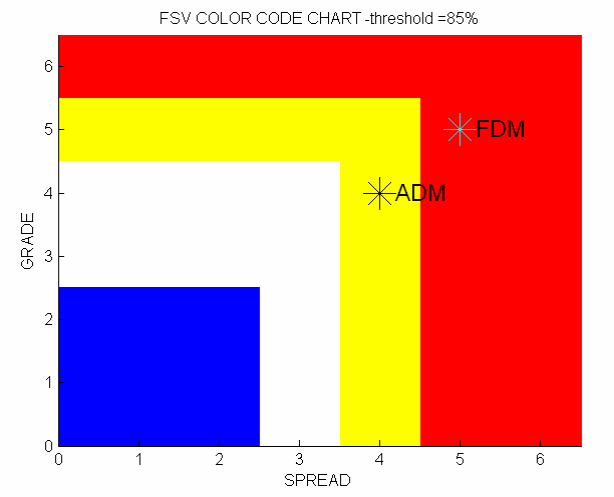

Figure 55—Another Grade and Spread chart

It was noted that the Grade and Spread approach could be used to address is the automatic weighting of the ADM and FDM when calculating the GDM. The current, default, approach is given in Equation (24).

$$GDM = \sqrt{ADM^2 + FDM^2} \tag{24}$$

However, considering that the Spread gives a measure of how much confidence can be placed in each of the components, it would seem appropriate to de-emphasize either the ADM or FDM if it has a much greater Spread than the other. If automatic weighting is to be done, it should be done in the manner of the following and built into the FSV method as listed previously between steps 11 and 12. It presumes that the Spread for the ADM and FDM have been previously determined.

If $\{\text{Spread}_{\text{ADM}} < \text{Spread}_{\text{FDM}}\}$

Then

$$K_{ADM} = 1$$

$$K_{FDM} = Spread_{ADM} / Spread_{FDM}$$

Else if $\{Spread_{ADM} > Spread_{FDM}\}$

Then

$$K_{ADM} = Spread_{FDM} / Spread_{ADM}$$

$$K_{FDM} = 1$$

Else

$$K_{ADM} = 1$$

$$K_{FDM} = 1$$

End if

$$GDM = \sqrt{(K_{ADM} \cdot ADM)^2 + (K_{FDM} \cdot FDM)^2} \quad (25)$$

Annex A

(informative)

Bibliography

[B1] ANSI C63.5-2006, American National Standard for Electromagnetic Compatibility – Radiated Emission Measurements in Electromagnetic Interference (EMI) Control – Calibration of Antennas (9 kHz to 40 GHz).

[B2] Antonini, G., Ciccomancini Scogna, A., Orlandi, A., Ritotta, C., and Duffy, A., "Application of FSV to EMC and SI Data," *IEEE International Symposium on EMC*, Chicago, IL, Aug. 2005.

[B3] Archambeault, B., "Concerns and approaches for accurate EMC simulation validation," *IEEE International Symposium on Electromagnetic Compatibility*, vol. 1, pp. 329–334, Aug. 2003.

[B4] Archambeault, B., and Brench, C., "Proposed standard EMI modeling problems," *IEEE International Symposium on Electromagnetic Compatibility*, pp. 173–176, Aug. 1994.

[B5] Archambeault, B., Brench, C., and Ramahi, O. M., *EMI/EMC Computational Modeling Handbook*, 2d ed. Boston, MA: Kluwer Academic Publishers, 2001.

[B6] Archambeault, B., Connor, S., and Duffy, A. P., "Comparing FSV and human responses to data comparisons," *IEEE International Symposium on Electromagnetic Compatibility*, Chicago, IL, Aug. 2005.

[B7] Archambeault, B., Pratapneni, S., Zhang, L., and Wittwer, D. C., "Comparison of various numerical modeling tools against a standard problem concerning heat sink emissions," *IEEE International Symposium on Electromagnetic Compatibility*, vol. 2, pp. 1341–1346, Aug. 2001.

[B8] Archambeault, B., and Ruehli, A., "Review of 1998 TC-9 challenging problems results and 1999 TC-9 challenging problems introduction," *IEEE International Symposium on Electromagnetic Compatibility*, vol. 2, pp. 667–672, Aug. 1999.

[B9] Balanis, C., *Advanced Engineering Electromagnetics*, John Wiley & Sons, 1989.

[B10] Balzano, Q., Garay, O., and Manning, T., "Electromagnetic energy exposure of the users of portable cellular telephones," *IEEE Transactions on Vehicular Technology*, vol. 44, no. 3, pp. 390-403, Aug. 1995.

[B11] Barton, D. K., *Modern Radar System Analysis*, Norwood, MA: Artech House, 1988.

[B12] Beard, B.B, and Kainz, W., "Review and standardization of cell phone exposure calculations using the SAM phantom and anatomically correct head models," Biomedical Engineering Online, vol. 3, no. 34, 2004,.
(http://www.biomedical-engineering-online.com/content/3/1/34)
(http://www.biomedical-engineering-online.com/content/pdf/1475-925X-3-34.pdf)

[B13] Beard, B.B, and Kainz, W., Onishi, T., Iyama, T., Watanabe, S., Fujiwara, O., Wang, J., Bit-Babik, G., Faraone, A., Wiart, J., Christ, A., Kuster, N., Lee, A.-K. Kroeze, H., Siegbahn, M., Keshvari, J., Abrishamkar, H., Simon, W., Manteuffel, D., and Nikoloski, N., "Comparisons of computed mobile phone induced sar in the sam phantom to that in anatomically correct models of the human head," *IEEE Transactions on Electromagnetic Compatibility*, vol. 48, no. 2, pp. 397-407, May 2006.

[B14] Berenger, J.-P., "Three-Dimensional Perfectly Matched Layer for the Absorption of Electromagnetic Waves," *Journal of Computational Physics*, vol. 127, pp. 363–379, 1996.

[B15] Bickford, William B., *A First Course in the Finite Element Method*, 2d ed. Irwin Publisher, 1994.

[B16] Blake, L. V., *Radar Range-Performance Analysis*, Norwood, MA: Artech House, 1986.

[B17] Blake, M. W., Kerr, P. A., Thorp, S. A., and Chou, J. J., "NASA Geometry Data Exchange Specification for Computational Fluid Dynamics (NASA IGES)," National Aeronautics and Space Administration Ames Research Center, Moffett Field, CA, NASA Reference Publication 1338, 1994.

[B18] Booton, Jr., Richard C., *Computational Methods for Electromagnetics and Microwaves*, New York: John Wiley & Sons, Inc., 1992.

[B19] Borovikovoch, V. A., and Kinber, B. Ye., *Geometrical Theory of Diffraction*, UK: IEE, 1994.

[B20] Brauer, John R., and Dekker, Marcel, ed., *What Every Engineer Should Know About Finite Element Analysis*, Dekker Publisher, 1993.

[B21] Capri, A. Z., and Panat, P. V., *Introduction to Electrodynamics*, Boca Raton, FL: CRC Press, 2002.

[B22] CGNS Project Group, CFD General Notation System (CGNS)*, The CFD General Notation System Overview and Entry-Level Document,* 15 May 1998.

[B23] Chavannes, N., Tay, R., Nikoloski, N., and Kuster, N., "Suitability of FDTD-based TCAD tools for RF design of mobile phones," *IEEE Antennas and Propagation Magazine*, vol. 45, no. 6, pp. 52-66, Dec. 2003.

[B24] Chew, W. C., Jin, J. M., Michielssen, E., and Song, J. M., (editors), *Fast and Efficient Algorithms in Computational Electromagnetics*, Boston, MA: Artech House, 2001.

[B25] Chew, W. C., *Waves and Fields in Inhomogeneous Media*, IEEE Press, 1999.

[B26] Chou, C. K., Bassen, H., Osepchuk, J., Balzano, Q., Petersen, R., Meltz, M., Cleveland, R., Lin, J. C., and Heynick, L., "Radio frequency electromagnetic exposure: Tutorial review on experimental dosimetry," *Bioelectromagnetics*, vol. 17, pp. 195-206, 1996.

[B27] Christ. A., *Analysis and Improvement of the Numerical Properties of the FDTD Algorithm*, PhD Thesis, Diss. ETH Nr. 15057, Zurich, 2003.

[B28] Christ, A., "Requirements for reliable worst-case assessment of human exposure to RF electromagnetic fields with known uncertainty," *Health Physics*, vol. 92, no. 6, pp. 554-564, June 2007.

[B29] Christ, A., Chavannes, N., Nikoloski, N., Gerber, H. U., Poković, K., and Kuster, N., "A numerical and experimental comparison of human head phantoms for compliance testing of mobile telephone equipment," *Bioelectromagnetics*, vol. 26, no. 2, pp. 125-137, Feb. 2005.

[B30] Christ, A., and Kuster, N., "Flat phantom setup for the performance check and system validation of measurement systems according to IEEE 1528 and IEC 62209," Technical Report, Foundation for Research on Information Technologies in Society, IT'IS, Zurich, Switzerland, May 2002.

[B31] Christopoulos, Christos, *The Transmission-Line Modeling Method: TLM*, IEEE Press and Oxford University Press, 1995.

[B32] Coleby, D., and Duffy, A., "Development of visual rating scale to aid validations," *IEE Seminar on Validation of CEM*, Farnborough, UK, pp. 75-79, March 2004.

[B33] Coleby, D. E., and Duffy, A. P., "A Visual Interpretation Rating Scale for Validation of Numerical Models," *COMPEL: International Journal for Computation and Mathematics in Electrical and Electronic Engineering*, vol. 24, no. 4, pp. 1078–1092, April 2005.

[B34] Coleby, D. E., "Assessment of Techniques for Electromagnetic Modelling Validation," PhD Thesis, De Montfort University, UK, 2004.

[B35] Crispin, J. W., and Siegel, K. M., *Methods of Radar Cross Section Analysis*, New York: Academic Press, 1968.

[B36] Dimbylow, P. J., "Fine resolution calculations of SAR in the human body for frequencies up to 3 GHz," *Physics in Medicine and Biology*, vol. 47, pp. 2835-2846, 2002.

[B37] Duffy, A. P., Martin, A. J. M., Orlandi, A., Antonini, G., Benson, T. M., and Woolfson, M. S., "Feature Selective Validation (FSV) for validation of computational electromagnetics (CEM). Part I – The FSV method," *IEEE Transactions on EMC*, vol. 48, no. 3, pp. 449–459, Aug. 2006.

[B38] Duffy, A. P., and Orlandi, A., "The influence of data density on the consistency of performance of the Feature Selective Validation (FSV) Technique," *Applied Computational Electromagnetics Society Journal*, vol. 21(2), pp. 164–172, July 2006.

[B39] Duffy, A. P., Orlandi, A., and Antonini, G., "Testing the robustness of the feature selective validation (FSV) method for EMC/SI applications," *EMC Europe 2006*, Barcelona, Spain, Sept. 2006.

[B40] Duffy, A. P., Martin, A., Antonini, G., Ciccomancini Scogna, A., and Orlandi, A., "Issues in validation of complex-valued simulations for signal integrity analysis," *IEEE International Symposium on EMC*, Santa Clara, CA, Aug. 2004.

[B41] Duffy, A. P., Drozd, A., Archambeault, B., and Coleby, D., "Measuring similarity for validation of computational electromagnetic modeling," *IEEE International Symposium on EMC*, Santa Clara, CA, Aug. 2004.

[B42] Durbano, J. P., Ortiz, F. E., Humphrey, J. R., Prather, D. W., and Mirotznik, M. S., "Hardware implementation of a three-dimensional Finite-Difference Time-Domain algorithm," *IEEE Antennas and Wireless Propagation Letters*, vol. 2, pp. 54-57, 2003.

[B43] Durney, C., Massoudi, H., and Iskander, M. F., *Radio Frequency Radiation Dosimetry Handbook*, Fourth Edition, USAFSAM-TR-85-73, Oct 1986.[26]

[B44] Edwards, T.C., *Foundations for Microstrip Engineering*, New York: John Wiley, 1981.

[B45] Electromagnetic Code Consortium (EMCC) Web Site: <https://www.vdl.afrl.af.mil/emcc>.

[26] Available at various Internet websites including: (http://www.emfdosimetry.org/handbook4.htm), (http://niremf.ifac.cnr.it/docs/HANDBOOK/home.htm).

[B46] EUREKA SARSYS Project, "Development of Procedures for the Assessment of Exposure to Electromagnetic Near-Fields from Telecommunications Equipment," Final Technical Report, 2001, (<http://www.sarsys.org/downloads.html>),.

[B47] Faraone, A., Balzano, Q., and Simunic, D., "Experimental dosimetry in a sphere of simulated brain tissue near a half-wave dipole antenna," *IEEE International Symposium on Electromagnetic Compatibility*, pp. 906-911, 1998.

[B48] Futter, P., Chavannes, N., Tay, R., Meili, M., Klingenböck, A., Pokovic, K., and Kuster, N., "Reliable prediction of mobile phone performance for realistic in-use conditions using the FDTD method," *IEEE Antennas and Propagation Magazine*, vol. 50, no. 1, pp. 87-96, Feb. 2008.

[B49] George, P. L., *Automatic Mesh Generation: Application to Finite Element Methods*, John Wiley & Sons, 1991.

[B50] Hafner, Christian, *The Generalized Multipole Technique for Computational Electromagnetics*, Artech House, 1990.

[B51] Hafner, C., *Post-modern Electromagnetics: using Intelligent Maxwell Solvers*, John Wiley & Sons, 1999.

[B52] Hartemann, Fredric V., *High-Field Electrodynamics*, Boca Raton, FL: CRC Press, 2002.

[B53] Harrington, Roger F., *Field Computation by Moment Methods*, Krieger Publishing Company, 1982.

[B54] Harrington, Roger F., *Time-Harmonic Electromagnetic Fields*, 2d ed. New York: Wiley-IEEE Press, 2001.

[B55] Hastriter, M. L., and Chew, W. C., "Role of Numerical Noise In Ultra Large-Scale Computing," *IEEE Antennas and Propagation Society International Symposium*, vol. 3, p. 3373-3376, Monterey, CA, June 2004.

[B56] Humphries, Jr., Stanley, *Field Solutions on Computers*, Boca Raton, FL: CRC Press, 1998.

[B57] Itoh, T., Pelosi, G., and Silvester, P. P., *Finite Element Software for Microwave Engineering*, New York: John Wiley & Sons, 1996.

[B58] IEEE EMC-S TC9 Subcommittee Web site:
<http://www.ewh.ieee.org/soc/emcs/tc9/tc9comms.htm>.

[B59] IEEE Std 1528-2003, IEEE Recommended Practice for Determining the Peak Spatial-Average Specific Absorption Rate (SAR) in the Human Head from Wireless Communications Devices: Measurement Techniques.

[B60] IEEE Std 1528a-2005, IEEE Recommended Practice for Determining the Peak Spatial-Average Specific Absorption Rate (SAR) in the Human Head from Wireless Communications Devices: Measurement Techniques, Amendment 1: CAD File for Human Head Model (SAM Phantom).

[B61] IEEE Std C95.1™-1999, IEEE Standard for Safety Levels with Respect to Human Exposure to Radio Frequency Electromagnetic Fields, 3 kHz to 300 GHz.

[B62] IEEE Std C95.3™-2002, IEEE Recommended Practice for Measurements and Computations of Radio Frequency Electromagnetic Fields With Respect to Human Exposure to Such Fields, 100 kHz–300 GHz.

[B63] IEEE P1528.1, Recommended Practice for Determining the Peak Spatial Average Specific Absorption Rate (SAR) in the Human Body from Wireless Communications Devices, 30 MHz - 6 GHz: General Requirements for using the Finite Difference Time Domain (FDTD) Method for SAR Calculations, IEEE PAR Sep. 2005.

[B64] IEEE P1528.2, Recommended Practice for Determining the Peak Spatial Average Specific Absorption Rate (SAR) in the Human Body from Wireless Communications Devices, 30 MHz - 6 GHz: Specific Requirements for Finite Difference Time Domain (FDTD) Modeling of Vehicle Mounted Antennas Configurations, IEEE PAR Sep. 2005.

[B65] IEEE P1528.3, Recommended Practice for Determining the Peak Spatial-Average Specific Absorption Rate (SAR) in the Human Body from Wireless Communications Devices, 30 MHz - 6 GHz: Specific Requirements for Finite Difference Time Domain (FDTD) Modeling of Mobile Phones/Personal Wireless Devices, IEEE PAR Mar. 2006.

[B66] IEEE P1528.4, Recommended Practice for Determining the Peak Spatial Average Specific Absorption Rate (SAR) in the Human Body from Wireless Communications Devices, 30 MHz - 6 GHz: Requirements for Using the Finite Element Method for SAR Calculations, specifically involving Vehicle Mounted Antennas and Personal Wireless Devices, IEEE PAR May 2008.

[B67] International Commission on Non-Ionizing Radiation Protection (ICNIRP), "Guidelines for limiting exposure to time-varying electric, magnetic, and electromagnetic fields (up to 300 GHz)," *Health Physics*, vol. 74, no. 4, pp. 494-522, Apr. 1998.

[B68] IPC-2251; "Design Guide for the Packaging of High Speed Electronic Circuits," Association Connecting Electronics Industries, Nov. 2003.

[B69] Jiang, Bo Nan, *The Least-Squares Finite Element Method: Theorems and Applications in Computational Fluid Dynamics and Electromagnetics*, Springer Verlag GmbH, 1998.

[B70] Jin, Jianming, *Electromagnetic Analysis and Design in Magnetic Resonance Imaging*, Boca Raton, FL: CRC Press, 1998.

[B71] Jin, Jianming, *The Finite Element Method in Electromagnetics*, John Wiley & Sons, Inc., 1993.

[B72] Kerr, D. E., et al., *Propagation of Short Radio Waves,* rev. ed. London: P. Peregrinus, 1987.

[B73] Kirkup, S. M., *BEMLAP—The Boundary Element Method for Laplace Problems: Manual and Fortran Codes*, Science-Books.net, April 2000.

[B74] Knott, E. F., Shaeffer, J. F., and Tuley, M. T., *Radar Cross Section*, 2d ed., SciTech Publishing, 2004.

[B75] Kodali, V. Prasad, *Engineering Electromagnetic Compatibility: Principles, Measurements, Technologies, and Computer Models*, 2d ed. New York: IEEE Press, 2001.

[B76] Kraus, John D., and Marhefka, Ronald J., *Antennas For All Applications*, 3d ed., McGraw-Hill, 2001.

[B77] Kunz, K. S., and Luebbers, R. J., *The Finite Difference Time Domain Method for Electromagnetics*, Boca Raton, FL: CRC Press, 1993.

[B78] Kuster, N., and Balzano, Q., "Energy absorption mechanism by biological bodies in the near field of dipole antennas above 300 MHz," *IEEE Transactions on Vehicular Technology*, vol. 41, no. 1, pp. 17-23, Feb. 1992.

[B79] Magnusson, Philip C., et. al., *Transmission Lines and Wave Propagation*, Boca Raton, FL: CRC Press, 2001.

[B80] Martin, A., "Feature Selective Validation." Ph.D. Thesis, De Montfort University, Leicester, U. K., 1999.

[B81] Martin, A. J. M., and Duffy, A. P., "A compensation technique to aid the comparison of experimental and modeled data," *IEEE International EMC Symposium*, Minneapolis, MN, Aug. 2002.

[B82] McNamara, D. A., *Introduction to the Uniform Geometrical Theory of Diffraction*, Artech House, 1990.

[B83] Mie, G., "A Contribution to the Optics of Turbid Media, Especially Colloidal Metallic Suspensions," *Annals of Physics*, vol. 25(4), pp. 377–445, 1908.

[B84] Miller, E. K., Medgyesi-Mitschang, L., and Newman, E. H., ed., *Computational Electromagnetics*, IEEE Press, 1992.

[B85] Mittra, R., ed., *Computer Techniques for Electromagnetics*, rev. ed. Hemisphere Publishing Corporation, 1987.

[B86] Morita, N., Kumagai, N., and Mautz, J.R., *Integral Equation Methods for Electromagnetics*, Artech House, 1990.

[B87] Mur, G., "Absorbing Boundary Conditions for the Finite-Difference Approximation of the Time-Domain Electromagnetic-Field Equations," *IEEE Transactions on Electromagnetic Compatibility*, vol. 23, pp. 377–382, 1981.

[B88] Nagaoka, T., Watanabe, S., Sakurai, K., Kunieda, E., Watanabe, S., Taki, M., Yamanaka, Y., "Development of realistic high-resolution whole-body voxel models of Japanese adult males and females of average height and weight, and application of models to radio-frequency electromagnetic field dosimetry," *Physic in Medicine and Biology*, vol. 49, pp. 1-15, 2004.

[B89] Orlandi, A., Antonini, G., Ritota, C., and Duffy, A. P., "Enhancing Feature Selective Validation (FSV) interpretation of EMC/SI results with Grade-Spread," *IEEE International Symposium on EMC*, vol. 2, pp. 362-367, Portland, OR, Aug. 2006.

[B90] Orlandi, A., Duffy, A. P., Archambeault, B., Antonini, G., Coleby, D. E., and Connor, S., "Feature Selective Validation (FSV) for validation of computational electromagnetics (CEM). Part II – Assessment of FSV performance," *IEEE Transactions on EMC*, vol. 48, no. 3, pp. 460–467, Aug. 2006.

[B91] Paul, C.R., *Introduction to EMC*, New York: John Wiley, 1992.

[B92] Peterson, Andrew F., Ray, Scott L., and Mittra, Raj, *Computational Methods of Electromagnetic Scattering*, New York: IEEE Press, and Oxford: Oxford University Press, 1998.

[B93] Pokovic, K., "Advanced Electromagnetic Probes for Near-Field Evaluation," Doc. Tech. Sci. Diss. ETH Nr. 13334, Swiss Federal Institute of Technology, Zurich, Switzerland, 1999, (<http://www.itis.ethz.ch/index/index_publications.html>), (http://e-collection.ethbib.ethz.ch/view/eth:23123).

[B94] Pozar, D. M., *Microwave Engineering*, 2d ed. New York: Wiley, pp. 156–157, 1993.

[B95] RL/ERS-96-027, "Transformable Scale Aircraft-like Model (TSAM) Antenna Measurement Program," Rome Laboratory / Air Force Research Lab Test Report, vols. 1-3, 11 June 1996.

[B96] Ruck, G. T., Barrick, D., Stuart, W., Krichbaum, C., *Radar Cross Section Handbook*, vol. 1, vol. 2, New York: Plenum Press, 1970.

[B97] Sadiku, Matthew N. O., *Numerical Techniques in Electromagnetics*, Boca Raton, FL: CRC Press, 2001.

[B98] Salazar-Palma, M., et. al., *Iterative and Self-Adaptive Finite Elements in Electromagnetic Modelling*, Artech House Publishers, 1998.

[B99] Salon, Sheppard J., and Chari, M. V. K., *Numerical Methods in Electromagnetics*, San Diego: Academic Press, November 1999.

[B100] Sandrini, L., Vaccari, A., Malacarne, A., Cristoforetti, L., Pontalti, R., "RF dosimetry: a comparison between power absorption of female and male numerical models from 0.1 GHz to 4 GHz. *Physics in Medicine and Biology*, vol. 49, pp. 5185-5201, 2004.

[B101] Sevgi, Levent, *Complex Electromagnetic Problems and Numerical Simulation Approaches*, New York: IEEE Press and Wiley & Sons, Inc., 2003.

[B102] Shen, J., *Computational Electromagnetics using Boundary Elements: Advances in Modelling Eddy Currents*, Computational Mechanics, 1995.

[B103] Shestopalov, Yu V., Smirnov, Yu G., and Chernokozhin, E.V., *Logarithmic Integral Equations in Electromagnetics*, Brill Academic Publishers, 2000.

[B104] Silvester, P. P. and Ferari, R. L., *Finite Elements for Electrical Engineers*, 2d ed. Cambridge: Cambridge University Press, 1991.

[B105] Silvester, Peter P. and Pelosi, Giuseppe, ed., *Finite Elements for Wave Electromagnetics*, IEEE Press, 1994.

[B106] Simpson, R., Jones, C., MacDiarmid, I., and Duffy, A., "The Integrated Error against Log-Frequency (IELF) method for CEM Validation," *IEEE International Symposium on EMC*, Chicago, IL, Aug. 2005.

[B107] Songoro, H., *On the Real-World Performance of ADI-FDTD*, <http://www.semcad.com/simulation/publications/hs_poster_05.pdf>, 2005.

[B108] Sorrentino, R., ed., *Numerical Methods for Passive Microwave and Millimeter Wave Structures*, IEEE Press, 1989.

[B109] Steele, Charles W., *Numerical Computation of Electric and Magnetic Fields*, 2d ed. Hingham, MA: Kluwer Academic Publishers, 1996.

[B110] Stratton, J. A., *Electromagnetic Theory*, Wiley-IEEE, 2007.

[B111] Stuchly M. A, Kraszewski, A., Stuchly, S. S., Hartsgrove, G. W., and Spiegel, R. J., "RF energy deposition in a heterogeneous model of man: Near-field exposures," *IEEE Transactions on Biomedical Engineering*, vol. 34, no. 12, pp. 944-950, Dec. 1987.

[B112] Sui, Wenquan, *Time-Domain Computer Analysis of Nonlinear Hybrid Systems*, Boca Raton, FL: CRC Press, 2002.

[B113] Sullivan, Roger J., *Microwave Radar: imaging and advanced concepts*, Norwood, MA: Artech House, 2000.

[B114] Taflove, Allen, *Advances in Computational Electrodynamics: The Finite-Difference Time-Domain Method*, Artech House, 1998.

[B115] Taflove, Allen, *Computational Electrodynamics: The Finite-Difference Time-Domain Method*, Norwood, MA: Artech House, 1995.

[B116] Taflove, A. and Hagness, S. C., *Computational Electrodynamics: The Finite-Difference Time-Domain Method*, 2d ed. Artech House, 2000.

[B117] Taflove, A. and Hagness, S. C., *Computational Electrodynamics: The Finite-Difference Time-Domain Method*, 3d ed. Norwood, MA: Artech House, 2005.

[B118] Tovmasyan, N. E., Kevorkian, L.Z., Giovanni, M.S., and Bobrova, M.N., *Non-regular Differential Equations and Calculations of Electromagnetic Fields*, World Scientific Publishing Company, 1998.

[B119] TR91-1-001.2, *Survey of Numerical Electromagnetic Modeling Techniques*, UMR EMC Lab Technical Report, 1 September 1991.

[B120] Tsai, Huan-Shang, *Real Time: A Two-Dimensional Electromagnetic Field Simulator*, Boca Raton, FL: CRC Press, 2000.

[B121] Tsuboi, H., and Sebestyén, I., *Applied Electromagnetics and Computational Technology*, IOS Press 1997.

[B122] Volakis, John L., Chatterjee, Arindam, and Kempel, Leo C., *Finite Element Method for Electromagnetics: Antennas, Microwave Circuits and Scattering Applications*, New York: IEEE Press, and Oxford: Oxford University Press, 1998.

[B123] Wadell, Brian C., *Transmission Line Design Handbook*, Artech House, 1991.

[B124] Wang, J.-Q., Fujiwara, O., Kodera, S., Watanabe, S., "FDTD calculation of whole-body average SAR in adult and child models for frequencies from 30 MHz to 3 GHz," *Physics in Medicine and Biology*, vol. 51, pp. 4119-4127, 2006.

[B125] Wang, Johnson J. H., *Generalized Moment Methods in Electromagnetics: Formulation and Computer Solution*, Wiley-Interscience, 1991.

[B126] Wriedt, T., (Editor), *The Generalized Multipole Technique for Electromagnetic and Light Scattering*, Amsterdam: Elsevier, 1999.

Annex B

(informative)

Basic descriptions of common CEM techniques

B.1 Adaptive Integral Method (AIM)

The AIM technique assists in making the iterative solution process more efficient and to speed up the matrix-vector multiplication.

B.2 Analytical Closed-Form Techniques

This method includes the use of non-numeric and quasi-discrete formulations that provide useful approximations and conservative or bounded analysis results. Most computational methods based on this approach are characterized in the frequency-domain. Many formulations in this category compute results based on real-valued (magnitude) quantities as opposed to computing complex magnitude and phase.

B.3 Bi-Conjugate Gradient Method with Fast Fourier Transform (BCG-FFT)

BCG-FFT techniques are useful in applications such as scattering and radar cross section (RCS), transient EM problems, the inverse problem, frequency selective surfaces (FSS), and optimum array processing. It considers Floquet's theory and the treatment of periodic conducting patches located in free space. Variations of this technique employ signal processing algorithms to arrive at solutions. BCG-FFT techniques are particularly useful in solving complex matrix equations generated by FEM/MoM methods.

B.4 Boundary Element Method (BEM)

BEM (like the FEM method) originated in the field of structural mechanics. It is a weighted residual technique that solves partial differential equations (PDEs) using mesh elements. It is essentially a MoM technique whose expansion and weighting functions are defined only on a boundary surface i.e., only the boundary of the domain of interest requires discretization. If the domain is either the interior or exterior to a volume, then only the surface is divided into mesh elements. The computational advantages of the BEM over other methods can be considerable. It is particularly useful for low frequency problems. The approach uses the simplest elements, is relatively easy to apply, and is versatile and efficient. BEM is mostly applicable to DC (electrostatics) and steady-state AC (EM) problems. Most general-purpose MoM modeling codes employ a boundary element method. Electrical engineers tend to use the more general term moment method to describe an implementation of this technique. Outside of electrical engineering however, the terms boundary element method or boundary integral element method are commonly used.

B.5 Conjugate Gradient Method (CGM)

The CGM technique is also based on the method of weighted residuals. It is very similar conceptually to conventional MoM techniques. Two features generally distinguish this technique from other moment methods. The first deals with the way in which the weighting functions are utilized. The second involves the method of solving the system of linear equations. Conventional moment methods define the inner product of a weighting function with another function *(*referred to as the *symmetric product*). The CGM technique uses a different form of the inner product called the *Hilbert inner product* that involves complex conjugation of real and complex weighting functions. When complex weighting functions are utilized, the symmetric product is a complex quantity and therefore not a valid *norm*. In this case, the Hilbert inner product is preferred. The other major difference between conventional moment methods and the CGM involves the technique used to solve the large system of equations these methods generate. Conventional

moment method techniques generally employ a Gauss-Jordan method or another direct solution procedure. Direct solution techniques solve the system of equations with a given number of calculations (N terms or unknowns). CGM utilizes an iterative solution procedure. This procedure, called the *method of conjugate gradients*, in conjunction with the *method of steepest decent*, can be applied to the system of equations or it can be applied directly to an operator equation. Iterative solution procedures such as the method of conjugate gradients are most advantageous when applied to large, sparse matrices.

B.6 Fast Multi-Pole Method (FMM)

FMM is a tree code-based method that uses two representations of the potential field: far field (multipole) and local expansions. The two representations are referred to as the "duality principle". This method uses a very fast calculation of the scalar potential field, which is computationally easier than dealing with the force vector (i.e., the negative of the gradient of the potential). The strategy of the FMM is to compute a compact expression for the potential phi (x, y, z), which can be easily evaluated along with its derivative, at any point. It achieves this by evaluating the potential as a "multipole expansion," a kind of Taylor expansion, which is accurate when $x^2 + y^2 + z^2$ is large.

B.7 Finite-Difference Frequency-Domain (FDFD)

Although conceptually the FDFD method is similar to the FDTD method, from a practical standpoint it is more closely related to the FEM method. Like FDTD, this technique results from a finite difference approximation of Maxwell's curl equations. However, in this case the time-harmonic versions of these equations are employed. Since there is no time stepping, it is not necessary to keep the mesh spacing uniform. Therefore, optimal FDFD meshes generally resemble optimal finite element meshes. Like the MoM and FEM techniques, the FDFD technique generates a system of linear equations. The corresponding matrix is sparse like that of the FEM method. Although it is conceptually much simpler than the FEM method, very little attention has been devoted to FDFD and very few available codes utilize this technique.

B.8 Finite-Difference Time-Domain (FDTD)

This method solves PDEs using a gridding technique with respect to a given boundary condition. In time-dependent PDEs, the FD method may be used in both space and time (i.e., FDTD) or it may be used for the spatial displacement component only for a given frequency (FDFD). FDTD techniques also require the entire volume to be meshed. Normally, this mesh must be uniform, so that the mesh density is determined by the smallest detail of the configuration. Unlike most FEM and MoM techniques, FDTD techniques are very well suited to transient analysis problems. Time stepping is continued until a steady state solution or the desired response is obtained. At each time step, the equations used to update the field components are fully explicit. No system of linear equations must be solved. The required computer storage and running time are proportional to the electrical size of the volume being modeled and the grid resolution. Because the basic elements are cubes, curved surfaces on a scatterer must be *staircased*. For many configurations this does not present a problem. However for configurations with sharp, acute edges, an adequately staircased approximation may require a very small grid size (0.1λ to 0.25λ edge dimensions). This can significantly increase the computational size of the problem. Surface conforming FDTD techniques with non-rectangular elements have been introduced to alleviate this problem. Like FEM, the FDTD methods are very good at modeling complex inhomogeneous configurations. Also, many FDTD implementations do a better job of modeling unbounded problems than FEM codes. As a result, FDTD techniques are often the method of choice for modeling unbounded complex inhomogeneous geometries.

B.9 Finite Element Method (FEM)

This method, originating in the structural mechanics engineering discipline, solves PDEs for complex, nonlinear problems in magnetics and electrostatics using mesh elements. FEM techniques require the entire volume of the configuration to be meshed as opposed to surface integral techniques that only require the surfaces to be meshed. However, each mesh element may have completely different material properties from those of neighboring elements. In general, FEM techniques excel at modeling complex

inhomogeneous configurations. However, they do not model unbounded radiation problems as effectively as MoM techniques. The method requires the discretization of the domain into a number of small homogeneous sub-regions or mesh cells and applying the given boundary condition resulting in field solutions using a linear system of equations. The model contains information about the device geometry, material constants, excitations and boundary constraints. The elements can be small where geometric details exist and much larger elsewhere. In each finite element, a simple (often linear) variation of the field quantity is assumed. The corners of the elements are called nodes. The goal of the FEM is to determine the field quantities at the nodes. Most FEM methods are variational techniques that minimize or maximize an expression that is known to be stationary about the true solution. Generally, FEM techniques solve for the unknown field quantities by minimizing an energy quantity. It is applicable to a wide range of physical/engineering problems and frequencies, provided it can be expressed as a PDE.

B.10 Finite Integration Technique (FIT)

Unlike the FDTD method, which uses the differential form of Maxwell's equations, the FIT discretizes Maxwell's equations written in their original (integral) form, on a 3-D domain. The unknowns are thus electric voltages and magnetic fluxes, rather than field components along the three space directions. Like all full 3-D methods (FEM, FDTD, TLM, etc.), the entire 3-D domain needs to be meshed. For Cartesian grids however, a special technique called Perfect Boundary Approximation (PBA) eliminates the staircase approximation of curved boundaries, for both PEC/dielectric and dielectric/dielectric interfaces. It allows even strongly non-uniform meshes, thus maintaining a manageable computational size. The FIT can be applied in both time domain (as the FDTD), and frequency domain (like FEM), on Cartesian, non-orthogonal-hexahedral, or tetrahedral grids. In the time domain, the explicit formulation leads to small memory requirements, and allows solving very large problems. From the time domain results, broad-band, high-resolution frequency-domain quantities are obtained by a discrete Fourier transform (DFT), virtually at no extra cost. If the FIT is used directly in the frequency domain, the resulting matrices are sparse. The FIT is applicable to a variety of EM problems: in bounded or unbounded domains, for electrically small or very large structures, in inhomogeneous, lossy, dispersive, or anisotropic materials. It performs well from DC up to the THz region.

B.11 Finite-Volume Time-Domain (FVTD)

This technique, an extension of the FDTD approach, permits each element in the grid to have an arbitrary shape. Frequency domain results are obtained by applying a (DFT) to the time domain results. This requires additional computation, but a wide-band frequency-domain analysis can be obtained by transforming the system's impulse response. The FVTD (and FDTD) methods are widely used for RCS analysis although they have been applied to a wide range of EM modeling problems. Flexibility is their primary advantage. Arbitrary signal waveforms can be modeled as they propagate through complex configurations of conductors, dielectrics, and lossy non-linear, non-isotropic materials. Another advantage is that they are readily implemented on massively parallel computers, particularly vector processors and single-instruction-multiple-data machines. The only significant disadvantage is that the problem size can easily become unwieldy for some configurations. Grid resolution is generally determined by the dimensions of the smallest features to be modeled. The volume of the grid must be large enough to encompass the entire object and most of the *near field*. Large objects with regions containing small, complex geometries may require large, dense grids. When this is the case, other numerical techniques may be much more efficient than the FVTD (or FDTD) methods.

B.12 Generalized Multi-pole Technique (GMT - Moment Method)

GMT is a relatively new method for analyzing EM problems. It is a frequency-domain technique that (like MoM) is based on the method of weighted residuals. This method is unique in that the *expansion* functions are analytic solutions of the fields generated by sources located some distance away from the surface where the boundary condition is being enforced. MoM generally employs expansion functions representing quantities such as charge or current on a boundary surface. GMT expansion functions are spherical wave field solutions corresponding to *multi-pole* sources. By locating these sources away from the boundary, the

field solutions form a smooth set of expansion functions on the boundary and singularities on the boundary are avoided. Like MoM, a system of linear equations is developed and solved to determine the coefficients of the expansion functions yielding the best solution. Since the expansion functions are already field solutions, it is not necessary to do any further computation to determine the fields. Conventional MoM techniques determine the currents and/or charges on the surface first and then integrate these quantities over the entire surface to determine the fields. This integration is not necessary at any stage of the GMT solution. There is little difference in the way dielectric and conducting boundaries are treated by the GMT. The same multi-pole expansion functions are used. For this reason, a general purpose implementation of the GMT models configurations with multiple dielectrics and conductors much more readily than a general purpose MoM technique. On the other hand, MoM techniques, which employ expansion functions that are optimized for a particular type of configuration (e.g., thin wires), are generally much more efficient at modeling that specific type of problem. Over the last ten years, the GMT has been applied to a variety of EM configurations including dielectric bodies, obstacles in waveguides, and scattering from perfect conductors. Work and new developments in this new method are continuing. Recent significant developments include the addition of a thin-wire modeling capability and a "ringpole" expansion function for modeling symmetric structures.

B.13 Geometrical Optics (GO)

The GO method applies exact ray tracing methods for light wave propagation through optical media. The method takes into account refraction, reflection and edge aberration phenomena and effects.

B.14 Geometrical/Uniform Theory of Diffraction (GTD/UTD)

UTD is an extension of the GTD method. These are high-frequency ray tracing techniques. They are only accurate when the dimensions of objects being analyzed are electrically large i.e., relative to the wavelength of the field. In general, as the wavelengths of an EM excitation approach zero, the fields can be determined using geometrical optics (GO). UTD and GTD are extensions of the GO method combining the effects of direct rays, reflection, diffraction and multi-path propagation around an EM structure comprised of canonical elements. Diffraction is a local phenomenon at high frequencies. Therefore, the behavior of the diffracted wave at edges, corners, and surfaces can be determined from an asymptotic form of the exact solution for simpler canonical problems. For example, the diffraction around a sharp edge is found by considering the asymptotic form of the solution for an infinite wedge. GTD and UTD methods add diffracted rays to GO rays to obtain an improved estimate of the exact field solution. Canonical problems include those that are comprised of simple objects such as right circular or elliptical cylinders with end caps, ellipsoids, N-sided plates, cones, frusta, and spheres. Certain formulations allow canonical geometry modeling elements to be of the non-PEC type.

B.15 Hybrid Lumped Circuit and Quasi-Transmission Line Method

This is a hybridization of lumped circuit and TLM methods. The TLM formulation is appropriately modified to account for lumped circuit characterizations in 3-D microwave applications.

B.16 Hybrid Techniques

No one technique is well suited to all (or even most) EM modeling problems. Most MoM codes will not model inhomogeneous, nonlinear dielectrics. Finite element codes cannot efficiently model large radiation problems. GMT and UTD codes are not appropriate for small, complex geometries or problems that require accurate determination of the surface and wire currents. Unfortunately, most practical printed circuit card radiation models have all of these features and therefore, cannot be analyzed by any of these techniques. One solution, which has been employed by a number of researchers, is to combine two or more techniques into a single code. Each technique is applied to the region of the problem for which it is best suited. The appropriate boundary conditions are enforced at the interfaces between these regions. Normally a surface integral technique such as the BEM will be combined with a finite method such as the FEM, FDTD, or TLM. Several successful implementations of hybrid techniques are described in the

literature. So far, none of the available hybrid techniques model the radiation from printed circuit cards very well. This is due to the fact that most of these methods were developed to predict RCS values or for other scattering problems where the source is remote from the configuration being modeled. The most widely used hybrid techniques also include MoM/GTD/FDFD/Eigen-Vector methods, MoM/PO, FEM/MoM, and MoM/MMP. Frequency and time-domain versions of several of these hybrid formalisms have been implemented in certain CEM codes which utilize FFT and inverse Fourier transform methods to relate time- and frequency-domain results. Recent work has been devoted to developing a fast finite element-boundary integral (FE-BI) technique.

B.17 Method of Moments (MoM)

This is a numerical technique based on the method of weighted residuals. It is synonymous with "surface integral technique" even though the method of weighted residuals can be applied to differential as well as integral equations. Moment method techniques apply thin-wire mesh/grid approximations or use perfectly electrically conducting (PEC) patch elements whose dimensions generally range between 0.1λ and 0.25λ. It is most appropriate in analyzing electrically small-to-moderately sized unbounded radiation problems and excels at analyzing PEC configurations and homogeneous dielectrics. Wire segments can be loaded or defined as non-PEC type in certain MoM formulations. EM fields are computed from wire mesh currents and patch surface current densities. In general, the method is not well suited to analyzing complex inhomogeneous geometries.

B.18 Multiple Multi-Pole (MMP)

The MMP is actually a code-based technique derived from the GMT method. It is a semi-analytic method for numerical field computations. Essentially, the field is expanded by a series of basis fields. Each of the basis fields is an analytic solution of the field equations within a homogeneous domain. The amplitudes of the basis fields are computed by a Generalized Point Matching Technique that is relatively efficient, accurate, and robust. Due to its close relations to analytic solutions, MMP is very useful and efficient when accurate and reliable solutions are desired.

B.19 Partial Element Equivalent Circuit (PEEC) Model

PEEC is based on the integral equation formulation. All structures to be modeled are divided into electrically small elements. An equivalent circuit describes the coupling between elements. Once the matrix of equivalent circuits is developed, then a circuit solver can be used to obtain a response for the system. It is mostly used for quasi-static partial inductance calculations to analyze printed circuit board EM radiation problems. One of the main advantages in using the PEEC method is the ability to add circuit elements into an EM simulator to model lumped circuit characteristics.

B.20 Pseudo-Spectral Time-Domain Method (PSTD)

PSTD applies spectral domain techniques to a variety of EM boundary value problems. Using elementary concepts and methods can easily solve complex problems.

B.21 Shooting Bouncing Rays (SBR), Physical Optics (PO), Physical Theory of Diffraction (PTD)

SBR is a high-frequency method based on “shooting” large numbers of rays from transmitter locations against a given geometry consisting of “receivers”. The rays are shot without regard to receiver location (unlike the UTD or GTD method). These rays then “bounce off” reflecting planar surfaces (i.e., facets) following the laws of reflection. Since no particular ray paths are being searched to determine local minima, maxima or inflection the path for each ray is found relatively quickly. Many more rays can be considered than with GTD, but each SBR is much faster to compute since the shooting and bouncing process is very straightforward for a geometry consisting entirely of planar surfaces. Using the SBR method, one initially evaluates the field at a particular point, since one cannot be assured that all of the

important SBR will pass through that point. One must use a "collection region" enclosing the point, and then use the rays that pass through this region to determine the field strength. The first-bounce PO plus the PTD contributions and the multi-bounce geometric optic ray contributions are included in the computation. These combined techniques work with planar, frequency selective surfaces (FSS) which are characterized by different types of impedance boundary conditions and complex material properties (i.e., non-PEC coatings, slabs or layers). Recent research has led to the development of non-planar or higher-order surface treatments.

B.22 Singularity Expansion Method (SEM)

Usual methods to treat time-dependent processes are either computation in the time domain by discretization with time steps or computation in the frequency domain and subsequent Fourier transform into the time domain. The SEM is a specific treatment of the time behavior via Laplace transform with complex frequencies. Response waveforms of complicated scatterers in the resonance range are dominated by a few damped sinusoids. Such objects exhibit resonance frequencies (with singularities of the field) whose positions in the complex frequency plane are also determined by radiation losses. The problem is to determine the essential singularities which characterize a given object. So SEM is not so much an alternative method for solving field distributions but a procedure to be used in conjunction with other methods, in order to determine broadband responses.

B.23 Spectral Domain Approach (SDA)

The idea of the SDA is to utilize the possibilities of the Fourier transform for functions in space. A spectral domain can be assigned to one, two or three coordinates. The problem is solved in this spectral domain. The solution of the original problem results from an inverse transform of the solution in the spectral domain. In the example of a planar transmission line, the Fourier transform is applied in the direction parallel to the substrate and perpendicular to the strip. In the case of complex geometries the problem in the spectral domain has to be solved by semi-analytical or numerical methods, and the subsequent inverse transform has to be done numerically.

B.24 Thin-Wire Time Domain Method (TWTD), Time-Domain Moment Method (TDMM)

These are variations of the TLM and MoM thin-wire formulation in the time domain. The methods are based on the Integral Equation technique.

B.25 Transmission Line Method (TLM)

TLM belongs to the general class of differential time-domain numerical modeling methods. It is similar to the FDTD method in terms of its capabilities. Like FDTD, analysis is performed in the time domain and the entire region of the analysis is gridded. The basic TLM approach is to obtain a discrete model that is then solved exactly by numerical means. Approximations are only introduced at the discretization stage. For EM systems, the discrete model is formed by conceptually filling space with a network of transmission-lines in such a way that the voltage and current give information on the electric and magnetic fields. The point at which the transmission-lines intersect is referred to as a node and the most commonly used node for 3-D work is the symmetrical condensed node. Additional elements, such as transmission-line stubs, can be added to the node so that different material properties can be represented. Instead of interleaving E-field and H-field grids however, a single grid is established and the *nodes* of this grid are interconnected by virtual transmission lines. At each time step, voltage pulses are incident upon the node from each of the transmission lines. These pulses are then scattered to produce a new set of pulses that become incident on adjacent nodes at the next time step. Excitations at the source nodes continue to propagate to adjacent nodes through these transmission lines at each time step. These stubs are usually half the length of the mesh spacing and have characteristic impedance appropriate for the amount of loading desired. The advantages of using the TLM are similar to those of the FDTD method. Complex, nonlinear materials are readily modeled. The disadvantages of the FDTD method are also shared by this technique. The primary

disadvantage being that voluminous problems that must use a fine grid require excessive amounts of computation. Nevertheless, both the TLM and FDTD techniques are very powerful and widely used.

B.26 Vector Parabolic Equation Technique (VPE)

VPE methods, used to analyze radio wave propagation in radar and radio communication systems, are new and powerful techniques that have become the dominant tool for assessing clear-air and terrain effects on propagation. The technique is key to engineers and researchers analyzing diffraction and ducting in radio communication systems.

Annex C

(informative)

Guidelines on the selection of CEM techniques and codes

C.1 Background

In IEEE P1597.1™/D4.3[27], the importance of applying the right techniques to the CEM modeling and simulation task involves a number of important decisions. These include the appropriate physics to be applied, the category of problem to be solved, desired accuracy, and the "observables" to be computed. A representation of the concept and decision scheme involved in selecting the appropriate solution method for validity and consistency is repeated here in Figure C.1.

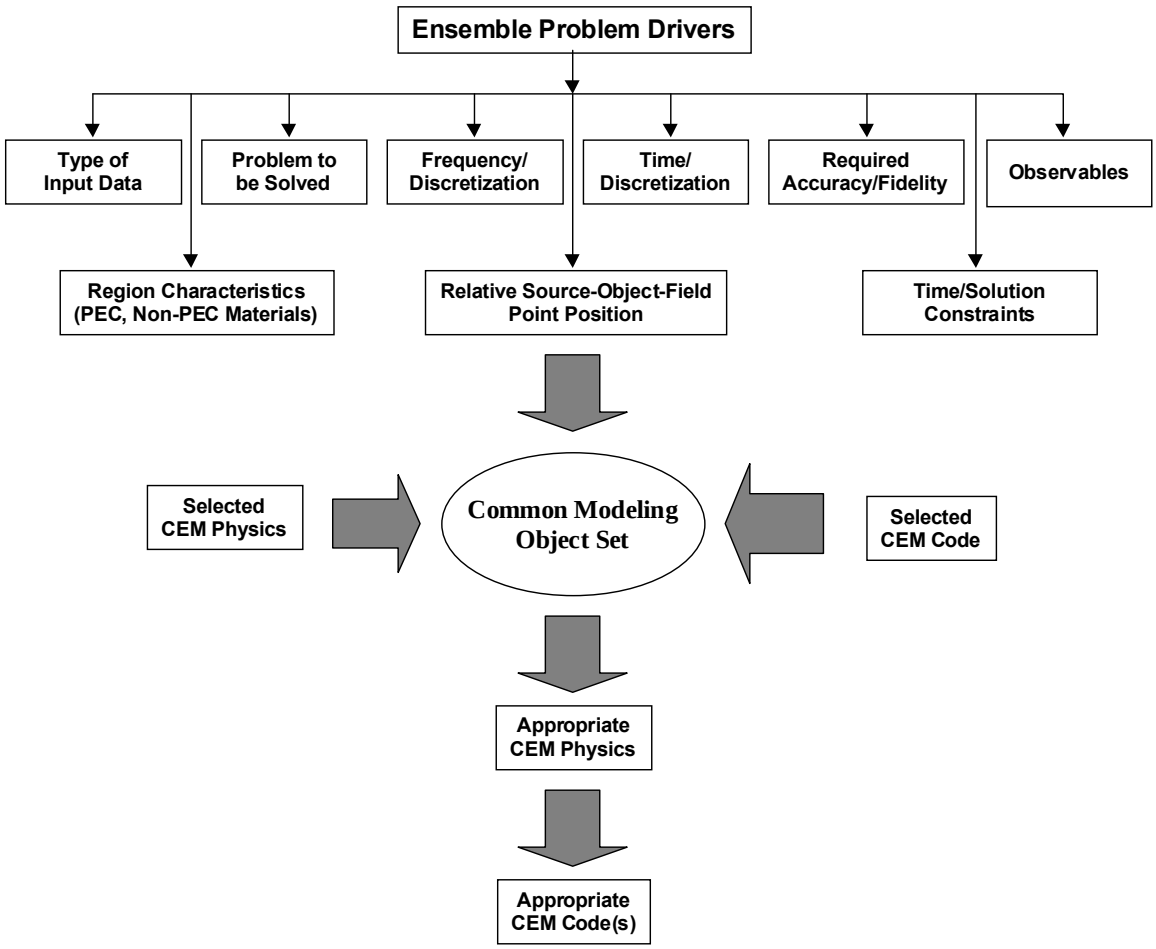

Figure C.1—Problem "drivers" influencing the CEM modeling/validation approach

[27] See Clause 2 for normative references.

Various types of computer software codes are available for modeling, simulating, and analyzing complex electromagnetics problems. Regardless of the code or computational method used, the applied engineering theories and physics formalisms are based fundamentally on the integral or differential forms of Maxwell's equations.

Next, computer methods for analyzing problems in EM generally fall into one of three categories: analytical techniques, expert systems, and computational techniques.

Analytical techniques make simplifying assumptions about the geometry of a problem in order to apply a closed-form (or table look-up) solution. However, most EMC problems of interest are simply too unpredictable to be modeled using this approach.

Expert systems do not actually calculate the field directly, but instead estimate values for the parameters of interest based on a rules database. Expert systems approach a problem in much the same way as a quick-thinking, experienced, EM engineer with a calculator would approach it.

Computational techniques attempt to solve fundamental field equations directly, subject to the boundary constraints posed by the geometry. Computational techniques generally require more computation than analytical techniques or expert systems, but they are very powerful EM analysis tools. Without making *a priori* assumptions about which field interactions are most significant, computational techniques analyze the entire geometry provided as input. They calculate the solution to a problem based on a full-wave analysis. A number of different computational techniques for solving EM problems are available. Each computational technique is well-suited for the analysis of a particular type of problem. The computational technique used by a particular EM analysis program plays a significant role in determining what kinds of problems the program will be able to analyze.

CEM techniques can also be subdivided into two other basic categories: frequency-domain techniques and time-domain techniques. These can be further expressed as either integral or discrete formulations of Maxwell's equations. Essentially, solutions to these equations involve a series of partial differential equations that are subject to boundary constraints, except for some variations that are particular to the physics of a given problem. For instance, a CEM technique can be used to solve the Laplace equation that describes the potential distribution of a closed boundary. Also, a CEM technique can be applied to solving the Helmholtz wave equation, which arises in many electromagnetic radiation problems in open space. The point here is that there are different techniques and formulations for different problem solving applications. When and which technique(s) to apply and how accurate the solutions will be are the central questions.

More specifically, these categories can be further subdivided into methods that deal with system topologies represented by Perfectly Electrically Conducting (PEC) smooth surfaces, or meshes consisting of elemental thin wires, small n-sided polygonal patches, or facets. One can extend and subdivide these methods even further by taking into account certain additional modeling constraints, boundaries, and topology variances that involve bounded or unbounded surfaces and the use of dissimilar materials.

There being a variety of electromagnetic modeling techniques, choosing the "best" technique is cause for a significant amount of debate, and often becomes a matter of past experience and personal choice or is driven by what tools are immediately available within the "toolbox". Many of the techniques are specialized for certain configurations, and require cumbersome tailoring when used for each problem. Some techniques are not particularly generic, and require in-depth knowledge of electromagnetics and the computational modeling technique. Still others are useful only for far-field problems, such as determining a radar cross section of a piece of military equipment.

C.2 Typical techniques for EMC modeling problems

For those who are new to the idea of applying computational electromagnetics (CEM) to solving EMC problems, two things become immediately apparent. First, there are a variety of numerical techniques available, each with unique strengths and weaknesses that need to be understood. Secondly, there is the

question of how these techniques can be accurately applied to a particular problem. These two issues create a tough barrier that must be overcome before further investigations of CEM are made. However, once these have been addressed it becomes easier to determine if CEM modeling will be a beneficial tool for any given situation.

The numerical techniques used in CEM are the means by which a set of equations is solved. For all EMC problems, it is Maxwell's equations that are being solved. However, in many cases the full set of equations is not necessary and constraints or simplifications can be applied. It is the addition of such constraints that result in the variety of techniques in use today for EMC modeling.

The three most common numerical techniques used in EMC modeling are the FDTD, Finite Element Method (FEM), and the Boundary Element Method (BEM), more commonly known as the MoM. These techniques are all used for solving a variety of field problems. Volumetric or surfaces meshes are generated based on a well defined set of rules that describe the geometrical problem, appropriate boundary constraints, and excitations.

Other techniques include the Partial Element Equivalent Circuit (PEEC) method and the Transmission Line Method (TLM). These two techniques were especially developed to provide a link between physical structures and circuit models. The TLM and BEM methods, which use similar definitions, are often used to study cable, trace, or transmission line radiated emissions and susceptibility to incident electromagnetic fields.

The most general solution to an EM problem might well be obtained using the FDTD technique, as there are very few constraints required in formulating a practical EMC tool. The FDTD approach, as discussed earlier, models EM wave propagation in two- and three-dimensional conductive media with or without dielectric loading. The price to pay for the flexibility afforded by FDTD is the magnitude of computational resources required for a given problem.

The MoM was developed to address a specific class of problems, namely antenna modeling. Different formulations, also using MoM, have been developed to address other specific tasks such as solving coupling problems.

The other numerical techniques mentioned have also been developed with the appropriate constraints to efficiently address a wide range of EMC related problems. This area is rapidly developing, with new customizations of these techniques being added frequently. Therefore, it is often equally important to consider what kinds of problems a tool is intended to solve rather than simply which technique should be used.

The application of numerical techniques to solving an EMC problem is the second hurdle to face. Some problems match so well to an easily implemented formulation of a particular numerical technique that the EM problem and numerical technique have almost become synonymous. The antenna modeling codes are a good example of this, where MoM has become so closely associated with such codes that many do not realize the wider range of applications that the MoM can be used to solve.

The creation of EMC models has much the same procedure as the preparation of a problem to be solved by any other means. The first three steps are to (i) determine what is wanted from the model, (ii) what is known as a starting point, and (iii) what pieces of information might be missing. This information is then incorporated into the framework of the available modeling tools and the best method of solving the problem can then be determined. The primary goal here is to help EMC engineers understand the subject so that they can decide on its relevance to their particular problems. Not everyone will need EMC modeling, and EMC modeling is not needed to address every problem.

While there is still much that can be done without the need to apply modeling, this is slowly changing. Design and analysis in the related discipline of signal integrity (SI) were once also performed by following rules and through the use of basic equations. However, as data rates increased and tools improved, SI

modeling grew from occasional use to a mainstay in the field. It is to be expected that EMC design and analysis work will develop in the same manner.

What is the "best" computational method? The answer to this question depends, to a great extent, on the particular problem that is to be analyzed. Analytical methods are very good at analyzing certain problems with a high degree of symmetry and they can provide a great deal of insight into the behavior of many configurations. However, an accurate evaluation of most realistic EM configurations requires a numerical approach. A brief overview of several common numerical EM methods is given in the following section C.3, and many good CEM references may be found in the bibliography, Annex A.

C.3 Commonly used CEM techniques

C.3.1 Method of Moments

Numerical techniques based on the method of weighted residuals are called moment methods or, method of moments (MoM). EM modelers have come to use the term MoM synonymously with BEM. The BEM is a moment method applied to the solution of surface integral equations. Most commercial MoM codes are boundary element codes, however the method of weighted residuals can be applied to differential equations as well as integral equations. In general, MoM techniques do an excellent job of analyzing unbounded radiation problems and they excel at analyzing PEC configurations and homogeneous dielectrics. They are generally not well-suited to the analysis of complex inhomogeneous geometries.

C.3.2 Finite Element Method (FEM)

Finite element techniques require the entire volume of the configuration to be meshed, as opposed to surface integral techniques that only require the surfaces to be meshed. The method is illustrated in Figure C.2. However, each mesh element may have completely different material properties from those of neighboring elements. In general, finite element techniques excel at modeling complex inhomogeneous configurations, but they do not model unbounded radiation problems as effectively as moment method techniques.

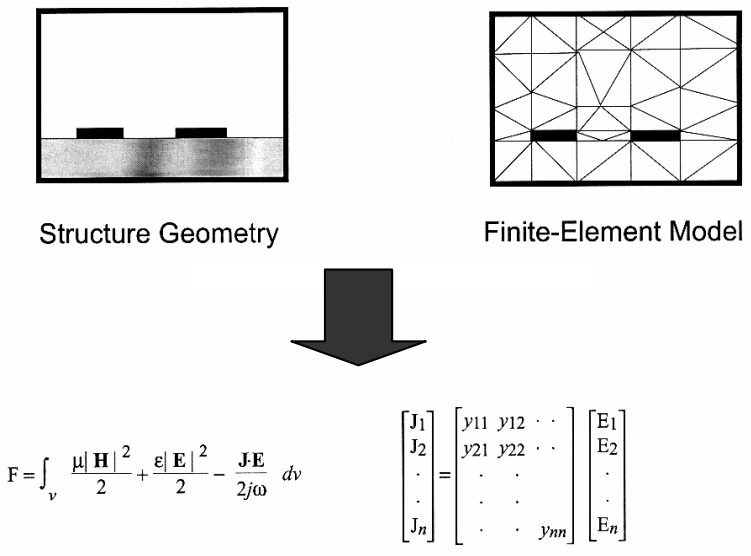

Figure C.2—Finite-Element modeling example

C.3.3 Finite-Difference Time-Domain (FDTD)

FDTD techniques also require the entire volume to be meshed. Normally, this mesh must be uniform, so that the mesh density is determined by the smallest detail of the configuration. Unlike most finite element and moment method techniques, FDTD techniques work in the time domain. This makes them very well-suited to transient analysis problems. Like the FEM, FDTD methods are very good at modeling complex inhomogeneous configurations. Also, many FDTD implementations do a better job of modeling unbounded problems than finite element modeling codes. As a result, FDTD techniques are often the method of choice for modeling unbounded complex inhomogeneous geometries. An illustration of the FDTD cell is given in Figure C.3.

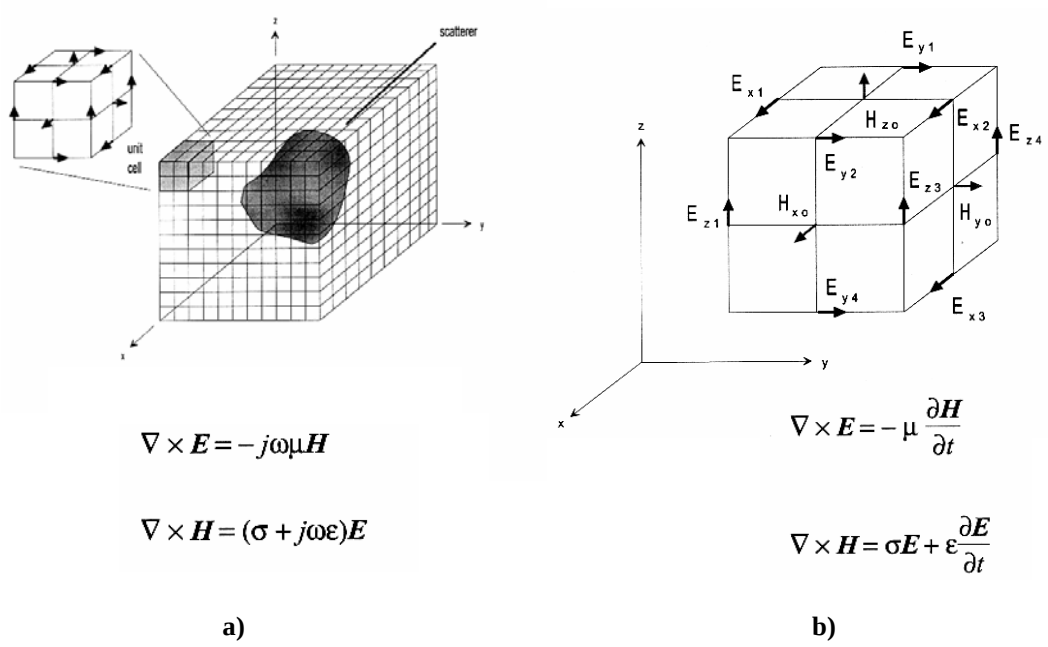

Figure C.3— a) Scatterer in an FDTD space lattice; b) Basic element of the FDTD lattice

C.3.4 Other Techniques

There are numerous other EM modeling techniques. Methods such as the Transmission Line Method (TLM), Generalized Multipole Technique (GMT), and others each have their own set of advantages for particular applications. The TLM model is illustrated in Figure C.4.

Recently, the so-called multiple multipole (MMP) and fast methods such as the multi-level fast multipole algorithm (MLFMA) method have obtained computational requirements proportional to $N \times \log(N)$, which allows for problems with millions of unknowns. Research being conducted by others are aiming to reduce N significantly without sacrificing the accuracy.

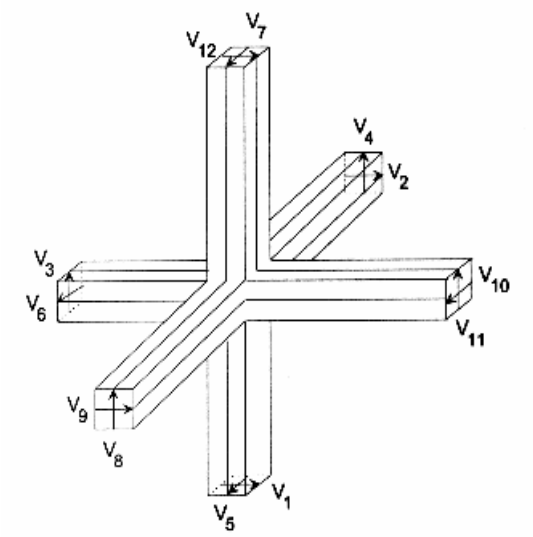

Figure C.4—The symmetrical condensed TLM node

Obviously, there are many computational methods to choose from depending upon the problem and the analyst's goals. There are yet other methods and solutions in addition to the techniques outlined above that will not be covered in detail here and are left as a research exercise for the reader. These are variations of some of the basic methods that more tightly tie together the physics formalism and the numerical solution method. These include Multi-Resolution Techniques (MRT), the Finite Integration Technique (FIT), Recursive Green's Function Method (RGFM), Adaptive Integral Method (AIM), and the Perfectly Matched Layers using a Partial Differential Equation (PML/PDE) solver method.

Some methods are highly specialized and are applicable to a certain class of problems. Certain other methods are considered to be more general purpose and are frequently used. Finite difference and volumetric techniques, for example, are very useful in modeling and analyzing three-dimensional EM wave propagation in air, or in the presence of dispersive or dielectric media for bounded geometries (i.e., interior cavity problems). FDTD methods can be used to study wave propagation and scattering in two-dimensional geometries as well. Problems involving smooth surface dielectric bodies are best dealt with using multi-pole methods and in certain cases, moment methods. Partial Element Equivalent Circuit methods are highly useful in studying mixed or printed circuit, cable, and electronic enclosure EM problems. Other methods are used to effectively model and analyze high-frequency antenna structures with or without dielectric media. Yet others, as the name of the method may imply, deal with energy propagation and scattering in two- and three-dimensional multiple non-PEC material layers as well as other types of frequency selective surfaces (FSS). Each of these methods is considered very powerful in spite of any inherent theoretical restrictions or limits on ranges of applicability. There are additional specialized modeling and computational methods based on Bodies of Revolution and Bodies of Rotation (BOR) schemes which take advantage of problem symmetry to more readily generate and analyze complex computational models.

The class of high-frequency ray tracing methods includes: the Geometrical Theory of Diffraction (GTD) and Uniform Theory of Diffraction (UTD), geometrical optics (GO), physical optics (PO), Physical Theory of Diffraction (PTD), and shooting bouncing rays (SBR) techniques. These techniques have been used quite extensively in analyzing high-frequency antenna radiation and scattered field effects for complex structures modeled with canonical elements. The UTD method, for instance, applies an asymptotic (*anzatz*-based) ray tracing method that reduces the computational requirements, but can also result in less accurate results in certain cases. These methods have been hybridized with lower frequency methods (e.g., MoM/UTD) to provide hybrid solutions that can be used to cover a broad range of frequencies. The hybrid MoM/UTD method is illustrated in Figure C.5.

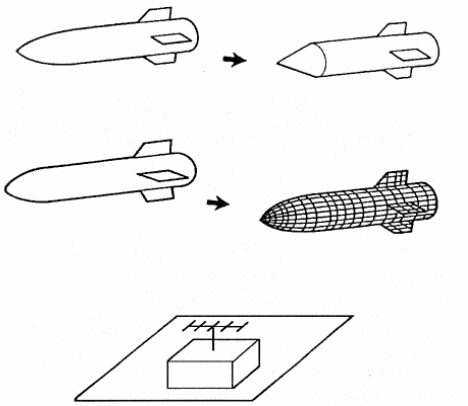

Figure C.5—Hybrid MoM/UTD examples

Current research and development for advancing CEM technologies is striving to develop new, accurate methods as well as further hybridizing existing methods in order to extend the range of problems that can be modeled in a single simulation. These also include the application of genetic algorithms and artificial intelligence or knowledge-based approaches to enhance the efficiency of the modeling and simulation task.

Annex D

(normative)

Validation problems: special cases

D.1 TSAM validation program

A series of EM measurements were performed on a selected test articles to generate meaningful data to be used in validating CEM codes. These measurements focus on far- and near-field scattering and EMI coupling/isolation phenomena at the system level. A survey was performed to identify existing measured EM data on canonical components such as circular and elliptical cylinders, ellipsoids, ogives, cones/frusta, and n-cornered plate structures. Sources of such data included the Air Force Research Laboratory, Rome Research Site (AFRL, RSS).

The AFRL, RSS conducted a measurement effort during the latter 1990s using the Transformable Scale Aircraft-like Model (TSAM) for the purposes of validating CEM codes. The report titled *Transformable Scale Aircraft-like Model (TSAM) Antenna Measurement Program,* RL/ERS-96-027 Test Report [B95] was reviewed. The TSAM Project objectives were the following:

— Record principle plane antenna pattern and gain data for six scale model antennas for seven TSAM configurations;

— Record antenna isolation data between each of the six scale model antennas for the seven configurations; and

— Compare this data with data obtained from CEM code simulations at 4.58 GHz, 68 GHz, and 8 GHz.

The TSAM report describes an effort to develop a scale model airplane to replicate what has been modeled by EM numerical modeling techniques. Figure D.1 shows the test article. This aircraft was used to mount antennas for the purpose of measuring radiation patterns and isolation. Figure D.2 shows measurement configurations and the test points considered. This effort was initiated in for two reasons. Previous scale modeling and numerical modeling results had been compared with qualitatively reasonable correlation, but there was concern that some differences needed to be defined and explained. The question to be answered was: is the numerical code in error or are the differences due to the fact that the numerical code cannot accommodate some details such as wing camber and washout? The second reason for this effort was to develop a model that is completely modular and can be assembled piece by piece in order to study the effects of individual components of the airframe. This model also allowed replacement of components from simple canonical shapes to more complex shapes as the numerical modeling techniques advance.

Advanced EM modeling techniques have progressed to the point that they can model complex structures such as aircraft with antennas and calculate antenna patterns that can compare favorably with measured data. The TSAM report provided typical comparisons of calculated and scale model measurements for various plane cuts of ultra high frequency (UHF) antennas mounted on top of a replica of a Boeing 707 type airplane. The patterns were very similar, but there were enough differences to cause concern that the modeling may not have been accurate or complete enough to be sensitive to small geometric changes. There was also the question of the quality of the measurement i.e., are structures in the environment perturbing the measurements? While EM modeling has reached a high degree of sophistication, many features were found to be difficult to incorporate, such as the camber and the washout in the wings, the eccentricity of the fuselage and the truncation of the nose. Many of these features could have been approximated by a repeated subdivision of the geometry which would consume a large amount of computer memory and require very long execution times. Many times the expenditure of these computer resources resulted in only a slight improvement in accuracy.

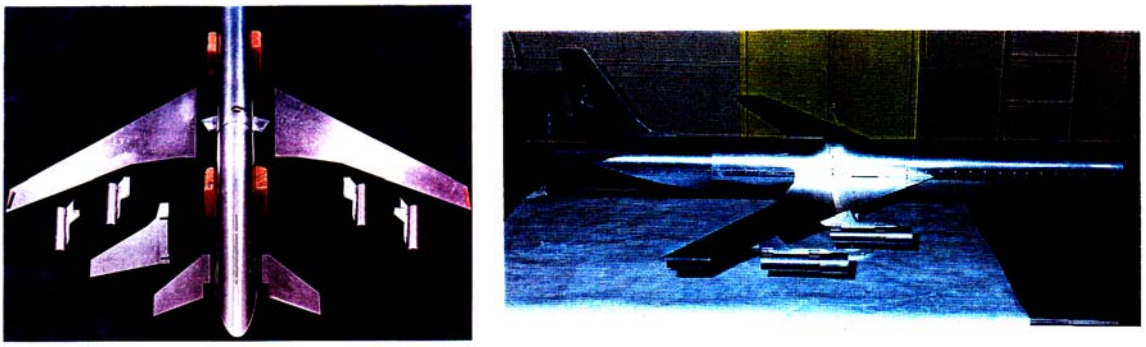

Figure D.1—Views of modular TSAM test article

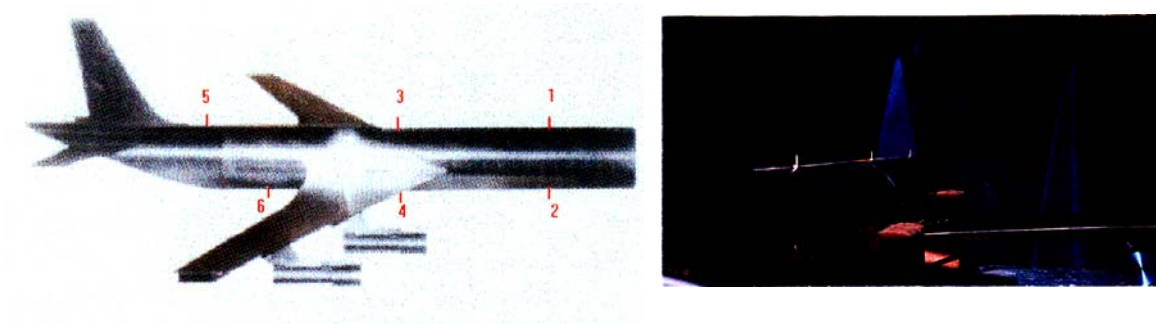

Figure D.2—TSAM antenna locations for coupling/isolation and pattern measurements

If one is looking to determine the correlation between an analytical technique and a measurement technique, the conventional approach is to model the structure being measured as close as possible. A better approach to consider is to construct a scale model to duplicate the current modeling capabilities and not visa versa since a real airframe has a more complicated shape than a model. Once the computer model and the physical scale model have been brought into correlation, then changes can be introduced in the scale model geometry in order to bring it more in line with a real structure and observe the convergence or divergence of the model.

One of the purposes of the TSAM effort was to build a model aircraft out of the canonical shapes (i.e., cylinders, plates and cones) that would accurately duplicate an airframe that has already been modeled by the selected CEM code(s). The geometry was adaptable to the extent that the various appendages such as the wings, engines and stabilizers could be removed or replaced with other geometries in order to perform a sensitivity analysis, which progressed from a simple canonical model to a close representation of a real aircraft. Furthermore, the TSAM provided the basis for a test-bed of benchmark data that could be used for CEM code validation purposes.

A canonical scale model aircraft, representative of a medium sized transport, was fabricated to facilitate comparisons to numerically modeled antenna patterns. This aircraft was designed to be identical to the aircraft in the numerical model. In order to be completely compatible with the computer model, selected antennas were used. These included: tuned resonate thin wires that have narrow bandwidths, antennas that functioned over the band of interest (225 MHz to 400 MHz), and a tuned bicone antenna that could be sized to $\lambda/4$. The bicone antenna was made to resonate over a 5:1 bandwidth, however, it becomes electrically long at the higher frequencies. Also, a Hertzian dipole was closely approximated using an electrically short dipole (such an antenna is not an efficient radiator since it is not tuned and has a high capacitive reactance).

A selected CEM was used to model antennas on operational airplanes and the results were compared with measurements taken on a 20:1 scale model of the same aircraft. It is uncertain as to whether the differences between the results were due to inaccuracies in the computer algorithms or due to the fact that the aircraft was numerically modeled as an assembly of canonical shapes (i.e., cylinders, flat plates, thin wires). Since actual aircraft are not exactly perfect canonical shapes, it was deemed best to make comparative measurements on a scale model that is made up of canonical objects that when assembled, closely approximates the general appearance of the aircraft under study. It was also determined that it would be best if these canonical shapes could be measured separately as well as collectively and anywhere in between. Where the pattern was sensitive to any geometric parameters, these parameters were made variable to the maximum extent practical. This scaled model aircraft comprised of canonical shapes was built so that any of the canonical shapes had a standard fit or attachment allowing for replacement by or with other canonical shapes having the same function. This also allowed the model to evolve as the computer models evolved. All shapes were made of electrically conducting material and electrical continuity between the pieces at the attachment points was assured. The 1:20 scale model aircraft was designed to approximate, as close as possible, a Boeing 707/300 and have, as a minimum, a cylindrical fuselage, two wings, one vertical stabilizer, two horizontal stabilizers, four wing pylons, and four engine nacelles. The wings were able to move up and down 10 degrees in each direction.

The goals of the TSAM effort included the validation of CEM codes, phenomenology studies in an attempt to quantify the effect of variations as physical configurations changes such as engines and wings are removed or if antenna locations are changed. Efforts were also directed at developing error budgets in both the measurement and simulation domains.

The TSAM report described the detailed pretest plan and testing procedures to measure both antenna patterns (pitch, roll, and yaw principle plane cuts) and isolation characteristics for the antennas mounted on the structure (with and without tail section, wings, engines, etc.). Sample results for the isolation measurements and simulation comparisons are shown here. Figure D.3, Figure D.4, and Figure D.5 show sample isolation results.

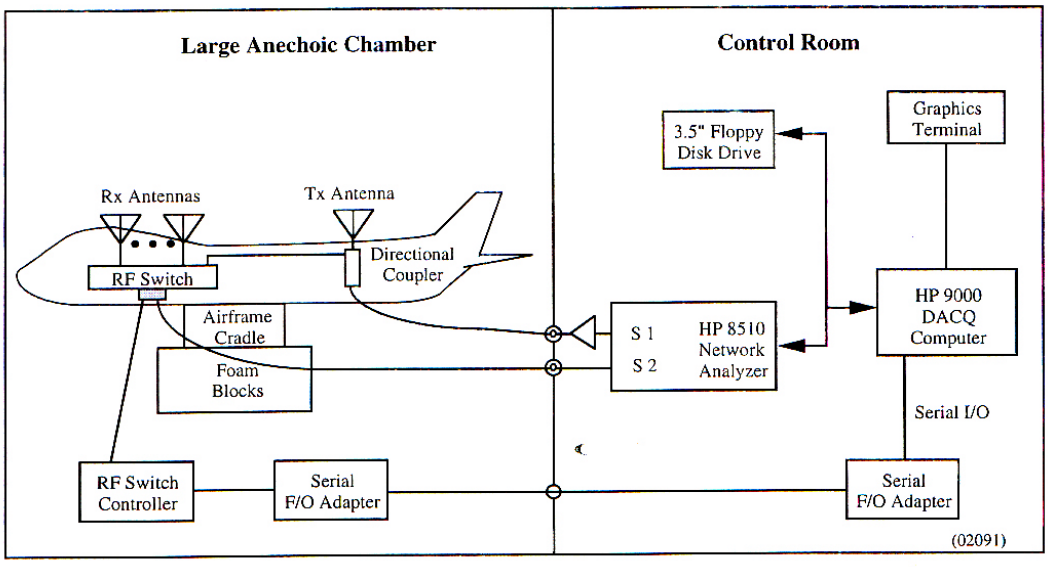

Figure D.3—Antenna isolation measurement system block diagram

The accuracy of the antenna isolation measurement system was based on determining the system error budgets. The Root-Sum-Square error value of ±1.03 dB was determined, which is acceptable for most EMC certification purposes.

Whereas differences between the measurements and code simulations were noted, the relative quantitative results were apparently published in this series of reports. Some relevant coupling/isolation data exist, for example, the geodesic coupling data associated with selected test points (corresponding to specific antenna locations) over the cylinder and wing structures of the TSAM test article.

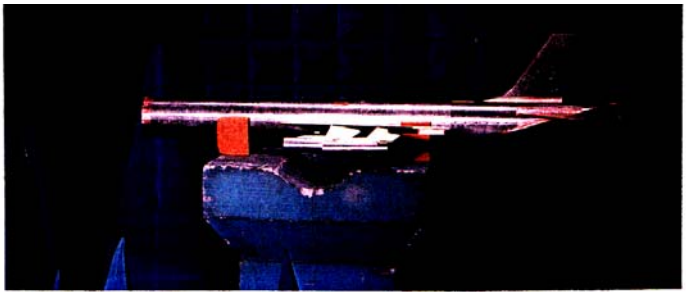

Figure D.4—TSAM mounted for isolation measurements

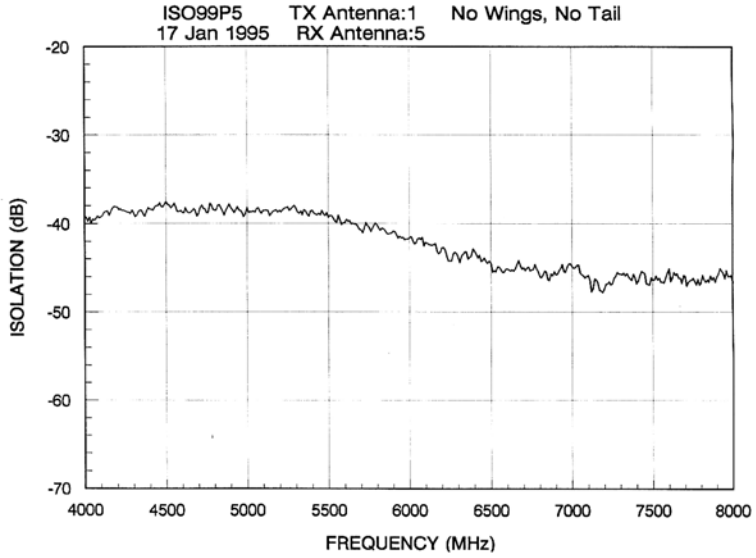

Figure D.5—Sample of TSAM measured isolation between antennas 1 and 5

The data on the results of the aforementioned measurements can be found in the reference below, which can also be downloaded from the IEEE EMC-S Web site,
<http://www.ewh.ieee.org/cmte/tc9/Problems/index.html>[28].

References:

[28] See Clause 2 for normative references.

[B95] RL/ERS-96-027, "Transformable Scale Aircraft-like Model (TSAM) Antenna Measurement Program," Rome Laboratory / Air Force Research Lab Test Report, vols. 1-3, 11 June 1996.

D.2 CEM and human exposure to electromagnetic fields

D.2.1 Standards

This sub-clause references standards development work being performed by the IEEE International Committee on Electromagnetic Safety Technical Committee 34 Subcommittee 2 (ICES TC34 SC-2)[29] on Wireless Handset Certification specific absorption rate (SAR) evaluation to develop a set of recommended practices for human exposure evaluation using CEM.

The IEEE P1528.1 project scope is to describe the concepts, anatomical models for compliance assessments, techniques, validation procedures, uncertainties, and limitations of the FDTD when used for determining the spatial-peak SAR in standardized human anatomical models exposed to wireless communication devices. It recommends and provides standardized anatomical models and provides general benchmark data for these models.

The IEEE P1528.2 project scope is to describe the concepts, techniques, vehicle models, validation procedures, uncertainties and limitations of the FDTD technique when used for determining the spatial-peak SAR in standardized human anatomical models exposed to vehicle mounted antennas. It recommends and provides vehicle models and provides general benchmark data for these models. It defines antenna locations, operating configurations, and exposure conditions, and defines positions of persons exposed to the vehicle mounted antenna.

The IEEE P1528.3 project scope is to describe the concepts, techniques, models, validation procedures, uncertainties and limitations of the finite-difference time-domain technique (FDTD) when used for determining the spatial peak specific absorption rate (SAR) in standardized human anatomical models. These models are exposed to personal wireless devices, e.g. mobile phones. It recommends and provides guidance on modeling of personal wireless devices and provides benchmark data for simulation of such models. It defines model contents and provides guidance on meshing and test positions at the anatomical models.

The IEEE P1528.4 project scope is to describe the concepts, techniques, models, validation procedures, uncertainties and limitations of general numerical simulation methods, e.g., finite-element method, when used for determining the spatial-peak specific absorption rate (SAR) in standardized human anatomical models exposed to personal wireless devices, in particular handheld mobile phones. It recommends and provides guidance on modeling of personal wireless devices and provides benchmark data for simulation of such models. It defines model contents, guidance on meshing and test positions at the anatomical models.

The validation data for these recommended practices are incorporated herein by reference.

References

[B63] IEEE P1528.1, Recommended Practice for Determining the Peak Spatial Average Specific Absorption Rate (SAR) in the Human Body from Wireless Communications Devices, 30 MHz - 6 GHz: General Requirements for using the Finite Difference Time Domain (FDTD) Method for SAR Calculations, IEEE PAR Sep. 2005.

[B64] IEEE P1528.2, Recommended Practice for Determining the Peak Spatial Average Specific Absorption Rate (SAR) in the Human Body from Wireless Communications Devices, 30 MHz - 6 GHz:

[29] Information about ICES and TC34 is available at Web sites (http://www.ices-emfsafety.org/), (http://grouper.ieee.org/groups/scc34/sc2/).

Specific Requirements for Finite Difference Time Domain (FDTD) Modeling of Vehicle Mounted Antennas Configurations, IEEE PAR Sep. 2005.

[B65] IEEE P1528.3, Recommended Practice for Determining the Peak Spatial-Average Specific Absorption Rate (SAR) in the Human Body from Wireless Communications Devices, 30 MHz - 6 GHz: Specific Requirements for Finite Difference Time Domain (FDTD) Modeling of Mobile Phones/Personal Wireless Devices, IEEE PAR Mar. 2006.

[B66] IEEE P1528.4, Recommended Practice for Determining the Peak Spatial Average Specific Absorption Rate (SAR) in the Human Body from Wireless Communications Devices, 30 MHz - 6 GHz: Requirements for Using the Finite Element Method for SAR Calculations, specifically involving Vehicle Mounted Antennas and Personal Wireless Devices, IEEE PAR May 2008.

D.2.2 Dipole antenna near lossy half-space benchmark validation problem

IEEE Std 1528-2003 and IEEE Std 1528a-2005 specify protocols and procedures for measurement of SAR induced by certain types of held-to-ear radio transceivers inside a generic simplified model of a human head. SAR measuring systems use a periodic validation procedure to evaluate the response and performance against numerically-calculated reference SAR values. The system validation test setup utilizes a flat phantom and a reference dipole, as shown in Figure D.6. IEEE Std 1528 provides system validation testing SAR target values, which were determined from modeling and measurements as described in Christ and Kuster [B30]. Results of [B30] are summarized here to provide a basic benchmark modeling problem for CEM codes.

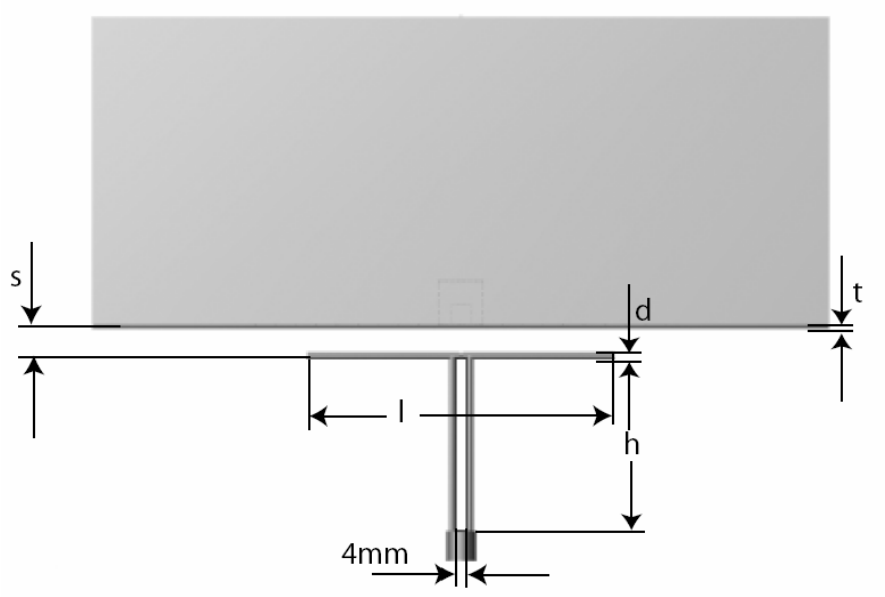

Figure D.6—Dimensions of the flat phantom model and test setup

The flat phantom setup consists of a resonant half-wave dipole antenna placed underneath a rectangular dielectric-material box shell filled with liquid that simulates the electrical properties of human tissue. Dimensions for the model parameters of Figure D.6 are given in Table D.1. The rightmost two columns of Table D.1 also give the transverse dimensions (length L, width W) of the rectangular box model.

Table D.1—Tissue-simulating liquid dielectric parameters and model geometry parameters

f, MHz	ε_r	σ	t, mm	d, mm	l, mm	h, mm	s, mm	L, mm	W, mm
450	43.5	0.87	6	6.3	270	166.7	15	700	600
835	41.5	0.9	2	3.6	161	89.8	15	360	300
900	41.5	0.97	2	3.6	149	83.3	15	360	300
1450	40.5	1.2	2	3.6	89.1	51.7	10	240	200
1800	40	1.4	2	3.6	72	41.7	10	220	200
1900	40	1.4	2	3.6	68	39.5	10	220	200

Numerical simulations were performed using a commercial FDTD code.[30] Liquid depth was 150 mm, the box shell dielectric material (ε_r = 3.7) was assumed to be lossless, and the dipole material to be perfectly conducting. Nonuniform meshing was used, with maximum cell size selected to not exceed $\lambda/15$ for all frequencies and dielectric parameters. Around the antenna feedpoint, antenna tips, and SAR maxima locations, the cell size was reduced to approximately 0.25 mm^3. Depending on simulation frequency and the setup dimensions, overall mesh sizes between three and twelve million cells. The mesh was truncated with PML absorbing boundary conditions. To verify the numerical results, SAR for the flat phantom setup was measured using a commercial system.[30] Input impedance of the dipole was measured with a network analyzer calibrated at the feedpoint of the dipole. Calculated and measured impedance results are shown in Table D.2. Calculated and measured SAR results are shown in Table D.3. Other details about related SAR measurements and computations are available in IEEE Std 1528-2003 [B59], IEEE Std 1528a-2005 [B60] and IEEE P1528.1 [B63]. Other benchmark SAR evaluation results are given for example in Beard, B.B, and Kainz, W. [B12], Beard, B.B, et al [B13], Faraone, A. et al [B47], EUREKA SARSYS Project [B46], Pokovic, K. [B93], Chavannes, N. et al [B23], Futter, P. et al [B48].

Table D.2—Measured and calculated antenna feedpoint impedance, and measured dielectric parameters

	measured		measured			Calculated		
f, MHz	ε_r	σ	Re{Z}, Ω	Im{Z}, Ω	S_{11}, dB	Re{Z}, Ω	Im{Z}, Ω	S_{11}, dB
450	44.5	0.86	56.6	-5.5	-21.9	54.9	-3.1	-25.2
835	41.9	0.89	48.5	-2.8	-29.8	51.0	1.4	-35.4
900	41.3	0.94	48.0	-3.0	-28.7	49.9	2.3	-32.8
1450	41.6	1.25	50.3	-1.2	-38.2	50.2	-2.4	-32.2
1800	40.5	1.35	48.4	-8.0	-21.7	50.6	1.1	-38.1
1900	39.1	1.47	45.0	-8.4	-19.8	50.6	0.7	-40.7

Table D.3—Measured and calculated SAR, normalized to 1 W input power

	Measured			Calculated		
f, MHz	1 g avg.	10 g avg.	peak	1 g avg.	10 g avg.	Peak
450	4.81	3.19	7.28	4.9	3.3	7.2
835	9.40	6.20	13.8	9.5	6.2	4.1
900	10.3	6.64	15.4	10.8	6.9	16.4
1450	29.1	16.4	48.8	29.0	16.0	50.2
1800	36.3	19.6	63.2	38.1	19.8	69.5
1900	40.4	21.2	71.2	39.7	20.5	72.1

References:

[30] Schmid & Partner Engineering, (http://www.semcad.com/simulation/index.php), (http://www.speag.com/measurement/index.php).

[B30] Christ, A., and Kuster, N., "Flat phantom setup for the performance check and system validation of measurement systems according to IEEE 1528 and IEC 62209," Technical Report, Foundation for Research on Information Technologies in Society, IT'IS, Zurich, Switzerland, May 2002.

[B59] IEEE Std 1528-2003, IEEE Recommended Practice for Determining the Peak Spatial-Average Specific Absorption Rate (SAR) in the Human Head from Wireless Communications Devices: Measurement Techniques.

[B60] IEEE Std 1528a-2005, IEEE Recommended Practice for Determining the Peak Spatial-Average Specific Absorption Rate (SAR) in the Human Head from Wireless Communications Devices: Measurement Techniques, Amendment 1: CAD File for Human Head Model (SAM Phantom).

[B63] IEEE P1528.1, Recommended Practice for Determining the Peak Spatial Average Specific Absorption Rate (SAR) in the Human Body from Wireless Communications Devices, 30 MHz - 6 GHz: General Requirements for using the Finite Difference Time Domain (FDTD) Method for SAR Calculations

Annex E

(informative)

Identifying sources of error in CEM modeling and simulation

E.1 Modeling complex large-scale problems

Large-scale CEM problems require the application of the *right tool for the right job* in order to minimize the potential for error generation and propagation during each step of the process. The subtleties of this issue are associated with knowing where sources of error can arise, how to quantify them, and what methods can be used to control errors. Sources of error can be categorized as *procedural*, *model-limited*, *technique-limited*, *problem dependent*, *numerical*, and *interpretive*. These by no means represent a complete taxonomy of error sources in CEM, but provide a means of better understanding basic error budgets and how these may be controlled. An overview of some of the sources of error to be mindful of and the potential pitfalls that may lend to computational uncertainty is given as follows.

E.2 Model-limited errors

This refers to the errors that arise because of limitations associated with the geometrical elements which are used to construct CEM models.

Sometimes the modeling elements are too gross or simplistic to faithfully represent the geometry at the frequency of interest. To overcome such difficulties, techniques have been developed to adapt detailed computer-aided design (CAD) models directly in order to derive high-fidelity CEM models. However, this results in a new source of error in that the CAD models themselves may contain subtle flaws that are not readily detected and which can result in other errors downstream of the modeling and simulation process.

E.3 Procedural errors

This refers to the step-by-step approach used in generating and analyzing a CEM model.

How one goes about modeling and analyzing a real-world problem is dependent on the type of problem to be solved and what EM phenomena and observables are of interest, among other considerations. For example, consider the problem of assembling a computational model, and integrating components and their individual EM contributions to compute a total budget solution ─ not to be confused with error budget. This problem is one of resolving a complex system into its parts, analyzing the EM interactions or relative contributions, and then integrating results in order to arrive at an accurate system analysis ─ a procedure called combinatorial modeling. First, this is an approximate idea. Linear superposition does not work. By solving a problem in components and later adding up the contributions, the total budget solution found this way is a lower bound to the true solution. The difference between the budget solution and the true solution is a function of how strongly the parts interact. The stronger they interact, the larger the difference between the budget solution compared to the true total solution.

An ill-posed problem can result in computational instabilities and numerical inaccuracies; for example, when an insufficient sampling criterion is used in an attempt to capture EM phenomena at resonance or about singularities or in the vicinity of near field caustic points.

The lesson to be learned here is this: building and analyzing a CEM model without some a priori understanding of the type of problem to be solved, the basic physics of the problem, and what observables are most appropriate based on the boundary conditions, frequency, and so forth, will likely lead to errors

and lend to the uncertainty. In other words ─ one needs to properly define the problem and the desired "metrics."

E.4 Technique-limited errors

This pertains to the approximations and potential errors that are introduced when Maxwell's equation are constrained to a particular subset of boundary conditions and modeling problems (also referred to as *quadrature error*), expressed either in differential or integral form.

As a result, the applied physics can exhibit certain inherent limitations. Some of the subtle issues here pertain to the applied mathematical algorithms and methods for truncating infinite series and controlling the number of second and higher order EM interactions (i.e., bounces) to be considered.

E.5 Problem-dependent errors

This pertains to errors that arise when the physical problem is not fully characterized and the solution approach does not match the problem to be solved.

For example, it is not necessarily prudent to use a full-matrix decomposition moment method (MoM) technique to solve a simple antenna coupling problem at 10 GHz. However, for scattering cross section problems at 10 GHz, moment method based techniques in conjunction with the use of fast solvers are desirable in order to obtain highly accurate results. Similarly, a transmission line method (TLM) technique may be quite suitable to analyzing an internal cable coupling problem for a closed or bounded cavity, but may not be appropriate for calculating antenna radiation effects for exterior problems involving large, complex structures.

Again, it is imperative that one start by defining the problem to be solved. The most suitable physics formalism(s) and solution method(s) can then be determined with a greater degree of confidence. Generally, at a very high level, problems can be classified as one of the following types: EMC, scattering cross section, antenna radiation, signal integrity, shielded enclosure problems, and materials problems. These categories can be further subdivided as necessary. EMC problems, for instance, can apply to printed circuit boards (PCBs) or devices as well as to large-scale systems. Here, we are invoking the fundamental rule ─ *use the right tool for the right job!*

Simply put, some techniques may be more or less error prone than others, not because they contain inherent limitations as such, but because their application does not match the type of problem(s) to be solved very well.

E.6 Numerical errors

Here, solution error is closely tied to technique-limited error in that the physics and the numerical solvers work together to provide a total budget solution.

In ultra large-scale CEM problems, a variety of errors can arise. In fact, the effects of numerical noise tend to become more pronounced due to round off and phase velocity errors in ultra large scale CEM problems. Solution errors are also attributed to the solver method employed. For example, banded matrix iteration involves approximations regarding the specification of the matrix band and the iterative convergence value, which sometimes can be a "best guess." Full wave or lower-upper decomposition (LUD) of matrices can result in numerical noise propagation for dense matrices. Inconsistent use of block matrix partitioning schemes in conjunction with an inconsistent Green's function along with applying asymptotic methods or other approximations in computing a total solution can clearly promulgate numerical inaccuracies.

The enhancement of numerical noise and round off error propagation stems, for example, from the application of an inconsistent Green's function and the process of solving for a large number of current or field unknowns (N) for a dense matrix system. There are actually various numerical noise contributions at

play in solving for the unknowns. These are product noise, subtraction noise, Gaussian elimination noise, matrix error noise (quadrature error in evaluating matrix coefficient terms), as well as phase velocity error where the phase velocity is incorrectly defined, which in turn can give rise to errors in the exponential function calculations. This is related to the process of solving an integral equation which formulates a cooperative behavior among the current elements so as to produce a field that exactly cancels the incident field within a metallic scatterer, for instance. Hastriter and Chew [B55] points out that this cooperative behavior requires that all the current elements "talk" to each other on the same "wavelength" or the same phase velocity. Hence, any inconsistency in the phase velocity will not allow the current elements to cooperate effectively with each other.

The sources of matrix error can be traced back to the problem of (i) geometrical modeling error; (ii) integral equation discretization (including basis function expansion error and quadrature error); (iii) matrix equation solution error (using iterative solvers, LUD, and banded matrices); (iv) matrix vector product error due to matrix equation factorization error (in the case of fast algorithms) and pre-corrected FFT errors; and (v) associated round off and numerical precision errors.

E.7 Interpretive errors

A person's attempt to interpret the computed observables can lead to erroneous conclusions about the data and detract from the real problem solution.

The process of modeling and analyzing problems that reveal singularities, caustics, and harmonic resonance behavior as well as situations where abrupt discontinuities of current or field point mismatches exist at/between multiple region (multilayer material) interfaces, can call into question the suitability of the technique as well as computational accuracy. Oftentimes, there is a balance of objective and subjective reasoning at play at this level of modeling and simulation. The proof comes in validating the results against ground truth or high-quality measurement benchmarks.

A standardized approach will most certainly be useful in performing a consistent, accurate, and repeatable validation and verification (V&V) of multiple EM observable data sets. A standardized method exists of interpreting computed data results in a highly objective and consistent way using novel technique comparison and Feature Selective Validation (FSV) designed to reduce the associated uncertainty in interpreting data. This method is briefly described below.

Reference:

[B55] Hastriter, M. L., and Chew, W. C., "Role of Numerical Noise In Ultra Large-Scale Computing," *IEEE Antennas and Propagation Society International Symposium*, vol. 3, p. 3373-3376, Monterey, CA, June 2004.

Annex F

(informative)

Guidelines for reporting solver performance

F.1 General

Reporting the performance of any new product or system is frequently a source of contention. Many times, this is because the developers wish to show their product/research in the best possible light. For end-users, this "ideal" case is infrequently (if ever) realized. Moreover, companies and researchers will use these performance numbers to compare the performance of their designs. Unfortunately, this is quite frequently an "apples and oranges" comparison. For example, how do we measure the performance of processors? Clock speed? FLOPS? Although neither metric fully describes a processor, both are used to compare and contrast processors from different manufacturers.

Similarly, performance of CEM solvers has been measured with several different metrics, including cells per second, nodes per second, and voxels per second (see also Taflove and Hagness [B117], Durbano, J. P. et al [B42], and Songoro, H. [B107]).. The basis of each of these metrics involves measuring the number of discretization points that can be "updated" per second. However, this measurement is not as straightforward as it sounds. For example, are they 2-D or 3-D nodes? 3-D nodes have more field components, and thus require more computations, as compared with 2-D nodes. Is a node considered processed after updating its electric or magnetic fields or both? What about the ABC chosen? Berenger's perfectly-matched layer boundary conditions are more accurate, but more computationally intensive than others, such as second-order Mur boundaries (see also Mur, G. [B87] and Berenger, J.-P. [B14]) . With the recent advent of hardware-based solvers, this issue has become even more important as these tools are focused almost entirely on speed. Without a clear mechanism to evaluate different solvers, tools will be unfairly compared to one another, misrepresentations will abound, and ultimately the users of these products will suffer.

F.2 Description

The performance of CEM solvers should be reported in terms of wall clock time, rather than metrics such as cells per second, nodes per second, or voxels per second. These metrics, although useful, can be confusing as different researchers and vendors use these terms interchangeably, but measure the performance differently. Additionally, if a particular solver is capable of solving the same problem using fewer nodes, due to adaptive meshing or exploitation of symmetry, the metric may provide misleading information. For example, if two solvers are each capable of updating 10 million Yee cells per second (Taflove and Hagness [B117]), but Solver A utilizes adaptive meshing and Solver B does not, Solver A can solve the problem faster despite being "equivalent" to Solver B. Furthermore, wall-clock time transcends the various solver categories, such as time-domain and frequency-domain solvers, in which such "per-second" metrics may not be meaningful, to enable direct performance comparisons amongst a range of solver implementations. Because the end user is ultimately concerned with how much time the simulation requires, the user should simply measure wall clock time.

When reporting the "wall-clock" time required to perform a given simulation, the user should also provide information about the underlying hardware platform used to carry out the simulations. This information should be disclosed so that those in the community can effectively review the results claimed by software vendors, researchers, etc. In order to fully describe the processing platform, those reporting run times should utilize the "level" system, which is described below and enumerated in Table F.1.

Level 1 reporting represents the minimum system information that should be reported when discussing solver performance. This information is relatively easy for even novice programmers and those that are not overly familiar with computer hardware to determine. Level 1 reporting includes details such as number of processors and total system memory and represents the base level of reporting.

For those who are more familiar with computer hardware and vendors who wish to sell their products commercially, it is recommended that a Level 2 or Level 3 reporting be used. These levels provide additional details that enable a more fair comparison between solvers, which is highly desirable for commercial solvers. Level 2 provides additional details regarding system memory and processing power, while Level 3 provides more details on the motherboard and hard drive that also impact overall solver performance. The reporting requirements of each level are outlined in Table F.1.

Table F.1—Performance reporting requirements

Level 1	Level 2	Level 3
• Run time • Processor Speed • Number of Processors • Cores per Processor • Total System Memory	• All Level 1 Information • Cache Size • Memory Type • Memory Speed • Processor Model	• All Level 2 Information • Motherboard Model • FSB Speed • Hard Drive Speed • Hard Drive Interface

This level reporting system can also be applied to vendors and researchers utilizing hardware-based CEM solvers. In addition to the host-computer specifications specified by the level system, users should also report:

— Accelerator model number (in the case of a commercial solver)

— Total accelerator memory

— PC Interconnect technology (e.g., PCI Express, PCI-X)

— Accelerator processor (e.g., FPGA, GPU)

For those who have purchased such tools, more accelerator details, such as exact FPGA model and type of memory on the GPU card, may not be immediately available. However, it is recommended that vendors (and researchers developing new hardware accelerators) disclose this information to the public. Such information should not be considered proprietary, as simply identifying the underlying hardware will not compromise the product (Note: this is because the real "intelligence" of the solver is the code used to program the platform). However, users wishing to compare platforms will find this information incredibly helpful and enable fair and accurate comparisons.

F.3 Detailed level descriptions

Below is a description of the items to be reported in each level, as well as their impact on the overall system performance. Typically, Level 1 reporting will be sufficient, but Levels 2 and 3 provide a more complete picture of the platform used to perform the simulations.

Level 1

— *Run Time* – perhaps the most obvious performance measurement, the run time measures the wall-clock time required to solve the problem at hand. Certainly, shorter runtimes are desired as this indicates a faster solver.

— *Processor Type/Speed* – processor speed refers to the clock rate of the processor(s) used to solve the problem. If a simulation finishes more quickly on a given platform, it may be because a faster code is used or simply because the hardware platform is better. Reporting processor speed will ensure that reported results can be compared on similar platforms.

— *Number of Processors* – if a system contains more than a single processor, this information should be reported so as to enable a more direct comparison and validation of performance results. Certainly, two or more processors will be able to solve the problem more quickly than a single processor. Note: this is the number of physical processing chips in the system, not the number of cores.

— *Cores per Processor* – just as multiple processors enable faster simulations, so do multiple cores. Because each core can solve aspects of the problem in parallel, it is important to report this information so that the reader can determine just how much processing power was used to perform the simulation.

— *Total System Memory* – this is an important value as too little memory will severely impact the performance of the solver. Specifically, if the problem is unable to fit into the system memory, data must be swapped to/from the hard drive which causes performance to drop off dramatically.

Level 2

— *Cache Size* – cache size (usually reported as L2 cache), represents "fast" memory located with the processor. This memory is independent of the system memory and allows for super-fast data accesses. Typically, larger cache sizes enable faster performance.

— *Memory Type* – this is the type of system memory used in the simulations. Examples include SDRAM, DDR, and DDR2. The type of memory directly impacts performance as newer memory architectures typically provide increased data throughputs, which allows data to flow more quickly to/from the processor, resulting in faster simulation times.

— *Memory Speed* – memory clock rate also impacts memory bandwidth, as a faster memory can read/write data more quickly.

— *Processor Model* – this information is important (although slightly redundant) as the model number indicates the type of processor, number of cores, cache size, etc. The model number will most likely grow in importance as the future of processor design continues to evolve from simply increasing clock rates to multiple cores and novel architecture designs. The model number may provide information about the processor that is otherwise omitted from this list.

Level 3

— *Motherboard Model* – similar to the processor model, the motherboard model number allows others to determine the exact components and configuration of the motherboard. This information includes aspects such as the north bridge chipset (which impacts memory performance), as well as NIC and RAID controller details, which impact data sharing and writeback performance.

— *FSB Speed* – although this information can be determined from the motherboard model, the front-side bus speed is important as it impacts how quickly data can travel to/from the processor.

— *Hard Drive Speed* – the faster the platters spin, the faster data can be read/written.

— *Hard Drive Interface* – the newer SATA interface provides increased data rates as compared to the older PATA IDE drives.

F.4 Examples

Below are examples of level-based reporting.

Level 1

"The simulation required 172 minutes on a desktop PC with 2 GB of memory and a 2.93 GHz quad-core processor."

Level 2

"The simulation required 172 minutes on a desktop PC with 2 GB of DDR2 800 memory and a 2.93 GHz Intel Core 2 Extreme QX6800 quad-core processor with 2 x 4 MB of L2 cache."

Level 3

"The simulation required 172 minutes on a desktop PC with 2 GB of DDR2 800 memory and a 2.93 GHz Intel Core 2 Extreme QX6800 quad-core processor with 2 x 4 MB of L2 cache. The system contained an Intel BOXDG965WHMKR motherboard with a 1066/800 MHz FSB and a 7200 RPM SATA 3.0 Gb/s hard drive."

References:

[B117] Taflove, A. and Hagness, S. C., *Computational Electrodynamics: The Finite-Difference Time-Domain Method*, 3rd ed. Norwood: Artech House, 2005.

[B42] Durbano, J. P., Ortiz, F. E., Humphrey, J. R., Prather, D. W., and Mirotznik, M. S., *Hardware implementation of a three-dimensional Finite-Difference Time-Domain algorithm*, IEEE Antennas and Wireless Propagation Letters, Vol. 2, pp. 54–57, 2003.

[B107] Songoro, H., *On the Real-World Performance of ADI-FDTD*, Web site <http://www.semcad.com/simulation/publications/hs_poster_05.pdf>, 2005.

[B87] Mur, G., *Absorbing Boundary Conditions for the Finite-Difference Approximation of the Time-Domain Electromagnetic-Field Equations*, IEEE Transactions on Electromagnetic Compatibility, Vol. 23, pp. 377–382, 1981.

[B14] Berenger, J.-P., *Three-Dimensional Perfectly Matched Layer for the Absorption of Electromagnetic Waves*, Journal of Computational Physics, Vol. 127, pp. 363–379, 1996.

Annex G

(informative)

Combinatorial modeling rules

G.1 General

The validation methodology should also investigate combinatorial schemes whereby components are assembled and measured or simulated in a certain prescribed order. Component-level measurements and procedures will to some extent determine the "order" of the simulation. By knowing how components were assembled and tested to begin with, we will know what to expect in the simulation to perform a first-order validation based on the measurements. The purpose of this piecewise approach beginning with one component, measuring its EM characteristics, and then adding a second component, measuring their joint characteristics, and so forth is to define the approach for effectively integrating the scattering effects of component structures. This draws upon methods used by the RCS community to identify and rank weakly and strongly interacting components. Interactions are superimposed nonlinearly (nth-order weighted summation of interaction terms as a function of component type, interaction type and order, etc. for a given frequency, position, orientation, polarization, and so forth) to obtain the total (budget) solution. This may result in quadratic, cubic, or higher order interaction terms. The component scattering contribution is determined from empirical results and then a weighting criterion (e.g., method of weighted averages) is applied to each component effect to compute the budget solution. The difference between the budget and true solution is a function of how strongly the parts interact. The accuracy of the models can be verified by comparing to the existing measurement benchmarks. Measured versus simulation error statistics can be computed to confirm accuracy and validity.

G.2 Integrating component contributions to achieve a total budget solution

This is also concerned with resolving a complex systems (e.g., an aircraft) into its parts, analyzing the EM interactions and relative contributions, and then integrating results in order to arrive at an accurate system analysis. First, this is an approximate idea. Linear superposition does not work. By solving a problem in components, finding its component RCS, for instance, and later adding up the total solution (i.e., budget solution), the total solution found this way is a lower bound to the true solution. The difference between the budget solution and the true solution is a function of how strongly the parts interact. The stronger they interact, the larger the difference between the budget solution compared to the true total solution. For example, five walls of a cavity are not strong scatterers individually, but when the five walls cooperate with each other to form a cavity, they can give rise to resonance scattering, which is much stronger than the scattering from the individual walls. So, a possible approach is to break the system up into weakly interacting components. Then the budget solution is not too different from the true solution. An adaptation of the Green's function method can be used to compute the total budget solution. The method can be modified to suit the requirements of subdividing a complex system into weakly interacting components.

G.3 Bounding uncertainty

Methods to bound uncertainty are meant to assure that valid and well-behaved CEM models are generated. One way to bound a simulation is to calculate the component solution, and assume that (a) they interfere constructively or (b) they interfere destructively. If there are N component solutions, one can add the solutions up constructively and destructively, giving rise to 2^N ways of adding up the solution. This still does not account for multiple scattering interactions, but will give an estimate of the lower and upper bounds of the interaction.

Annex H

(informative)

Data used for FSV comparison

The two columns give the original data used for the comparison discussed in clause 7.2 and can be used to verify the performance of any FSV implementation.

There is no "*x*-axis" (abscissa) data supplied. Should a user want to include this in their implementation, they are at liberty to choose and append this data as they desire.

Data set 1	Data set 2	0.046429	0.069950	0.051542	0.065548
0.012993	0.005201	0.030858	0.064323	0.046711	0.070976
0.013990	0.004959	0.060038	0.073414	0.038589	0.072311
0.015652	0.005208	0.020235	0.094452	0.033686	0.066288
0.017790	0.005697	0.033602	0.102192	0.029346	0.055784
0.020280	0.006092	0.053036	0.088234	0.058649	0.042583
0.023428	0.006325	0.065498	0.059738	0.173874	0.024825
0.027315	0.005800	0.086544	0.023422	0.195732	0.020205
0.032804	0.011920	0.106964	0.023067	0.148918	0.027351
0.040045	0.015485	0.125732	0.055359	0.123055	0.041103
0.050596	0.016501	0.137062	0.081207	0.109524	0.075695
0.063725	0.019867	0.136292	0.082272	0.102871	0.121761
0.076012	0.026566	0.126312	0.078949	0.099236	0.149956
0.082584	0.041096	0.113007	0.064751	0.092468	0.133759
0.085201	0.046831	0.101948	0.054573	0.120304	0.125885
0.089828	0.025555	0.093235	0.048758	0.142639	0.129959
0.099506	0.021559	0.085842	0.037262	0.155502	0.150803
0.116135	0.016902	0.079918	0.026402	0.167580	0.159805
0.147041	0.019456	0.075142	0.056931	0.170967	0.186295
0.195847	0.035746	0.071739	0.102264	0.156746	0.199356
0.212456	0.055326	0.067730	0.126076	0.120602	0.187141
0.196068	0.116001	0.062370	0.116390	0.116093	0.153542
0.156960	0.075157	0.055273	0.100933	0.115334	0.125168
0.124012	0.040676	0.042429	0.088242	0.164688	0.117493
0.101074	0.045473	0.020955	0.077545	0.164619	0.107937
0.084267	0.032957	0.135277	0.067646	0.135780	0.090229
0.070675	0.021251	0.106182	0.058500	0.109653	0.071133
0.055658	0.009499	0.088573	0.048901	0.090530	0.051497
0.039948	0.010509	0.079453	0.040533	0.076900	0.064404
0.110619	0.041052	0.074455	0.034393	0.070633	0.064228
0.102478	0.083866	0.071510	0.030655	0.061451	0.062117
0.096989	0.112732	0.067101	0.027801	0.075493	0.049110
0.102158	0.126030	0.063427	0.018178	0.068218	0.035820
0.112221	0.106518	0.060249	0.020003	0.065220	0.020262
0.096706	0.054300	0.054201	0.048185	0.054531	0.015710

0.029159	0.050642	0.217468	0.046114
0.030663	0.032211	0.239235	0.055355
0.030912	0.024133	0.167870	0.068970
0.030857	0.019192	0.096588	0.059259
0.031435	0.017967	0.081234	0.067982
0.031700	0.014424	0.072453	0.059420
0.024025	0.014550	0.067707	0.052073
0.021782	0.024175	0.067085	0.039444
0.023407	0.019393	0.062359	0.080490
0.024854	0.012118	0.068417	0.130463
0.024017	0.028598	0.091370	0.219254
0.008286	0.033693	0.139046	0.122086
0.010965	0.025064	0.168266	0.027756
0.012557	0.031809	0.120438	0.063553
0.012972	0.038263	0.087711	0.065514
0.012861	0.043623	0.088154	0.165520
0.012547	0.037722	0.092747	0.129532
0.012175	0.028859	0.114552	0.122467
0.011296	0.040136	0.166870	0.071346
0.009573	0.034361	0.244392	0.094769
0.007334	0.024857	0.348434	0.058752
0.014520	0.051249	0.265228	0.072304
0.051411	0.037937	0.200836	0.117470
0.107334	0.039751	0.172607	0.121819
0.086903	0.031167	0.155182	0.141487
0.068657	0.005396	0.161415	0.133575
0.067230	0.063156	0.153503	0.080864
0.134216	0.082054	0.147423	0.082569
0.093670	0.065670	0.091442	0.043915
0.098637	0.060495	0.085079	0.065918
0.081108	0.045910	0.097828	0.089558
0.100445	0.053583	0.101585	0.088001
0.147636	0.077477	0.119419	0.037455
0.225449	0.111618	0.153427	0.108677
0.279861	0.090588	0.212440	0.056519
0.211380	0.077766	0.263123	0.111511
0.159828	0.071495	0.217308	0.227074
0.131989	0.049702	0.167694	0.274353
0.116737	0.067787	0.179230	0.152184
0.097973	0.185448	0.133652	0.129906
0.087620	0.287369	0.099926	0.057528
0.084320	0.227806	0.098789	0.099438
0.121071	0.167641	0.109379	0.103374
0.116711	0.114437	0.105122	0.096081
0.105820	0.114120	0.100475	0.076649
0.103268	0.125267	0.084263	0.026834
0.110054	0.123390	0.038954	0.040123
0.130760	0.081928	0.015528	0.060429
0.176544	0.024426		

Annex I

(informative)

Glossary

algorithm: (A) completely determined finite sequence of instructions by which the values of the output variables can be calculated from the values of the input variables [IEV 351-21-37]; **(B)** a finite set of well-defined rules for the solution of a problem in a finite number of steps [IEV 714-21-02]

benchmark: (A) A standard against which measurements or comparisons can be made. *See also:* benchmark program; benchmark problem. **(B)** A procedure, problem, or test that can be used to compare systems or components to each other or to a standard as in definition (A). [IEEE 100]

calibration: The process of adjusting numerical or physical modeling parameters in the computational model for the purpose of improving agreement compared with results whose veracity is accepted under the circumstances of the calibration... (modified AIAA G-077-1998)

problem: an inquiry starting from given conditions to investigate or demonstrate something. (http://www.askoxford.com/)

validation: (CFD simulations) The process of determining the degree to which a model is an accurate representation of the real world from the perspective of the intended uses of the model. (AIAA G-077-1998)

verification: The process of determining the degree to which a model is an accurate representation of the problem space from the perspective of the intended uses of the model. (modifed AIAA G-077-1998)